Final Report

Development and Field Trial of Dimpled-Tube Technology for Chemical Industry Process Heaters

Prepared by:
Yaroslav Chudnovsky, Ph.D.
Aleksandr Kozlov, D.Sc.
Gas Technology Institute

September 2006

U.S. DOE Award DE-FC07-01ID14089

DEVELOPMENT AND FIELD TRIAL OF DIMPLED-TUBE TECHNOLOGY FOR CHEMICAL INDUSTRY PROCESS HEATERS

Final Report

(September 2001 – June 2006)

Prepared by:

Yaroslav Chudnovsky, Ph.D.

Aleksandr Kozlov, Sc.D.

Energy Utilization Center/Process Heating
Gas Technology Institute
1700 S. Mount Prospect Rd.
Des Plaines, IL 60018

Prepared for:

Industrial Technology Program
U.S. Department of Energy
Golden Field Office
1617 Cole Blvd, Golden, CO 80401

Project Manager, Chemicals and Combustion
Mr. Bill Prymak
303-275-4931 phone
303-275-4753 fax

September 2006

Legal Notice

Acknowledgments

This R&D was cofunded by the U.S. Department of Energy Industrial Technologies Program, GTI's Sustaining Membership Program, Gas Research Institute and ExxonMobil Research Engineering Corporation. Project team is grateful to all the Sponsors for their strong financial support as well as to Industrial Partners for their valuable comments in design review as well as results analysis. Special thanks are to BP Cherry Point refinery for hosting the GTI pilot-scale evaluation and providing exceptional support to this challenging development.

Research Summary

Title:	Development and Field Trial of Dimpled-Tube Technology for Chemical Industry Process Heaters
Contractor:	Gas Technology Institute
DOE Contract Number:	DE-FC07-01ID14089 (61142/15320)
GRI Contract Numbers:	8414 (32054/15144), 8477 (30797/15058), 8827 (20400)
SMP Contract Number:	80042/15401
Principal Investigator:	Yaroslav Chudnovsky, Ph.D.
Report Type	Final Report
Report Period:	September 2001 – June 2006
Objective:	To develop and field-test a cost-effective Dimpled Tube Technology for significantly improving the energy efficiency of chemical industry gas-fired process heaters.
Technical Perspective:	Most approaches to increasing heat transfer rates in the convection sections of gas-fired process heaters involve the incorporation of fins, baffles, turbulizers, etc. to increase either the heat transfer surface area or turbulence or both. Although these approaches are effective in increasing the heat transfer rates, this increase is invariably accompanied by an associated increase in convection section pressure drop as well as, for heaters firing 'dirty' fuel mixtures, increased fouling of the tubes – both of which are highly undesirable. GTI has identified an approach that will increase heat transfer rates without a significant increase in pressure drop or fouling rate. Compared to other types of heat transfer enhancement approaches, the proposed dimpled tube approach achieves very high heat transfer rates at the lowest pressure drops. Incorporating this approach into convection sections of chemical industry fired process heaters may increase energy efficiency by 3-5%. The energy efficiency increase will allow reducing firing rates to provide the required heating duty while reducing the emissions of CO_2 and NO_x.
Technical Approach:	Based on the results of previously conducted fundamental studies, experimental data from a University of Utah subcontract, and results of in-house CFD modeling, a bench-scale unit (BSU) was developed, fabricated and extensively evaluated in GTI's Applied Combustion Research Laboratory. There were six test sections under comparative testing. Each replaceable section was comprised of 20 tubes arranged in a staggered bundle containing smooth, finned, or dimpled tubes. Air flow over the tube bundle simulated the heating medium (flue gas) while water flow inside the tubes simulated the heated medium (chemical product). The test section was thermally insulated to minimize heat losses. During the tests, the following parameters were measured and registered by a data acquisition system: air inlet/outlet temperature, pressure, and flow rate, and water

inlet/outlet temperature and flow rate. Based on the results of the bench-scale evaluation, a field trial system was developed, fabricated, and installed at an industrial partner's refinery. A slip-stream approach was selected and approved by the industrial partner as the most promising approach for GTI's field trial and post-trial performance monitoring.

Results:

The BSU design was based on the modeling results. It was fabricated by a local vendor with advisory support from KTI Corporation, a world leader in the engineering of fired heaters. Six test sections were evaluated in GTI's research laboratory, according to the test plan, and the data was processed for comparative analysis. Heat transfer enhancement (up to 25% more than a smooth surface) was obtained for dimpled tubes with certain configurations.

In comparison with finned tubes (widely used in the chemical industry) the following benefits were established:

- Relative heat transfer coefficient (Nu/Nu_{finned}) ~ 3.0
- Relative pressure drop (Eu/Eu_{finned}) ~ 0.4
- Relative cost ($\$/\$_{finned}$) ~ 0.5

Based on bench-scale evaluation results, a field trial unit (FTU) was designed, employing the slip-stream approach. Bypass streams on both sides of the existing economizer enable simultaneous data collection from the finned-tube test section and dimpled-tube section in an actual industrial environment. KTI engineered the FTU design, fabricated and provided procurement services to the host site's local contractors for FTU installation. Field evaluation results demonstrated the anticipated benefits in heat transfer enhancement and fouling rate mitigation.

Project Implications:

This technology could be very beneficial for a variety of heat transfer applications in the petrochemical industry, since it provides a significant increase in heat transfer coefficient with a minimal pressure drop penalty and a potential for fouling rate reduction.

Contents

List of Figures

List of Tables

Introduction

Overall Objective

The overall objective of the entire project is to develop and demonstrate a cost-effective dimpled tube technology for significantly improving the energy efficiency of chemical industry fired process heaters. Specific goals include a 15-20% increase in overall thermal efficiency of the convective section, with no significant increase in pressure drop or fouling rate.

Project Description

A number of approaches can be used to increase heat transfer rates in the convection section of fired process heaters. These approaches, in general, involve the incorporation of fins, baffles, turbulizers etc. to increase either the heat transfer surface area or turbulence or both. These approaches are effective in increasing heat transfer rates, but this increase is invariably accompanied by an associated increase in convection section pressure drop as well as, for heaters firing 'dirty' fuels, increased fouling of the tubes – both of which are highly undesirable.

GTI has identified an approach that will increase heat transfer rates without a significant increase in pressure drop or fouling. It involves the use of specially shaped dimples, as shown in Figure 1. Compared to other types of heat transfer enhancement approaches, as illustrated in Figure 2, the proposed dimpled approach achieves higher heat transfer rates at lower pressure drops, because of vortex flow patterns within the dimples; moreover, it is expected the dimpled approach will not increase (and may even reduce) fouling rates. The red line in Figure 2 represents the equality of heat transfer gain and pressure drop penalty associated with this gain reached by majority of the heat transfer enhancement techniques. Figure 2 shows that VHTE (vortex heat-transfer enhancement) provides a better balance of pressure drop and heat transfer than most other available techniques.

Studies[1] have confirmed that flowing a gaseous medium over surfaces with specially shaped dimples can generate extremely stable vortices. As illustrated below, each dimple works as a vortex generator that intensifies the rate of convective heat transfer and mass transfer to the dimpled surface from the core of the gaseous medium. The following benefits were established by majority of previous studies:

- Increased dimpled side heat transfer coefficients by 30-40%;
- No significant fouling is expected on dimpled surfaces when used in gaseous media with entrained particulate matter;
- No significant increase in pressure drop compared to smooth surfaces.

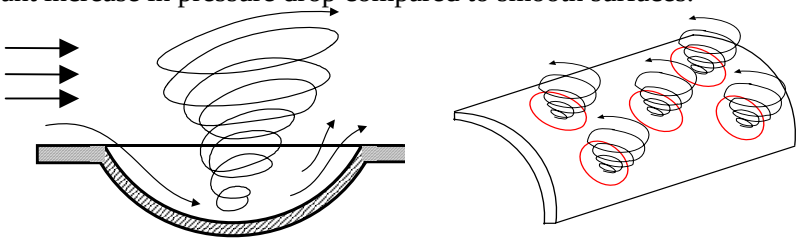

Figure 1. Mechanism of Swirl Formation in a Dimple[2] and a Cluster of Vortices on a Tube Surface

---

[1] A. Schukin, A. Kozlov, Y. Chudnovsky, R. Agachev, "Intensification of Heat Exchange by Spherical Depressions. A Survey," Applied Energy: Journal of Fuel, Power and Heat Systems, vol 36, no. 3, pp.45-62, 1998.

[2] Ya. Chudnovsky, "Heat Transfer and Fluid Flow in a Spherical Cavity," Paper presented at Second European Thermal Sciences and UIT National Heat Transfer Conference, Rome, Italy, May 1996.

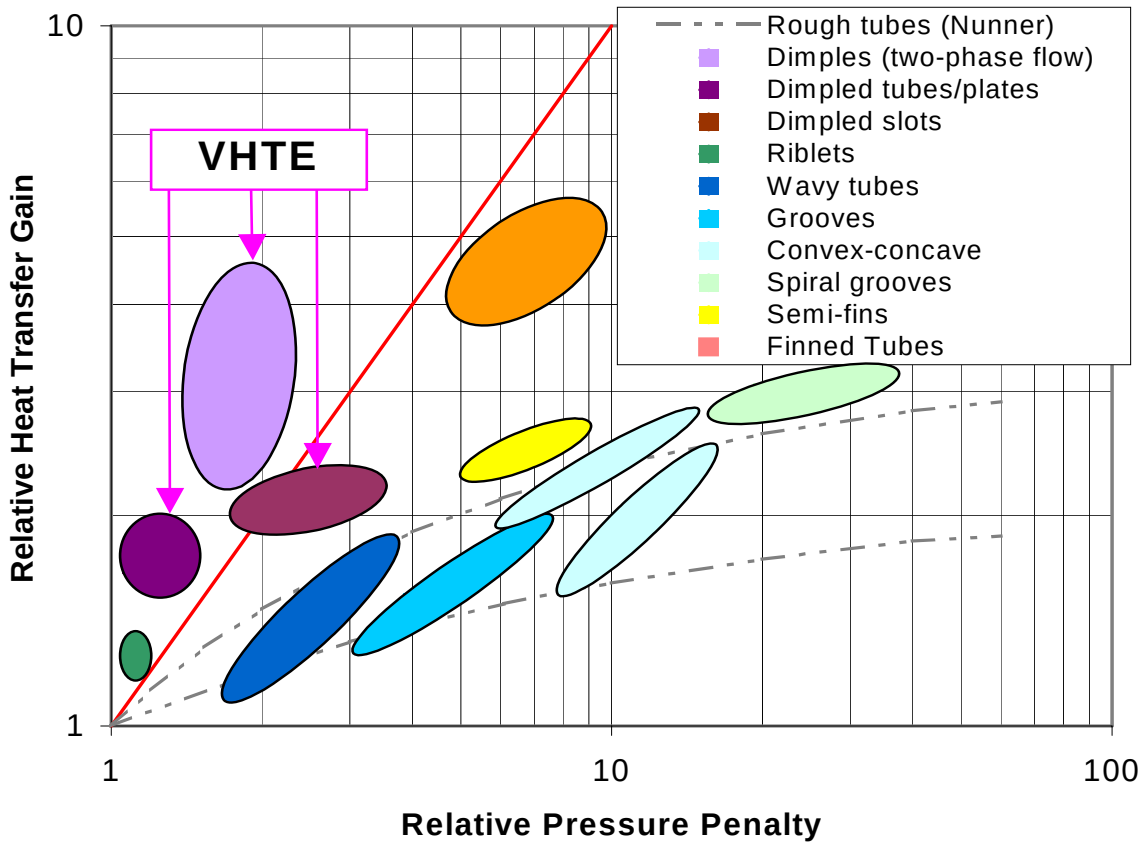

Figure 2. Efficiency of Various Heat Transfer Enhancement Methods

Along with previous experimental work, computational fluid dynamics (CFD) modeling has also been carried out. This modeling demonstrated the existence of stable 3-D vortices in the dimple (Figure 3). The internal structure of the vortex inside a single dimple was also determined and partially investigated.

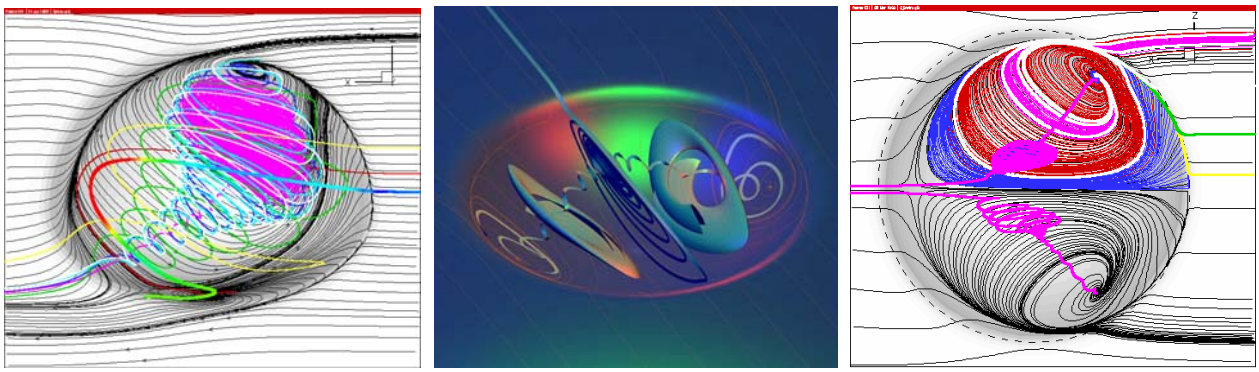

Figure 3. Vortex Structures Were Identified Through CFD Modeling[3]

[3] S.Isaev et al, "Identification of Self-Organized Vortex Structures In Numerically Simulated Turbulent Flow," Technical Physics Letters, vol. 26, no. 1, pp. 15-18, 2000.

The project work scope had two major phases:

Phase I: Profile Development and Bench-Scale Laboratory Evaluation

- Development of an efficient surface relief for heat transfer enhancement and fabrication of a set of test sections for laboratory evaluation.
- Design and fabrication of a bench-scale unit to determine the expected performance range in the laboratory.
- Evaluation (jointly with industrial partners) of the bench-scale results on technical merit and economic payback, as a basis for a go/no-go decision for Phase II.

Phase II: Technology Scale-Up and Pilot-Scale Field Trial

- Development of a pilot-scale field trial approach and selection of the appropriate host site for the technology demonstration.
- Design and fabrication the field trial hardware, including test sections and measurement and data acquisition systems.
- Conducting (jointly with industrial partners) a pilot-scale field trial that includes data collection and 6-12 months performance monitoring of the test sections for further comparative analysis of anticipated benefits.

<u>The key hurdles for this development:</u>

- The risk of applying a new technology into an operating fired process heater. This risk was minimized by involving industrial partners with a strong presence in the Chemical Industry and which complement the effort by proving the technical and economic benefits of the technology in the field.
- The risk that laboratory results do not adequately represent full-scale performance. Thorough laboratory testing and the use of CFD modeling reduced this risk to the high confident level.
- Convincing potential users that the benefits of dimpled-tube technology outweigh its costs. This will be addressed by examples that illustrate satisfactory monetary rates of return in the follow-on full-scale demonstration effort.

Approach, Methodology and Accomplishments

Application Concept

Implementation of dimpled tube technology into industrial applications will require packaging the existing (or newly constructed) convection sections of process heaters with vortex-heat-transfer-enhanced VHTE-tubes, which should be comparable to the standard practice of replacing damaged tubes in the field. The typical convective section of the fired heater is shown in Figure 4a [4]. It usually consists of one or more process coils including shock tubes. Shock tubes are the first 2-3 rows of the convection section tubes handling the hot combustion products flow (~1300-1500ºF) coming out of the furnace. They are typically bare, since fins cannot last long in this high-temperature environment.

The general layout of the originally proposed application concept is shown in Figure 4b.

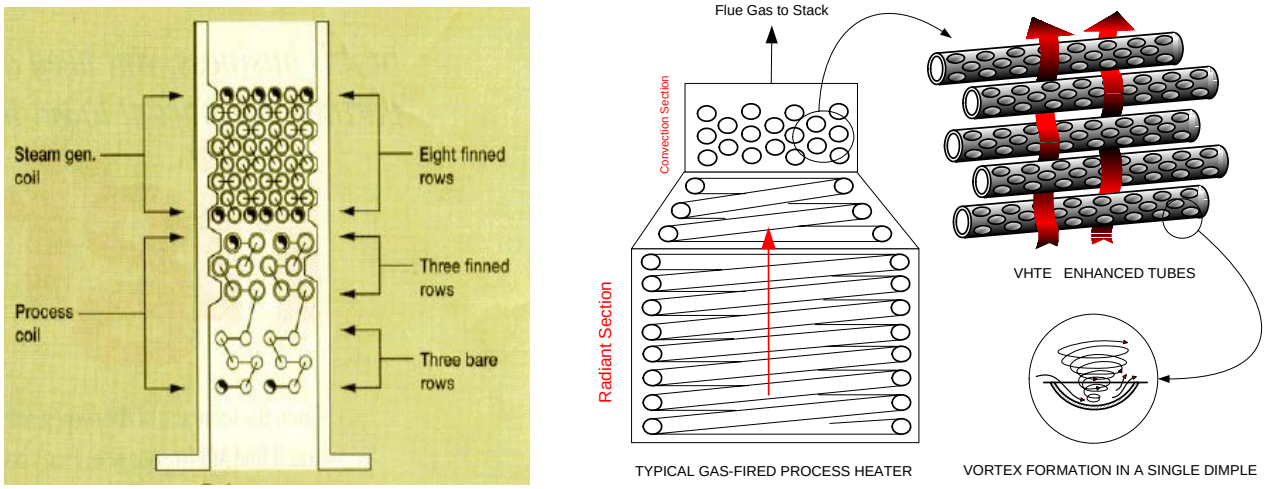

Figure 4. Typical Outline of the Fired Heater Convective Section (a) and Application Concept of VHTE Enhancement of Convection Section (b)

Tri-Evaluation Approach

For the successful project performance a tri-evaluation approach was selected: numerical evaluation, laboratory evaluation and field evaluation. The following was accomplished:

CFD modeling to develop efficient dimpled-surface profiles and experimental validation of the CFD model results were performed with support of FLUENT Inc. and Convective Heat Transfer Laboratory of the Utah University.

Laboratory bench-scale evaluation following the comparative analysis of six tube banks (test sections) comprised of the various types of tubes: smooth, finned, and dimpled and demonstrated the significant heat transfer enhancement of the dimpled tube banks over other tested.

A slip-stream field trial approach was selected; a host site was identified and evaluated for its suitability for a field trial. Concept design of the field trial unit was developed and a set of dimpled tubes were fabricated per selected surface geometry.

---

[4] A.Garg. Fired Heaters Engineering School, Houston, TX, December 10-12, 2001

The field trial unit was engineered and fabricated by KTI with GTI support. All the fabrication drawings were carefully reviewed by GTI project team and industrial partners and modified per their comments appropriately to meet host site technical and safety requirements.

The field trial system (including control, measurement and data acquisition units) was installed at the host site facility by local service contractors. Instruments and data acquisition system were calibrated and checked for proper operation. The field trial system was then placed in service by GTI project team with the help of host site personnel. Thermal and hydraulic performance data were collected and processed for three test sections (finned tubes in in-line arrangement, dimpled tubes in in-line arrangement, dimpled tubes in staggered arrangement).

Post-trial fouling performance monitoring was carried out without water flow from middle of September 2005 to the end of March 2006. The visual observation of the tested tubular banks clearly demonstrated superior fouling performance of the dimpled surfaces over the traditional finned surfaces.

CFD Modeling

Model Development

In order to develop and optimize the new tubular heat exchanger, we had to mathematically model the hydrodynamics and heat transfer processes in the dimpled-tube bundle.

FLUENT software was selected for CFD modeling. GTI has a licensed copy of the FLUENT solver, which is packaged with the GAMBIT mesh-generation code. GTI asked Fluent Inc. to develop and validate the computational numerical model, including meshing, for a computational domain (provided by GTI) and converging of the numerical solution (for a proper functional check). The validation was based on comparing the calculation results for dimpled tubes with the calculation results for smooth tubes. Calculation results for smooth tubes also had to be validated against published reference data.

Using the computational model developed by Fluent Inc., GTI carried out extensive in-house parametric calculations for smooth and dimpled tube bundles at various flow conditions (inlet flow velocity and temperature) and dimple geometry (diameter and depth). Two different computational approaches (2D and 3D) were chosen to describe the smooth and dimpled tube banks. The 2D computational domain geometry for smooth tubes is shown in Figure 5a. Two symmetry surfaces limit the computational domain in a way that required only 8 semi-tubes to be included in the domain.

A 3D modeling was chosen for the dimpled tubes case. The details of the computational domain for the dimpled tubes bank are shown in Figure 5b. Four symmetry surfaces limit the computational domain in a way that required only 8 semi-tubes and 24 semi-dimples on each tube to be included in the domain.

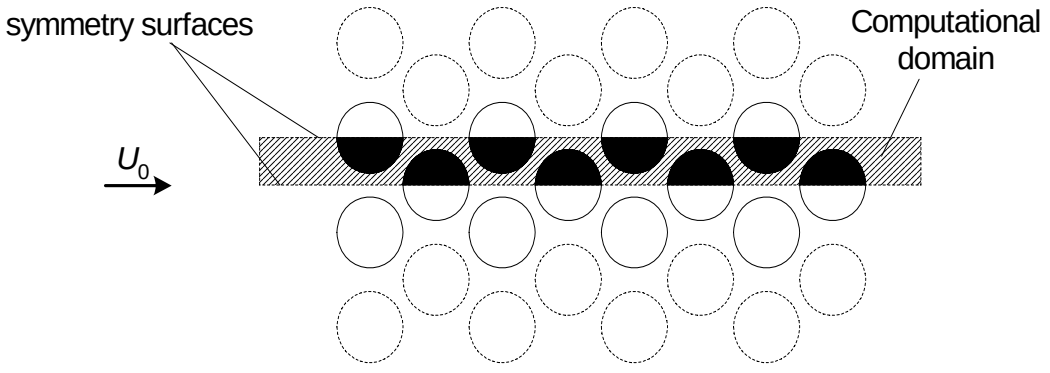

Figure 5a. Computational Domain Geometry for Smooth Tubes (2D Approach)

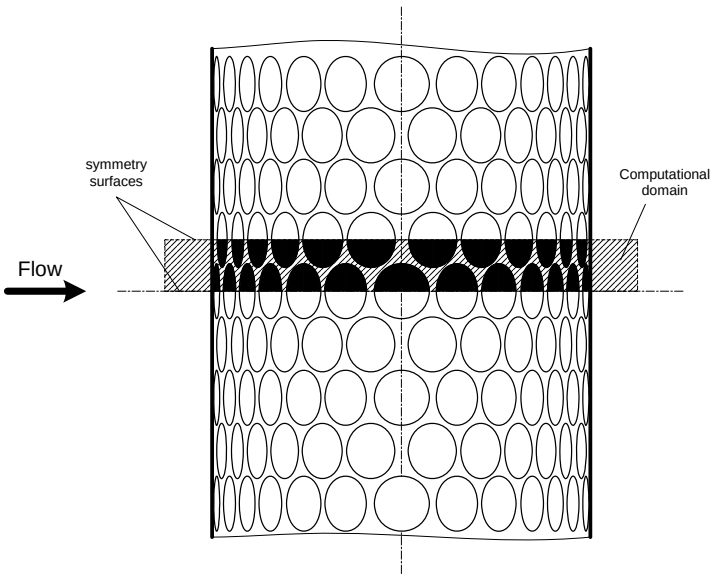

Figure 5b. Computational Domain Geometry for Dimpled Tubes (3D Approach)

A uniform incoming velocity profile that is located at a distance of 5 tube diameters from the first tube row was used at the tube bank inlet. Inlet turbulence intensity was ~1%. Inlet longitudinal and cross-flow turbulence integral scale was accepted as 3 tube diameters. A uniform zero static pressure profile behind the tubes located at a distance of 10 tube diameters from the last row was used at the outlet. Symmetry boundary conditions were used at the symmetry surfaces.

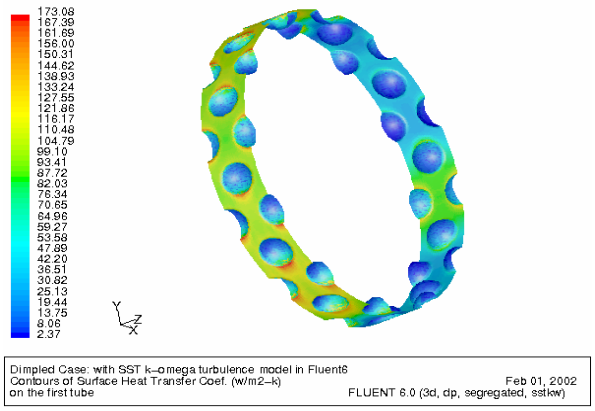

Figure 6. Heat transfer Coefficient Along the Dimpled Tube Surface (Slice View)

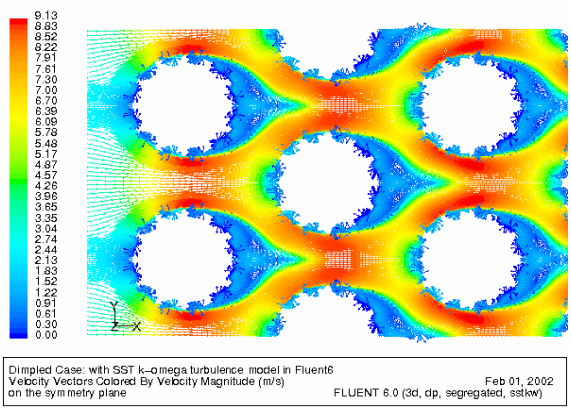

Figure 7. Velocity Distribution Between the Dimpled Tubes in a Staggered Bank

A detailed description of the modeling and validation approaches as well as discussion of the results obtained is given in the Summary of CFD Modeling enclosed to this report in Appendix I. Figures 6 and 7 represent just a portion of modeling results on heat transfer and fluid flow over dimpled tubes in a staggered arrangement.

The essential heat transfer enhancement behind the dimple can be explained by the influence of the vortex that is formed inside each dimple and escapes from the dimple. These vortices (see Figure 8) increase turbulence intensity substantially and, therefore, increase heat transfer.

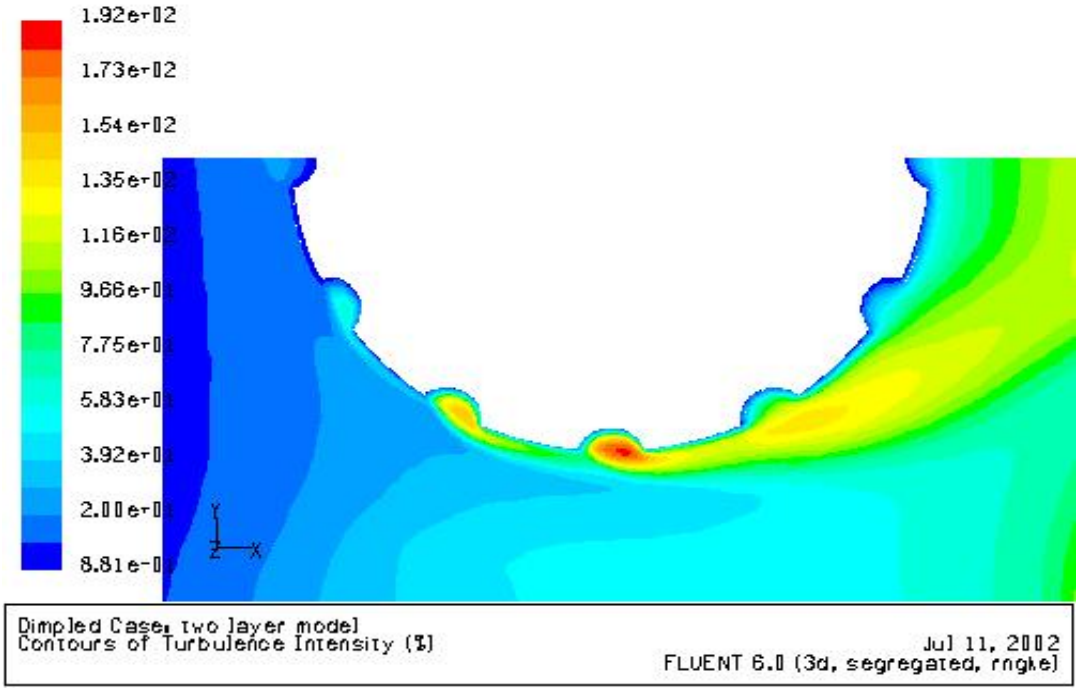

Figure 8. Contours of Turbulence Intensity Near the Tube

Model Validation

The developed CFD model was validated with the existing data on smooth tubes and with experimental results obtained from the Heat Transfer Laboratory of the University of Utah under subcontract to GTI (see Appendix II).

CFD Modeling Summary

The computational model for heat transfer and pressure drop calculations (smooth and dimpled-tube cases) was developed by Fluent, Inc. with GTI's technical assistance. Based on GTI in-house CFD evaluation, the RNG k-ε turbulence model with two-layer zonal model was selected as a better predictor of heat transfer for smooth and dimpled tubes than the k-ω turbulence model.

The modeling results for smooth tubes were successfully validated with available published reference data. The modeling results for dimpled tubes were acceptably validated with the University of Utah's experimental results.

The major results obtained for dimpled tubes are:

- Heat transfer enhancement (over smooth tubes) of up to 15-20%.
- Pressure drop penalty of less than 5-10%.

The resulting trends and other information obtained under the parametric modeling study were used in bench-scale unit design for laboratory evaluation of the tube bank models.

Bench-Scale Unit Development

To evaluate smooth, finned, and dimpled tube banks in terms of heat transfer and pressure drop the bench-scale unit (BSU) and test sections (replaceable tube banks) were designed and fabricated by a local vendor. Figure 9 represents the general layout of the experimental unit installed at the GTI Applied Combustion Research Laboratory.

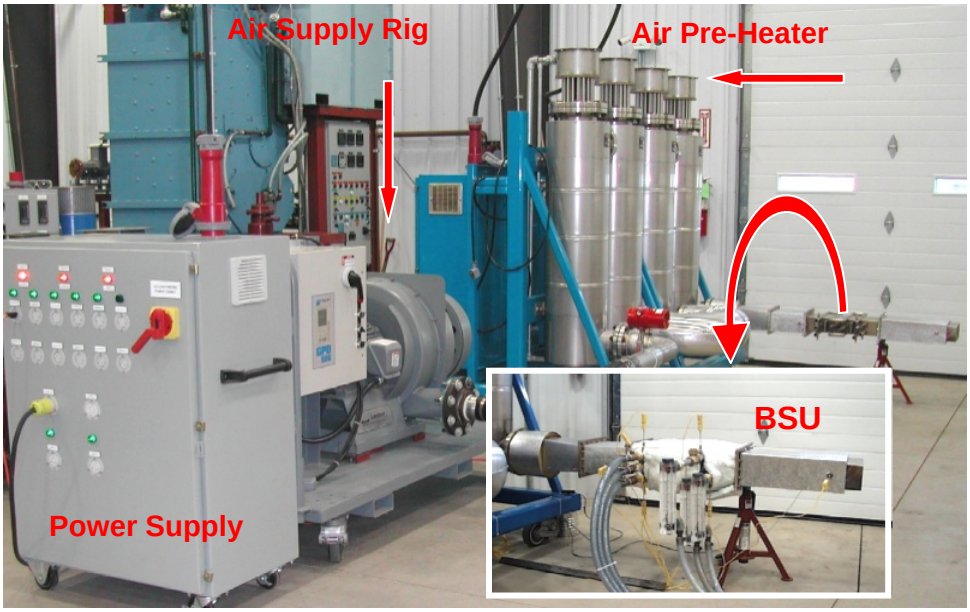

Figure 9. Experimental Unit at GTI

The entire experimental unit contained the following major components:

Air supply module (including Sierra 780 mass flow meter, 0-25,000 SCFH).
Air heating system (four OGDEN electrical heaters, 41.5 kW each).
Water supply system (including ABB Mini-Mag flow meter, 0-26 GPM).
Test sections (smooth, finned and dimpled).
Measurement system (including data acquisition based on OPTO22 modules).

A test section consists of a rectangular air channel with 20 tubes installed in a staggered arrangement. The pre-heated air (up to 1100°F) flowed over the tube banks while city water flowed inside the tubes to remove heat from the BSU. Six test sections were developed and fabricated for BSU evaluation:

Section 1 – 4" by 8" cross section with smooth tubes (1" OD x 0.083" wall thickness).
Section 2 – 4" by 8" cross section with finned tubes (1" OD x 0.083", 6 fins per inch).
Section 3 – 4" by 8" cross section with dimpled tubes (1" OD x 0.083", shallow dimples).
Section 4 – 4" by 8" cross-section with dimpled tubes (1" OD x 0.083", deep dimples).
Section 5 – 3" by 8" cross-section with dimpled tubes (1" OD x 0.083", shallow dimples).
Section 6 – 3" by 8" cross-section with dimpled tubes (1" OD x 0.083", deep dimples).

Figure 10 shows the three types of test sections (with smooth, finned and dimpled tubes).

a **b** **c**

Figure 10. BSU Test Sections: a **– smooth,** b **– finned,** c **– dimpled**

Each test section was equipped with pressure measurement taps, thermocouple couplings, and water connection nipples. To minimize heat loss to the ambient environment, the test section was heavily insulated during the testing (see Figure 11).

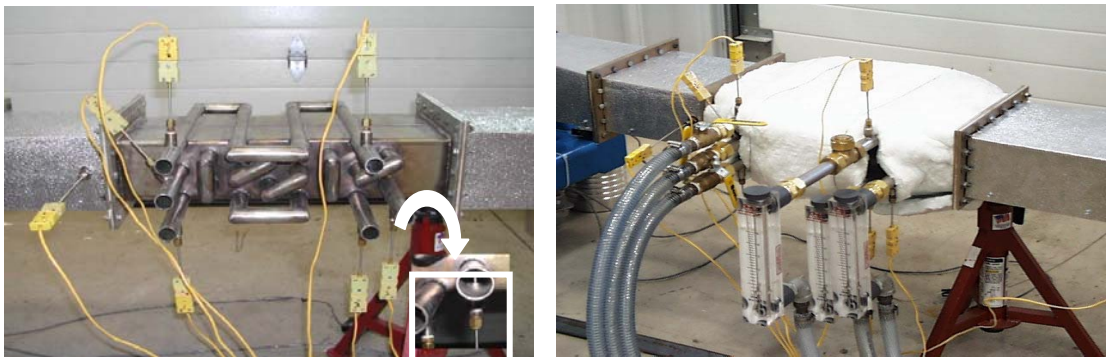

Figure 11. Test Section Installed in the BSU at GTI

All the measurement sensors had 4-20 mA outputs compatible with the data acquisition system (DAS) based on OPTO22 modules. The measurement system included the following means for measuring of test parameters:

- K-type thermocouples for measuring air and water temperature.
- Sierra 780 mass flow meter for measuring incoming air flow.
- ABB Mini-Mag flow meter for measuring water flow.
- Dwyer 606 pressure transducers for measuring pressure drop across the test section.

Measured signals were displayed on the DAS monitor, along with the simultaneous recording to the data-files that were further converted into MS Excel spreadsheets for processing and analysis.

Comparative evaluations of all test sections were performed according to the following test approach:

Incoming air was pre-heated by four electrical heaters (OGDEN CK8A-0500-M5) to 1100-1200ºF and delivered to the BSU test section for heating the water-cooled tube bank. The air flow rate was varied in order to evaluate heat transfer and pressure drop, at incoming flow velocities of 10-80 ft/s.

City water flow rate through the tubes was varied to keep water temperature below 150ºF to prevent unwanted boiling.

During the test run, the following parameters were measured, collected by the DAS, and electronically recorded in an output file (for each test section):

- Air flow rate, SCFH.
- Water flow rate, GPM.
- Air temperature before test section, ºF.
- Air temperature after test section, ºF.
- Water inlet temperature, ºF.
- Water outlet temperature, ºF.
- Pressure drop across the tube bank, in. w.c.

Data from the output file was converted into MS Excel spreadsheet format and further processed. The processed results were presented in criteria/dimensionless form and analyzed.

Major Bench-Scale Evaluation Results

The overall heat transfer coefficient and pressure drop across the tube bank for each of the six test sections were obtained. The results for dimpled tubes were compared with smooth and finned tubes

Heat Transfer

Based on temperature and flow measurements the following results were obtained. Criterion **Nu** constructed per bare tube diameter (**Nu=hD/k**) versus criterion **Re** constructed per inlet flow velocity ($\mathbf{Re_d=UD/\nu}$) are given in Figure 12. Here, **D** is the tube outside diameter, **h** is heat transfer coefficient, **U** is inlet velocity, **k** is heat conductivity, and **ν** is kinematic viscosity. Area $\mathbf{A_0}$ in the figure relates to the outside surface area of the bare tubes and area **A** relates to the outside surface area of the finned tubes. It is obvious that in the **Re** number range of 5000-6500 the heat transfer coefficient is more than twice the value for dimpled tubes compared to finned tubes.

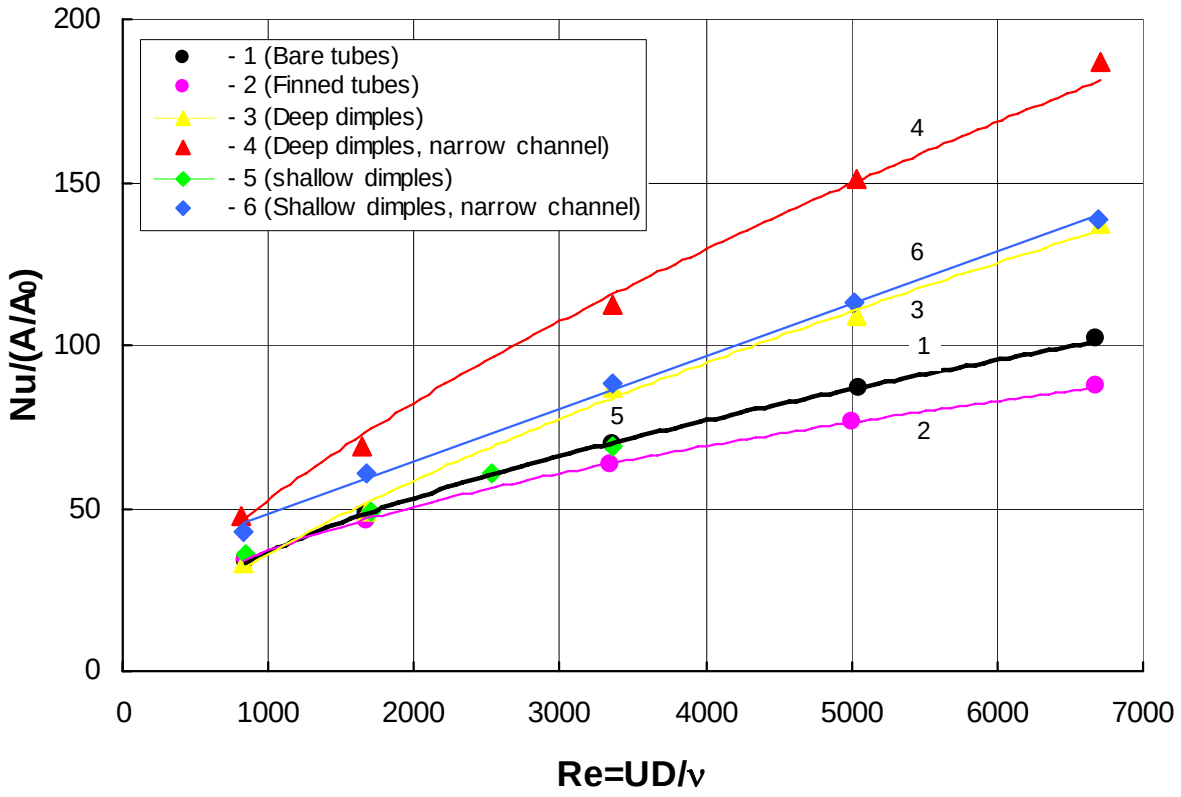

Figure 12. Heat Transfer Versus Air Velocity for Bench-Scale Tests

Pressure Drop

In Figure 13 the criterion **Eu** is presented versus criterion **Re** that represents the mean air velocity $\mathbf{U_m}$ between the tubes. Here, **ΔP** is a pressure drop across the test section and **ρ** is a density of the hot air flow. As the **Re** value ranges from 15,000-25,000 a corresponding reduction in pressure (three fold) is encountered with the dimpled surface. Mean air velocity in the minimum inter-tube space was determined based on the recommendations[5] commonly accepted in engineering practice.

[5] Heat Exchangers Design Handbook, G.Hewitt ed., Begell House Inc., 2002

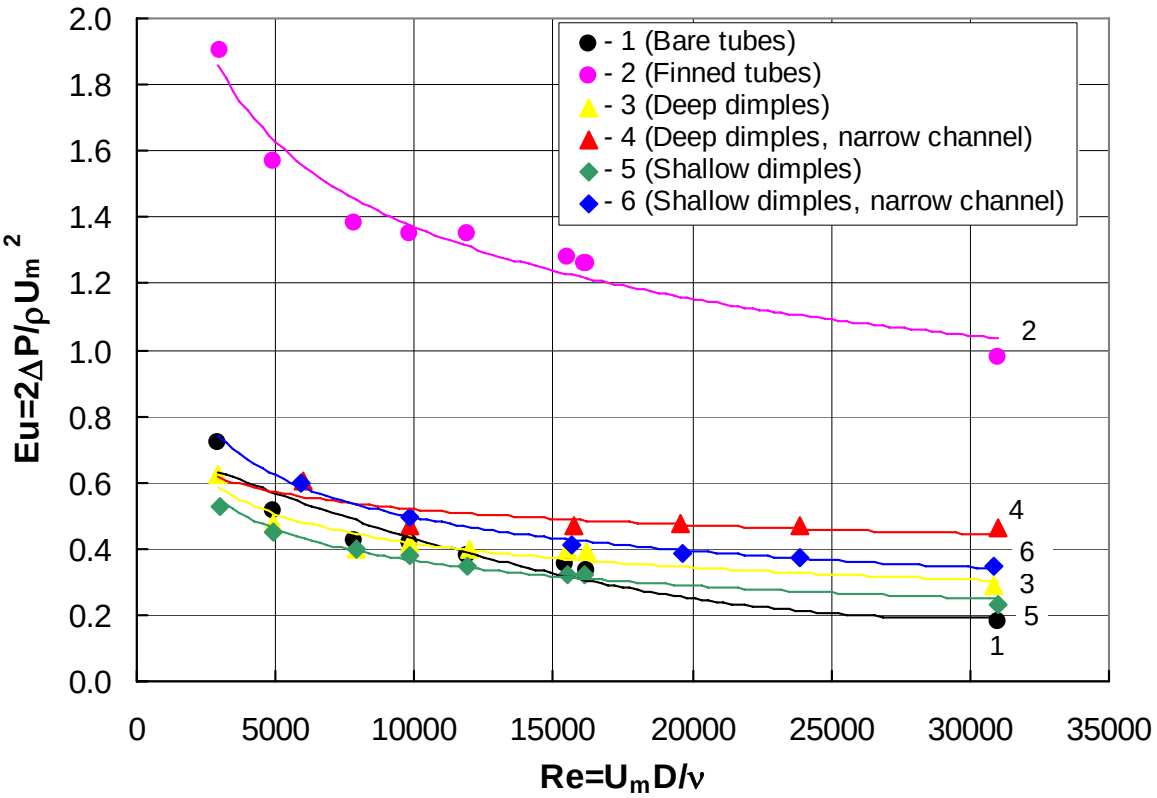

Figure 13. Pressure Drop Versus Air Velocity for Bench-Scale Tests

Figure 13 demonstrates the obvious advantage of the dimpled tubes (for all studied dimple depths and profile densities) over the finned surface.

Additional details on data processing and uncertainty analysis can be found in Appendices III and IV.

Bench-Scale Evaluation Summary

Based on bench-scale evaluation, a preliminary comparison of the VHTE and typical finned tubes was conducted to establish benchmark trends for further field trial and potential industrial benefits. Table 1 represents a preliminary comparison of dimple technology to typical finned-tube convection sections of chemical industry fired process heaters. Heat transfer coefficient, heat transfer area, total heat rate and total tube cost were compared.

For comparison purposes, the data in Table 1 are normalized with respect to smooth tubes. The subscript o represents the parameter for smooth tubes. Data entries labeled “Typical” are for finned tubes with 2D tube spacing.

Table 1. Convection Section Comparison, Typical (Finned) Tubes Vs Dimpled Tubes

a – Equal Tube Quantities (2D Spacing)

	Qty	h/ho	A/Ao	Q/Qo	$/$o
Typical	88	0.7	4.7	1.9	2.0
VHTE	88	0.9	1.4	1.2	1.0
Comparison		30% higher	70% lower	30% lower	50% lower

b – Equal Total Heat (2D Spacing)

	Qty	h/ho	A/Ao	Q/Qo	$/$o
Typical	88	0.7	4.7	1.9	2.0
VHTE	198	1.0	3.1	1.9	2.0
Comparison	125% higher	40% higher	30% lower		none

c – Equal Total Heat (1.1D Spacing)

	Qty	h/ho	A/Ao	Q/Qo	$/$o
Typical	88	0.7	4.7	1.9	2.0
VHTE	96	1.9	1.5	1.9	1.0
Comparison	9% higher	170% higher	70% lower		50% lower

d – Equal Capital Investment (1.1D Spacing)

	Qty	h/ho	A/Ao	Q/Qo	$/$o
Typical	88	0.7	4.7	1.9	2.0
VHTE	192	2.0	3.0	2.3	2.0
Comparison	120% higher	190% higher	40% lower	20% higher	

The preliminary analysis demonstrates the potential for significant savings in energy (fuel), capital costs and increase in throughput by manufacturing or retrofitting the convection section for fired process heater with dimpled tubes as opposed to finned and shock tubes.

Based on the experimental data obtained in the course of bench-scale evaluation the following benefits were estimated for the industrial application, based on a natural gas price of $6-7/MMBtu and a domestic population of 700 high-temperature fired heaters:

- Energy savings per each 1% of fuel use decrease = $350-450K per heater annually.
- Reduced expenses per each 1% retrofit of installed base = $50-100K annually.
- Gain per each 1% increase in throughput = 10,000 tons of product per heater (assuming $500/ton of ethylene this corresponds to $5M per year).
- Lower operating costs due to reduced maintenance, cleaning, easy replacement, etc.

Pilot-Scale Field Trial Preparation

Approach Development

A slip-stream approach was selected for the upcoming field trial as the most likely approach to minimize intrusion into the operating unit and risk of loss product. Two slip-streams, one with finned tubes and one with dimpled tubes bypass the existing economizer, as shown in Figure 14.

The slipstream ductwork is connected to the existing unit through shut-off guillotines to eliminate, in case of emergency, any negative effect on actual production. The test sections will be operated at similar flue gas and product flow conditions for heat transfer and pressure drop measurements, followed by long-term monitoring of fouling performance.

Dimpled Tube Development

To meet ASME code, the standard tube SA178A was selected for the field trial unit. The dimpled profile developed in the course of bench-scale evaluation (see Figure 15) was formed on the test tubes surface by an automatically operated tool that was specially designed for this purpose in collaboration with Energetic System Consulting (St-Petersburg, Russia). Figure 16 demonstrates the major elements of the "dimpling machine."

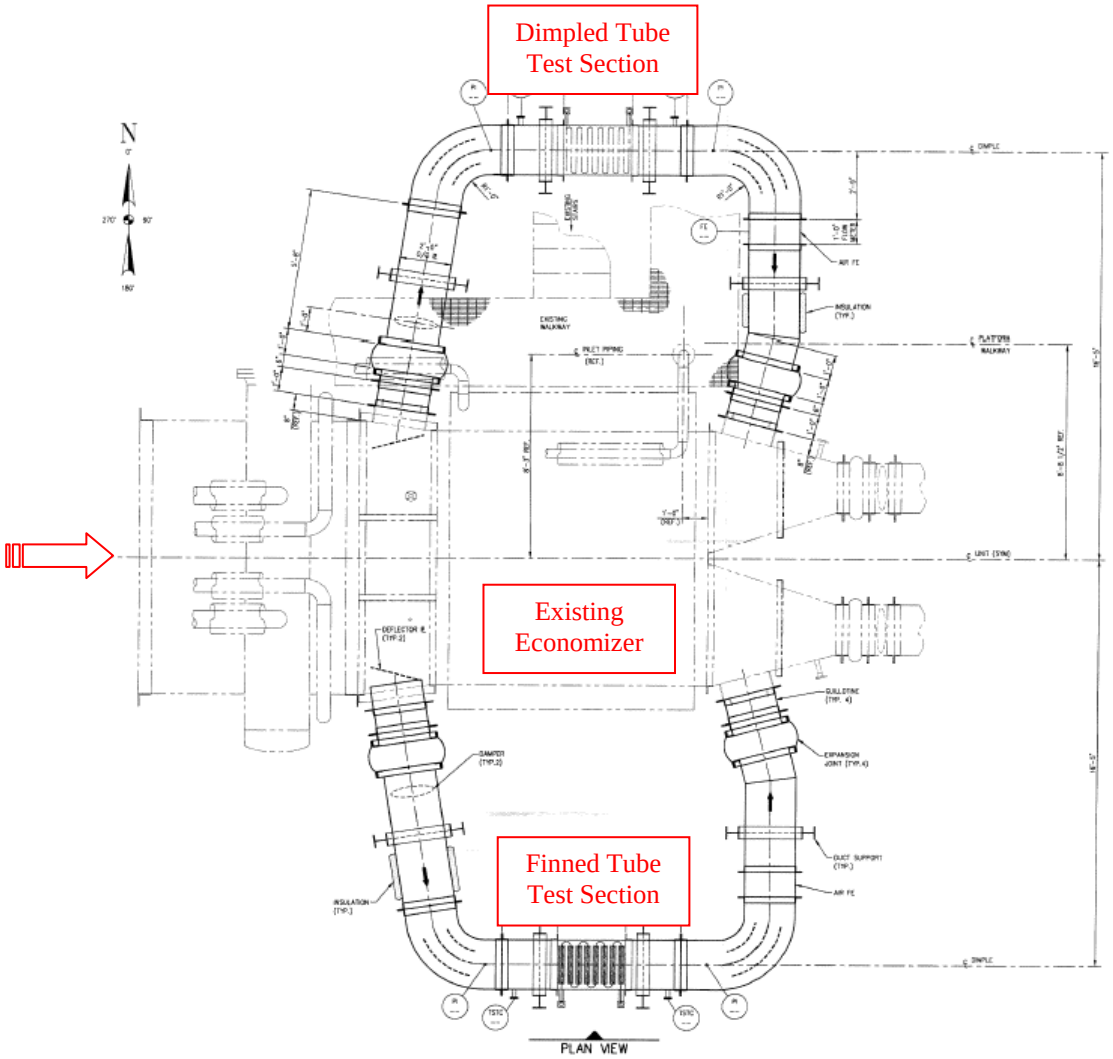

Figure 14. Slip-Stream Layout for Field Trial

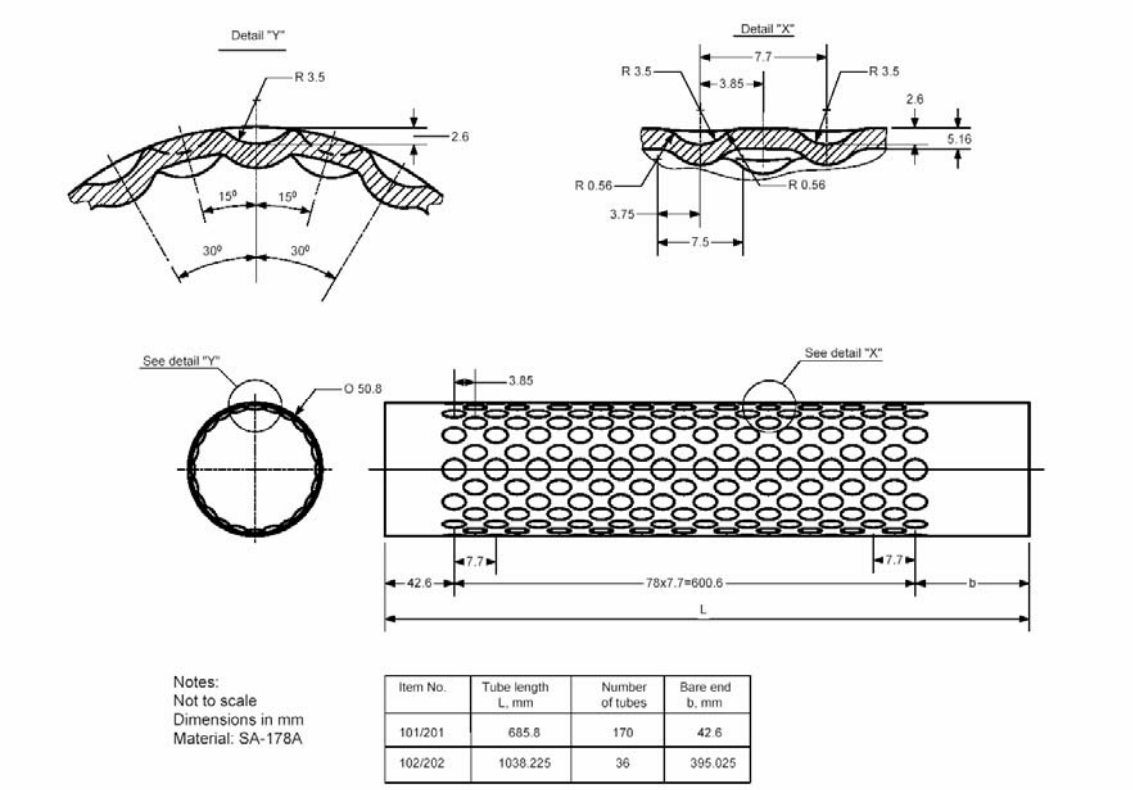

Item No.	Tube length L, mm	Number of tubes	Bare end b, mm
101/201	685.8	170	42.6
102/202	1038.225	36	395.025

Figure 15. Dimpled Tube Surface Profile Geometry

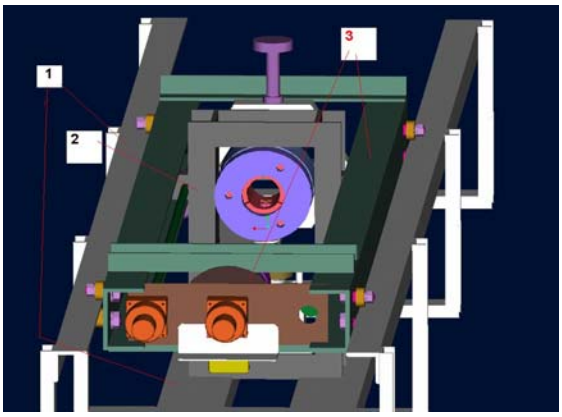

Dimpling Machine General Layout:
1 – Frame, 2 – Support, 3 – Pressing Head

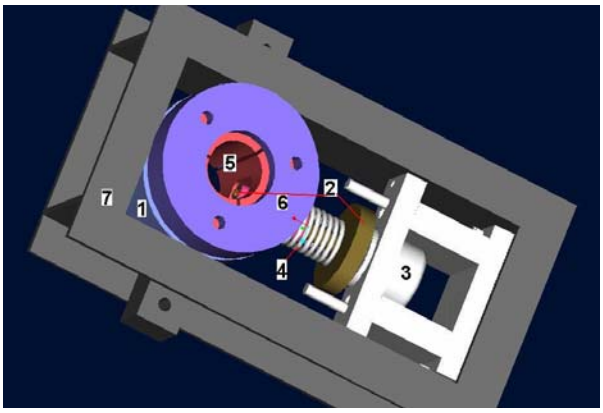

Dimple-Pressing Head Design:
1– Stationary Body, 2 – Punch, 3 – Hydraulic Cylinder, 4 – Return Spring, 5 – Collet, 6 – Clamping Nut, 7 – Press Support

Figure 16. Components of the Dimpling Machine

The strength of randomly selected tubes was evaluated by means of stressed-deformed state analysis and destructive testing. The destructive testing results demonstrated a secure safety factor. The burst pressure significantly exceeded the operating pressure of the existing economizer. (See the "burst" testing protocols, Appendix VI, attached).

For the stressed-deformed state analysis, the dimpling geometry was copied directly from the fabricated samples shown in Figure 17.

a  b 

Figure 17. Dimpled-Tube Samples Used as a Basis for Deformed-State Analysis: a – cuts for profile measurement, b – profiles (wall thickness of 0.2", 0.15" and 0.1")

Two values of internal pressure (7,500 psi and 1,400 psi) were considered for all calculations. The first pressure value of 7,500 psi was selected from the destructive test results. The second pressure value, 1,400 psi, is twice the 700-psi working pressure of the tubes. Figure 18 shows part of a finite element stress-deformed state analysis.

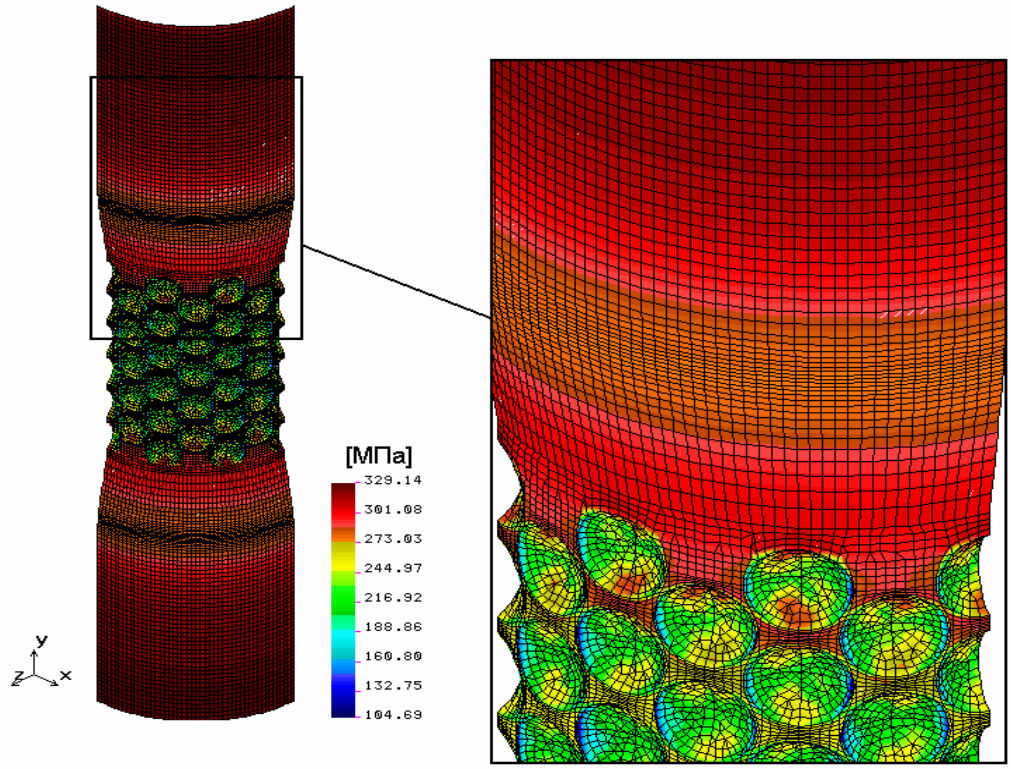

Figure 18. Finite Element Stressed-Deformed State Analysis of a Dimpled-Tube Sample

In Figure 18, the yield strength of SA-178A is in the range of 180-255 MPa (green/yellow). Figure 18 clearly indicates that the obtained maximum stresses (red areas) exceed the yield point, which means that the material is in its plastic range. Based on the analysis performed, it is expected that all the stresses will be related to the elasticity range, so all the calculated results may be considered as real characteristics of the tube in a stress-deformed state. More details on stressed-deformed analysis of the dimpled tube is given in Appendix V.

Pilot-Scale Field Trial System

The field-trial system (FTS) included two flow ducts bypassing the existing economizer on both sides, as shown in Figure 14. Figure 19a illustrates a finned-tube branch of the FTS and Figure 19b illustrates the overall view of the entire pilot-scale facility. Each duct was equipped with adjustable deflector, control damper and turning vanes to set and maintain the equal flow rates in both test sections.

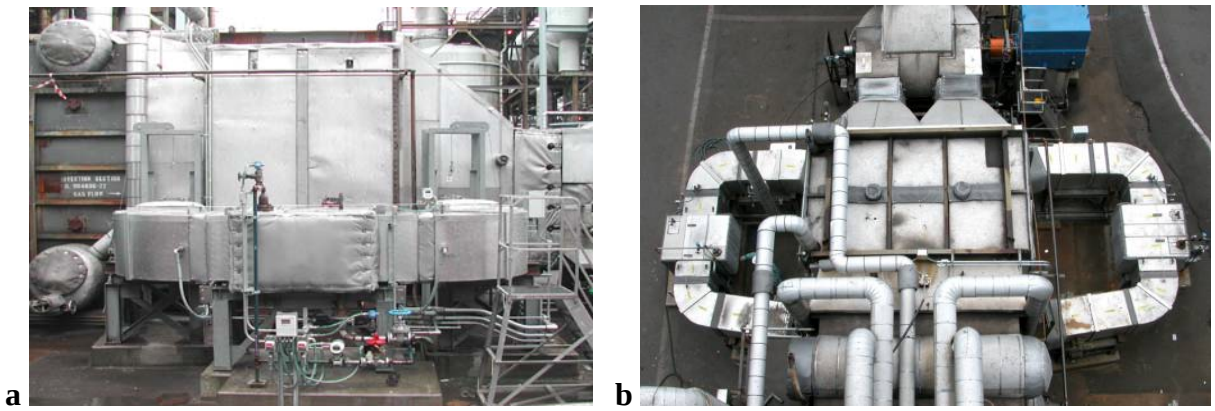

a **b**

Figure 19. Overall Views of the Pilot-Scale Test Facility:
a- Finned Tubes Branch, b - Overall View

Three test sections were fabricated for the field trial - finned tube (industry standard with 2D spacing between the tubes), dimpled tube (in-line arrangement to provide the same heat transfer as finned tubes test section) and dimpled tube (staggered arrangement to provide the same pressure drop as finned test section). Figure 20 shows finned and dimpled tube banks prior to the trial.

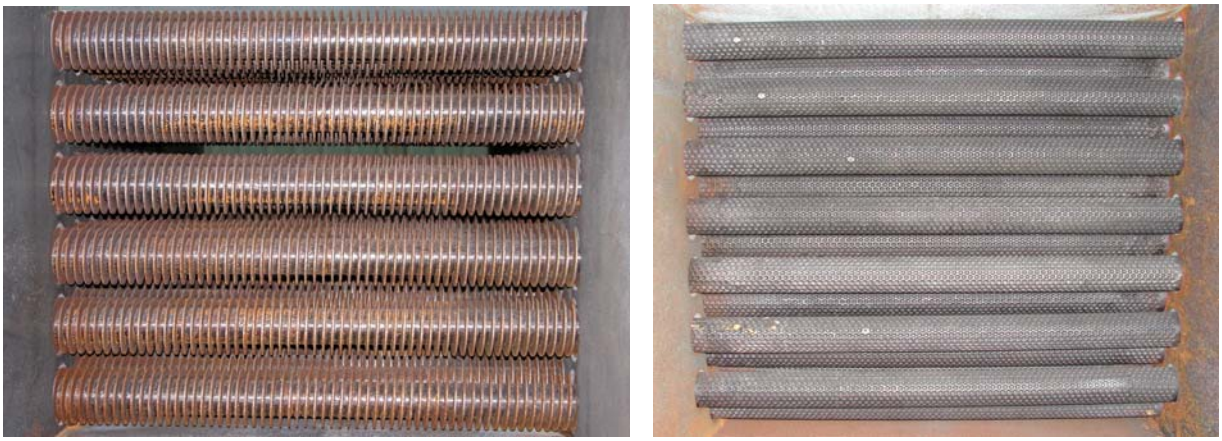

a b

Figure 20. Test Sections: a – finned (in-line), b – dimpled (staggered)

Mass flow meters were installed at the flow outlets, while temperature sensors were installed at the flow inlet and outlet. Pressure drop across the test section was measured by differential pressure gauge. Some measurement equipment was installed at the existing economizer to monitor the baseline unit operation. The measurement test point locations are shown in Figure 21.

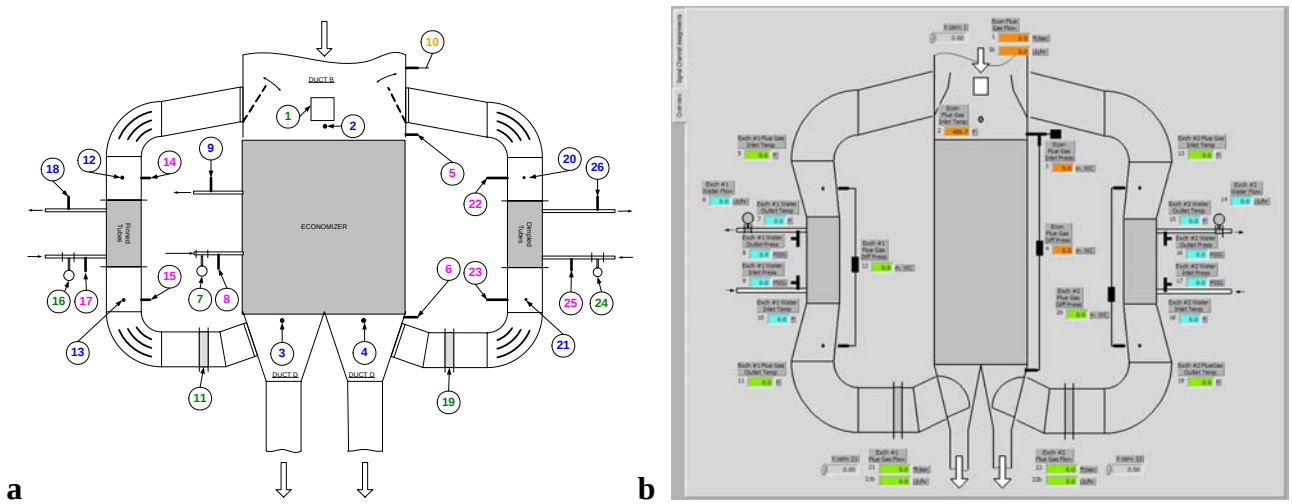

a b

Figure 21. Measurement System Layout (a) and Control Screen (b):

1, 7, 11, 19, 16, 24 (flow sensors), 10 (gas analyzer),
2-4, 9, 12-13, 18, 20-21, 26 (thermocouples), 5-6, 8, 14, 15, 17, 22-23, 25 (pressure gauges),

The comparative data collection was carried out at the following experimental conditions:

- Flue gas flow rate for each test section: 2800-3200 CFH
- Flue gas inlet temperature: 480-540°F
- Flue gas outlet temperature: 260-280°F
- Water mass flow rate for each test section: 10-15 GPM
- Water inlet temperature at the test section: 60-65°F
- Water outlet temperature at the test section: 95-125°F

All the e-signals from the field sensors were collected by sophisticated data acquisition system developed using National Instruments FieldPoint hardware/software. Data acquisition system was integrated with the FTU measurement system that was located in the MobileMini trailer set aside of the FTU as shown in Figure 22.

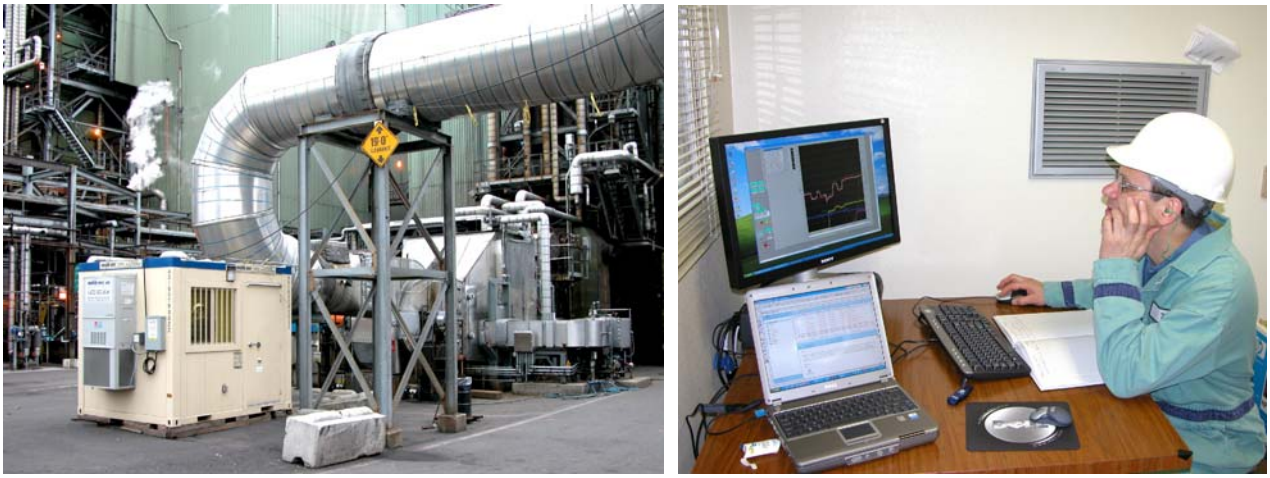

a b

Figure 22. Trailer Position on the Field Site (a) and Trailer's Interior View (b)

Field Point software permitted assigning the different measurement parameters to multiple acquisition channels and performance of simultaneous reading, displaying and recording of the measured values. Figure 23 illustrates the channel setup screen while Figure 24 illustrates the signal displaying screens.

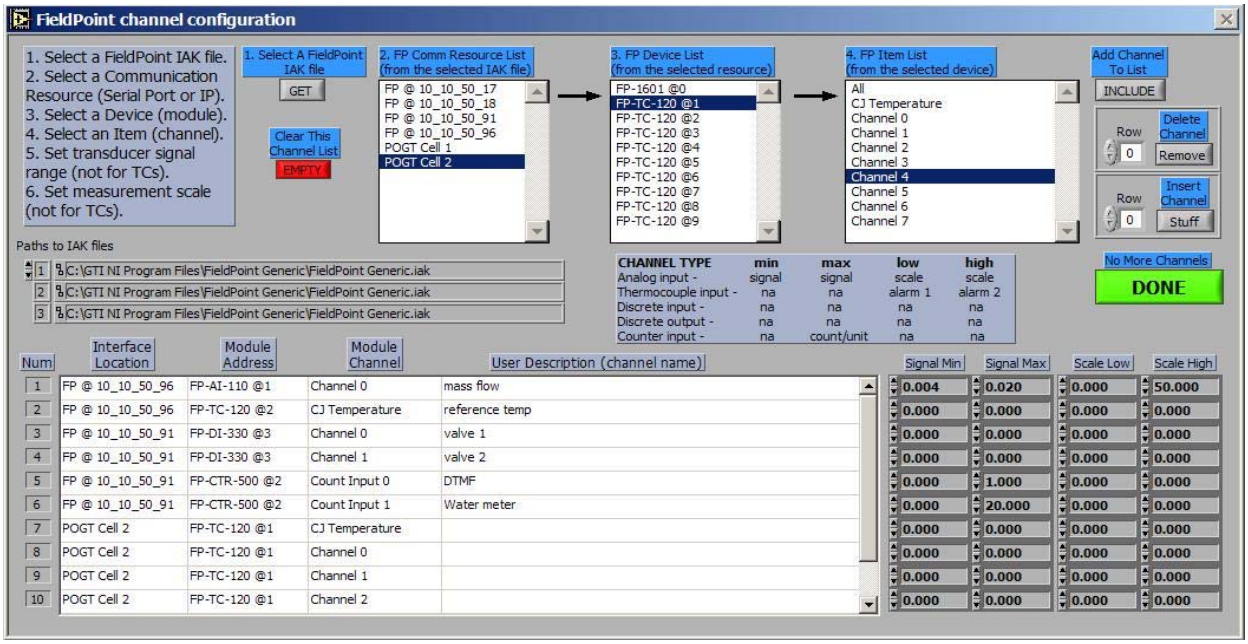

Figure 23. Data Acquisition Setup Channels Screen

a 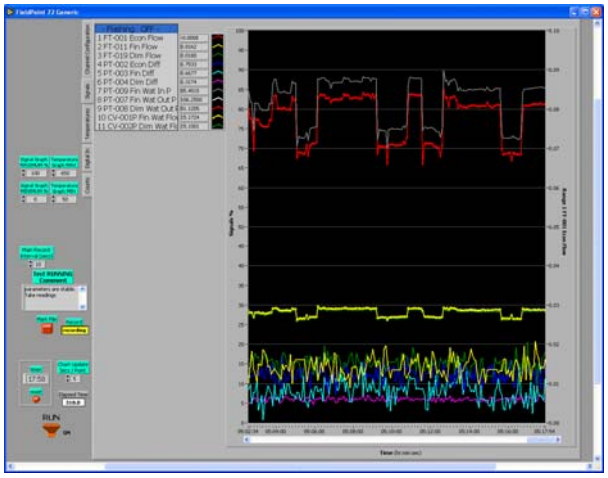 b 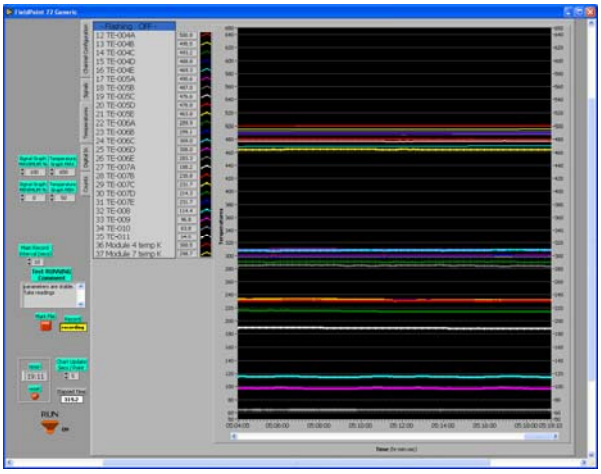

Figure 24. Data Collection Screens: a - flow and pressure signals; b - temperature signals

Operating parameters of the FTS were measured and auto-recorded in conventional MS Excel spreadsheet format (.XLS) and further processed and analyzed per standard engineering procedure.

In the course of data processing it was discovered unintended heat transfer that was possibly caused by air flow infiltration into the test sections due to insufficient sealing and negative operating pressure inside the economizer (between -5.7"WC and -6.2"WC per control room data) as shown in Figure 25a. Based on enthalpy balance we performed the detailed analysis of possible air infiltration, estimated the impact on heat transfer calculations and corrected the measured data (see Figure 25b).

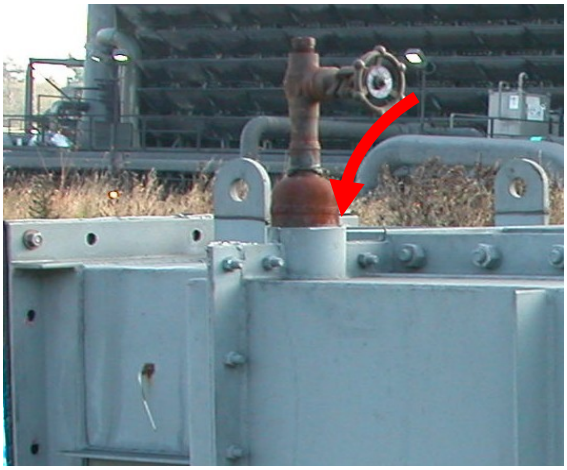

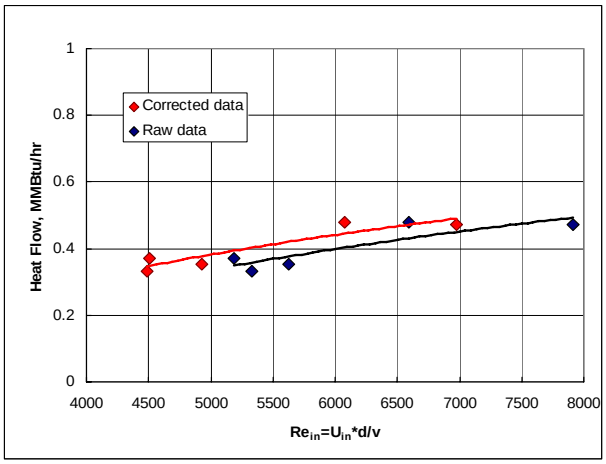

a **b**

Figure 25. Air Infiltration into the Test Section (a) and Data Correction (b)

Below is the example of the air infiltration estimate based on the measured data for finned tube test section for regime #1 data collected on March 17, 2005.

The following parameters were measured:

- total outlet mass flow rate including air infiltration $\mathbf{m_{out}}$ = 11226 lb/hr
- flue gas inlet temperature $\mathbf{T_{in}}$ = 495.4ºF
- gas outlet temperature $\mathbf{T_{out}}$ = 282.2ºF
- water flow rate $\mathbf{m_w}$= 6922 lb/hr
- water inlet temperature $\mathbf{(T_w)_{in}}$=49ºF
- water outlet temperature $\mathbf{(T_w)_{out}}$=107.1ºF
- ambient air temperature $\mathbf{T_{air}}$=65ºF

Flue gas heat flow $\mathbf{Q_{FG}}$ calculated as (without taking into account air infiltration):

$$\mathbf{Q_{FG}=m_{out}(Cp_{in}T_{in} - Cp_{out}T_{out})} = 645{,}805 \text{ Btu/hr.}$$

Water heat flow $\mathbf{Q_w}$ was calculated as

$$\mathbf{Q_w=m_wCp_w[(T_w)_{out} - (T_w)_{in}]} = 401{,}963 \text{ Btu/hr.}$$

Heat flow difference between flue gas and water heat flows would be

$$\mathbf{(Q_{FG}-Q_w)/Q_{FG}}*100\%=(645{,}805-401{,}963)/645{,}805*100 \approx \mathbf{38\%},$$

that is obviously too high for heat losses.

Estimated heat losses through the walls should not exceed $\mathbf{Q_{loss}}$=7322 Btu/hr, which is about 2% of water heat flow $\mathbf{Q_w}$. The heat losses were estimated based on reference data for combined (natural and force) convection.

The number of 38% for the heat flow difference can be explained by measuring error or by air infiltration only. In order to eliminate the measuring error we checked all measuring equipment, replaced thermocouples and duplicated measurements using different measuring devices.

Assuming some air infiltration to the test section due to insufficient sealing and negative operating pressure inside the economizer (between -5.7"WC and -6.2"WC per economizer control room data) we calculated infiltrated air and corrected the measured data as described below.

Figure 26 illustrates the heat sources and sinks at the test section including heating of water and air infiltration.

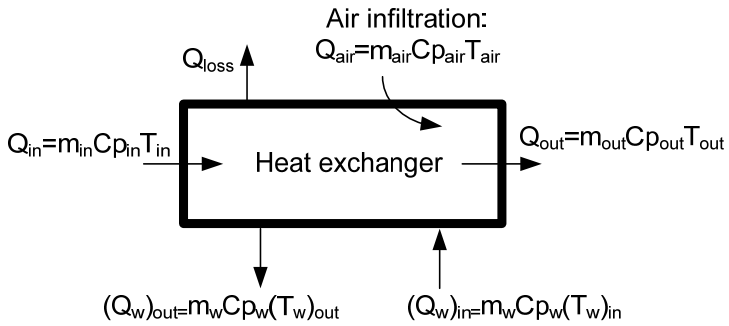

Figure 26. Enthalpy balance of the test section

$\mathbf{m_{in}}$, $\mathbf{m_{out}}$, $\mathbf{m_{air}}$, $\mathbf{m_{air}}$, and $\mathbf{m_w}$ are gas inlet and outlet mass flow rates, air mass flow rates, and water mass flow rate; $\mathbf{Q_{loss}}$ is heat loss. Value $\mathbf{m_{out}}$ was measured by a flow meter. Temperatures $\mathbf{T_{in}}$, $\mathbf{T_{out}}$, $\mathbf{T_{air}}$, $(\mathbf{T_w})_{in}$, and $(\mathbf{T_w})_{out}$ were measured by thermocouples. Specific heat values $\mathbf{Cp_{in}}$, $\mathbf{Cp_{out}}$, $\mathbf{Cp_{air}}$, and $\mathbf{Cp_{water}}$ are estimated based on the measured temperatures. Flue gas inlet flow rate can be found as $\mathbf{m_{in}=m_{out}-m_{air}}$ if air flow rate is known. Based on the inlet mass flow rate, then we can estimate flue gas inlet velocity and Reynolds number.

Outlet flow enthalpy $\mathbf{Q_{out}=m_{out}Cp_{out}T_{out}}$ is a sum of the flue gas and air enthalpies:

$$\mathbf{m_{out}Cp_{out}T_{out}=m_{in}Cp_{FG\ out}(T_{FG})_{out}+m_{air}Cp_{air}T_{air}} \quad (1)$$

Here $\mathbf{(T_{FG})_{out}}$ is outlet temperature of flue gas which is mixed with air. This temperature is higher than flue gas/air mixture outlet temperature $\mathbf{T_{out}}$.

Change in flue gas enthalpy can be estimated as

$$\mathbf{Q_{FG}=m_{in}(Cp_{in}T_{in}-Cp_{FG\ out}T_{FG\ out})} \quad (2)$$

Moreover, at the same time $\mathbf{Q_{FG}=Q_w+Q_{losses}}$.

Joint resolution of equations (1) and (2) allowed us to find two unknowns, namely, flue gas outlet temperature $\mathbf{T_{FG\ out}}$=344ºF and air infiltration rate $\mathbf{m_{air}}$=1194 lb/hr. The air infiltration rate value was about **10.6%** of the outlet gas mass flow rate $\mathbf{m_{out}}$=11226 lb/hr. See Table 2 below for other values.

In order to check this result for air infiltration, we calculated a flue gas heat flow and compared it with water heat flow. Flue gas flow rate was equal to $\mathbf{m_{in}=m_{out}-m_{air}}$=11226-1194=10032 lb/hr and the flue gas heat flow $\mathbf{Q_{FG}}$ based on the equation (2) was equal to 409,365 Btu/hr, which is about 2% higher than water heat flow $\mathbf{Q_w}$=401,963 Btu/hr.

Table 2. Air Infiltration % per each data collection run

Test Date	3/17/05	3/17/05	3/17/05	3/17/05	6/21/05	6/21/05	6/22/05	6/22/05	6/23/05	6/23/05
Air, %	**10.6**	**15.8**	**10.8**	**15.2**	**6.9**	**1.2**	**5.0**	**3.0**	**6.7**	**1.4**
Test Date	8/16/05	8/16/05	8/17/05	8/17/05	8/17/05	8/17/05	9/13/05	9/13/05	9/13/05	9/13/05
Air, %	**0.3**	**12.4**	**1.4**	**11.9**	**1.8**	**15.8**	**6.9**	**8.0**	**6.6**	**13.1**

Major Accomplishments and Results

The following major accomplishments were made in the course of the project performance:

CFD model to predict heat transfer and flow dynamics in the dimpled tube bank was developed and validated with experimental data. The results of numerical modeling employing commercial software (FLUENT) demonstrated high potential of the heat transfer enhancement with no significant pressure penalties.

The bench-scale evaluation of the three heat transfer surfaces was performed at GTI's Applied Combustion Research Laboratory. A VHTE profile was evaluated to significantly increase the heat transfer coefficient by about 30-40%.

Slip-streaming of the existing economizer was selected as the preferred approach for pilot-scale field trial. All the partners and host site approved the approach.

The field-trial unit (FTU) was designed, engineered, and fabricated, with strong support of the project partners and field trial host. Three test sections were developed for the field trial: finned (typically used in industry), dimpled (with in-line tube arrangement), and dimpled (with staggered tube arrangement).

The field-trial system (the FTU, plus the measurement and data acquisition equipment) was installed at the host site for data collection and long-term monitoring. Installation followed by instruments calibration, startup/shakedown and data collection.

Collected data was further processed, analyzed and presented to project partners in the form of Field Trial Results Review meeting. Upon field trial completion FTU was set for the post-trial performance monitoring to evaluate the dynamics of the test sections performance and validate the measurements repeatability.

Figure 27 illustrates the superior heat transfer performance at reduced pressure drop for the tested dimpled tube bank over the conventional finned tube bank. The accuracy of the heat flow and pressure drop measurements was calculated with 95% confidence level. The maximum uncertainty for the heat flow measurement was identified as 14% at lowest water flow regime. The maximum uncertainty for the pressure drop across the test section was identified as 6% at the lowest flue gas flow.

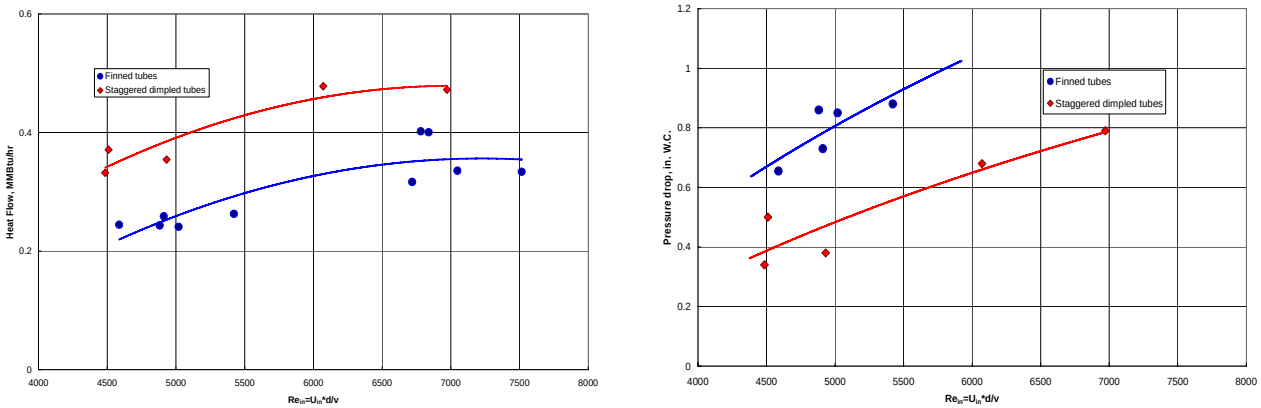

Figure 27. Major Field Trial Results: a – heat flow, b – pressure drop

Post-Trial Performance Monitoring

Upon completion of the data collection the FTU was set for the long-term post-trial fouling performance monitoring to compare the dynamics of test section performance over the approximately 6 months period. Data monitoring results for both sections are given in Figure 28.

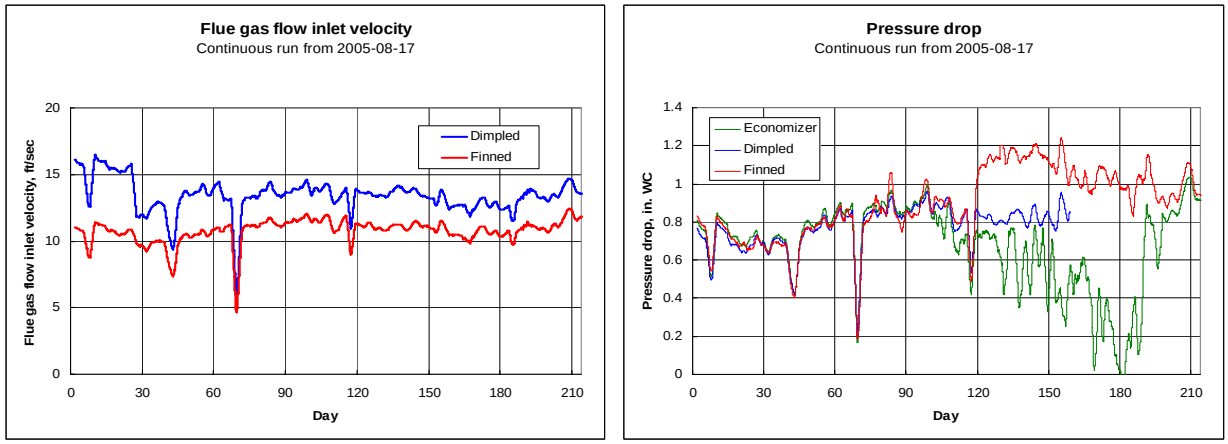

Figure 28. Post-Trial Monitoring Data
(economizer's pressure sensor was out after 120 days of operation)

Visual inspection of the test sections after FTU demolition clearly demonstrated the superior performance of the dimpled tube sections over the traditional finned tube bank. The test sections views before the trial and after performance monitoring are shown in Figure 29. Obviously the dimpled test sections were much less fouled than the finned one. That effect could be roughly explained by additional intensive turbulization of the flow due to dimpled-generated vorticity near the tube surface as well as staggered arrangement of the tubes that provide additional flow disturbance between the tubes which further reduces deposition rate on the tube surface.

a b c

Figure 29. Visual State of the Test Sections Internals After the Trial:
a -finned, b - dimpled (in-line arrangement), c - dimpled (staggered arrangement)

Conclusions and Recommendations

Presented R&D work clearly demonstrated the strong potential of the VHTE approach for significant energy savings (fuel savings), capital costs and increase in throughput by manufacturing or retrofitting the convective section for fired process heater with dimpled surfaces as opposed to finned and studded tubes.

The pilot-scale field trial results indicated up to 40-60% increase in heat flow for the dimpled tubes in staggered arrangement while decreasing in pressure drop about 50-60% over the industry accepted finned tubes (see Figure 27 above). Post-trial fouling performance run has proven cost-effective potential for reducing fouling rates in convection passages of industrial fired heaters (see Figure 29 above).

The project findings provided the basis for the pre-commercial design of the VHTE-enhanced convective unit for the full-scale demonstration in real production environment. Below are major design considerations for the pre-commercial unit:

- "deep" dimple surface profile (H/D > 0.3) to be developed with maximum dimple density on the tubular surface permitted by fabrication technology;
- spacing between the tubes should be calculated assuming maximum permitted pressure drop for the selected equipment;
- foulant collection tray must be incorporated into design for periodical removal of the fouling material out of the convective unit while in operation.

Preliminary estimation of the full-scale unit performance employing the conventional arrangement of the industry-accepted finned tubes versus best dimpled performer (deep dimples on the tubular surfaces in staggered arrangement) and bare tube bank is shown in Table 3.

Table 3. Comparison of the Full-Scale Economizer with Funned, Dimpled and Bare Tubes

Parameter	Finned tubes	Dimpled tubes	Bare tubes
Tube transversal spasing, in	4.0	3.20	3.20
Tube longitudinal spacing, in	4.0	2.46	2.46
Number of tube rows longitudinal to flow	18	29	29
Number of tube rows transversal to flow	34	42	42
Total number of tubes	612	1218	1218
Bare tube surface area, ft2	3363	6694	6694
Tube total surface area A_t, ft2	17711	9311	6694
Average velocity between tubes, ft/sec	41.9	34.4	34.4
Heat absorbed, MM Btu/hr	8.4	8.2	7.0
Pressure drop, in W.C.	1.1	1.3	1.9
Tube outside surface heat transfer coefficient ***h***, Btu/(ft2*hr*F)	7.7	19.4	14.9
Flue gas outlet temperature **Tfgo**, F	386	389	405
A_t***h**, Btu/(hr*F)	135582	180323	99720

The rough data clearly indicates that a tested arrangement of the dimpled tubes is 33% more efficient rather than typical (2D spacing) finned tubes arrangement and 181% over bare tube bank with the same as dimpled tubes layout. Adding more benefits such as lower fouling rate (extended duty cycle) and lower tube cost as well as easier replacement and maintenance, this technology would attract not only the refineries but other petrochemical plants employing convective heat transfer units.

GTI has a strong expertise to adjust the surface profile and tubular arrangement for the particular application using the CFD models and engineering empirical estimations.

The proposal for the follow-on effort (Full-Scale Field Trial of the Convective Heat Transfer Unit) was submitted by GTI and Partners to U.S. Department of Energy in response to "Innovative Energy Systems Challenge" announcement in early 2006.

Future Development Plans and Commercialization Path

During the project performance GTI team closely worked with industrial partners to develop a basis for the future technology commercialization. Optional license agreement was prepared and sent to KTI Corporation for manufacturing partner's review. Joint interim review meetings were arranged at the both partners' locations - ExxonMobil Research Engineering (Fairfax, VA) and BP Cherry Point Refinery (Blaine, WA). All the industrial partners - KTI, EMRE and BP - are strongly interested in further technology development and successful commercialization across Petrochemical Industry.

Market Characterization

The Chemical Industry consumes about 33% of all energy used in the U.S. for manufacturing. By developing and adopting more energy efficiency technologies, U.S. industry can boost its productivity and competitiveness while strengthening national energy security, improving the environment, and reducing emissions linked to global climate change. Most processes used by the chemical industry occur at elevated temperatures and pressures. Temperature is typically added to different hydrocarbon streams through the use of fired process heaters. There are an estimated 1,400 process heaters currently serving the chemical industry, approximately 700 of which are high temperature process heaters. The total energy consumption in these heaters, according to a study prepared for the U.S. EPA[6], was 0.34 quads or 0.34×10^{15} Btu's per year. Natural Gas consumption makes up 0.28 quads, or 48%, of the total energy used.

Market Being Addressed - In addition to the 700 high temperature process heaters identified above, the U.S. has 154 refineries which vary in capacity from a few thousand Bbl/day to as much as 500,000 Bbl/day capacity[7]. For the larger refineries (greater than 100,000 Bbl/day) typical fired process heaters would include crudes, vacuums, reboilers, hydrotreaters, CCR's, hydrogen reformers (or third party suppliers with a reformer), and cokers (depending on how complex the facility is). In addition to these process heaters, most large facilities will also have boilers for steam generation equipment. All of these fired heaters would employ both radiant heat transfer and/or heat transfer through convection, and all are potential candidates for implementation of the dimpled tube technology.

Why is the VHTE Technology an Improvement over Current Practices - Energy is a major factor in the technology equation for the Chemical Industry. Increasingly stringent environmental regulations associated with the combustion of fuels, and the growing volatility of energy markets, is moving energy efficiency to the forefront. In addition, the use of petroleum as a feedstock for commodity chemicals increases our dependence on imported oil and impacts US energy security. The VHTE technology employs dimpled surface that greatly increases the heat transfer without the "fins" or other protuberances that increase system pressure drop and enhance the possibility of the surface fouling when hydrocarbon fuels are burned. In so doing, the VHTE technology has the ability to decrease energy consumption by approximately 5%. The combined potential benefit from employing dimpled tube technology is the sum of the energy savings and NO_x credits, and is estimated to be ≈ $44 million per year if the technology is applied to all of the 700 existing high temperature process heaters. These benefits do not include cost reductions associated with reduced down time resulting from reduced fouling of the tubes. Based on energy savings alone, the payback to the chemical company is anticipated to be between one to three years.

Size of the Domestic Market - Given all of the above facts, the annual domestic market for chemical industry new installations and retrofits is estimated to be $50 million. This is obviously an average and can vary from year to year. Other issues beyond general maintenance and repair that all units experience can also affect the market, including governmental regulations mandating low sulfur gasoline and diesel, which would compel refiners to modify their processes, which may include an additional furnace and temporarily inflate the market.

---

[6] Radian Corporation for the U.S. EPA (EPA-453/R-93-034)

[7] Worldwide Refining and Gas Processing Directory 2000, 56th edition, Penn Well Corporation

Competition - There are a variety of heat transfer enhancement techniques used in state-of-the-art heat exchangers, including fins (circular, spiral, longitudinal, serrated, etc.), artificial roughness elements, and turbulizing inserts (projections in the heat exchanger that increase the turbulence of the air flow). However, all of these technologies increase the pressure drop in the heater, increasing back pressure as well as creating "dead zones" that enhance fouling, requiring down time to remove soot from the heat exchanger units. The dimpled tube technology does not possess these negative characteristics. Instead, interactions between the vortices created by the "dimples" fosters a high-intensity, extremely stable pattern that significantly enhances all near-wall hydrodynamics and thermal transfer processes.

Based on previous research, it is estimated that the improved heat flux of dimpled tubes, combined with the lower potential of fouling, will increase the convection section thermal effectiveness by 25%, which in turn will increase the heat absorbed from 20% to 25%. The total fried process heater thermal efficiency then will become 90-95% rather than the current 80-85%.

Based on the above, the industry-wide energy benefit due to the energy efficiency improvement from all 700 (100% market penetration) units having dimpled tubes is:

(700 units) (56.1MMBtu/H/unit) (8600H/yr) (0.85-0.80) = **≈ 16.9 Trillion Btu per year saved**.

At a natural gas fuel cost of $6.50 per MMBtu, the energy savings is **≈ $ 110 Million per year**

Market Pull - The domestic market is a mature market from a standpoint of new plants. For the foreseeable future, the existing refiners and chemical processors will be concerned about upgrading their facilities in lieu of building new ones. Based on this point, a key aspect of implementing the VHTE technology domestically will be to maintain or improve the heat transfer of existing systems with limited modifications to the existing furnaces. The buyer would be looking for the process pressure drop to remain constant at the same capacity while transferring the same amount or more heat in the same amount of physical space in the furnace itself with little or no additional weight and at a competitive price. This limits the initial potential market, the chemical industry to retrofits of the existing units on a 5 to 10 year replacement cycle that is common to the industry, and with the assumption that the industry can be given sufficient justification to replace existing finned or other heat enhancement tube technology with the dimpled tube technology.

Potential Market Growth - For the Chemical Industry, we have used the 5.3% growth rate in Ethylene[8]-capacity in the last decade worldwide as a starting point. However, since there is a worldwide over capacity in ethylene capacity[9], our commercialization plan has assumed a growth rate of only0.5 to 1.5% over a 20-year horizon, with a capturable market (conservative estimate) of 40-60% of potential market. When introducing this product, it is our intent to begin in the domestic market. Given that GTI, ExxonMobil and BP are either all based in the United States or have a large presence here; focusing on the domestic market is our first and foremost target.

Market Penetration Process and Product Cycle

Market Penetration Process - Market penetration usually begins slowly and gradually builds, particularly in the conservative chemical and refining markets. Without the assistance of our industrial partners Exxon Mobil and BP, the first two years of the commercial development could see no sales with two or three applications in the third year and more after that. The key to implementation of this technology is for ExxonMobil and BP to install full-scale units, thus lending credibility to the product technical credence. ExxonMobil and BP are strong end users in the industry and would affect the market opinion of a product. The general impression would be if it is accepted in ExxonMobil and BP then it can be accepted anywhere.

Estimated Revenue Stream for Dimpled Tubes - Of the retrofitted furnaces, approximately 70% would include either new convection sections or require modifications to their existing convection sections.

---

8 "Ethylene-capacity growth slowed in 1998," pp. 50-61, March 29, 1999, Oil & Gas Journal.

9 Ibid.

Convections represent 10 to 50% of the cost depending on a combination of tube material, thickness, and material type. This makes the over all cost of the convection section between $3.5 MM to $17.5 MM per facility, with the tubes representing 30% of that amount. The total annual tube market is thus $1.05 to $5.25 million. If we further assume a range of market penetration of 0% to 90%, the final range of sensitivity of the domestic market would be between $0.0 and $4.73 million per year.

Competing Technologies in the next 5 years

The Chemical Industry is focusing on incremental improvements to existing heat enhancement technologies rather than a quantum step process like the dimpled tube technology, although ExxonMobil and BP are both very interested in the success of this process and will likely adopt it if the energy and operational savings observed in the pilot plant can be achieved in a full scale version.

Intellectual Property Management

GTI provided an invention disclosure to the Department of Energy for the VHTE Technology in 2004 (Patent Invention Disclosure GTI-04-1582).

Based on successful results of pilot-scale evaluation at participating refinery GTI will negotiate a licensing arrangement with potential OEMs (optional license agreement was drafted up and sent to KTI corporation for the review and comments) that will allow the end user (chemical plant) to deploy the technology throughout their chemical plant sites under favorable terms, while permitting GTI and/or its licensees to market the technology to the remainder of the industry at a later time. GTI will also select an OEM (or group of OEMs) as a licensee to sell the technology throughout the Chemical Industry: licensees for this activity will be based on merit, with team members getting the most favored opportunity to qualify; the commercially operated system will be a showcase for the technology that can be used to “sell” prospective customers in the Chemical Industry on the concept.

Partners needed to reach Commercialization Goals

GTI will work with OEM manufacturers like KTI who have sales staffs and strong connections to the chemical industry as a major focus of our plans to reach commercialization goals. Licenses will be issued to OEMs as described above.

Potential Market Barriers

The major potential market barrier is the conservatism of the Chemical Industry. New technologies must provide significant improvements in either capital cost, energy savings, reduced operations and maintenance costs, enhanced production, or enhanced environmental impacts (coupled with regulations that mandate environmental improvements) before the industry will make a change. The GTI team believes that the pilot tests have indicated the potential for improvements in all of the above areas, and a concerted technology marketing approach will be developed to “sell” the industry on the new technology. This approach will include: a successful commercial demonstration, presentation of the results through out associated vendors that do business within the Chemical Industry and through trade and professional associations like the AISI, AISE, ABMA, ASME, AIChE,, participation at technical meetings, presentation to GTI member companies (150 gas and electric utilities), and meetings with engineering companies that are active in the Chemical Industry, and with which GTI has working relationships, including Kellogg Brown and Root, Kinetics Technology International, Ralph M. Parsons, Bechtel, Fluor, Stone & Webster, Sargent & Lundy, and Foster Wheeler. Naturally, if a licensee is selected to sell the technology within the chemical industry, these efforts will be directed through that entity. For future use of the technology by the refining industry, GTI will also introduce the technology to the American Petroleum Institute.

To provide the greatest chance for success of this technology with the Chemical Industry the following are essential:

- Positive test data (already obtained from the pilot-scale field test at BP's Cherry Point Refinery).
- Refinement of the technology using modeling and data from the pilot scale tests
- Implementation of a full scale operating application with the assistance of ExxonMobil and/or BP in their own facilities where more test data can be collected and testimonies for marketing purposes could be offered.
- Development of computerized design tools for proper design of any heat transfer equipment utilizing the dimple tubes technology by KTI. In order to be cost effective, a minimal amount of time to take an application from basic process requirements to detailed design is the only way to make the technology feasible without some other strong, compelling advantage.

Planned Commercialization Schedule

Based on the schedule for the Phase I and Phase II efforts, the GTI Team anticipates the following commercialization schedule:

2007 - 2009 - preparation for the full-scale demonstration at participating refinery
2009 - 2010 - pre-commercial full-scale demonstration of the technology
2010 - 2012 - commercial design, engineering, fabrication and installation
2012 - 2014 - first full-scale unit in commercial operation at participating refinery
2015 - 2020 - 420 to 630 units converted to dimpled tube technology

Publications, Presentations, Patents

1. March 2002 - AIChE Meeting "Technologies for Tomorrow's Chemical Industry" (New Orleans, LA).
2. April 2003 - DOE/Partners Phase I review and Go/No Go decision meeting (Fairfax, VA).
3. February 2004 - Dimpled Tube Technology For Heat Transfer Enhancement In Chemical Industry Process Heaters, by Y. Chudnovsky, H. Kurek, A. Kozlov. Natural Gas Technologies II Conference and Exposition (Phoenix, AZ).
4. April 2004 - Vortex Heat Transfer Enhancement For Waste Heat Recovery In Chemical Industry Process Heaters by Y. Chudnovsky, H. Kurek, A. Kozlov - AIChE Spring National Meeting (New Orleans, LA).
5. July 2004 - Method and Apparatus for Heat and Mass Transfer Augmentation, by A. Kozlov, Y. Chudnovsky, and V. Kunc, GTI Invention Disclosure 04-1582.
6. April 2005 - Heat Transfer Enhancement And Fouling Rate Reduction In Chemical Industry Process Heaters Through Dimpling Of The Product Tubes, by Y.Chudnovsky and A.Kozlov - DOE/AIChE Spring National Meeting (Atlanta, GA)
7. September 2005 - Vortex Heat Transfer Enhancement For Industrial Applications: Experimental and Numerical Study of Dimpled Wall in Rectangular Channel by Y.Chudnovsky, A.Kozlov, A.Maskinskaya, E.Sergievsky. 5th International Conference on Enhanced, Compact and Ultra-Compact Heat Exchangers (Whistler, Canada)
8. December 2005 - Heat Transfer Enhancement and Fouling Rate Reduction in Chemical Industry Fired Heaters, by Y.Chudnovsky at the Field Trial Review Meeting, GTI Headquarters (Des Plaines, IL).
9. January 2006 - Dimpled Tubes (VHTE) for Performance Improvement of the Convective Heat Transfer Equipment in Chemical Industry, by Y.Chudnovsky - Field Trial Results Review at EMRE Heat Transfer Equipment and Energy Section (Fairfax, VA)
10. April 2006 - Effects Of Exterior Surface Dimples On Heat Transfer And Friction Factors For a Cross-Flow Heat Exchanger, by L. Sherrow, P. Ligrani, Y. Chudnovsky, A. Kozlov, Journal of Enhanced Heat Transfer, 2006, #1, pp. 1-18.

Nomenclature

h Heat transfer coefficient [Btu/hr/ft^2/^{o}F]
A Total heat transfer area for the tube bank [ft^2]

D Tube diameter [in]

Q Total heat transferred through the tube bank [Btu/hr] – defined as $hA\Delta T$, where h is the heat-transfer coefficient, A is the total heat transfer area, and ΔT is the temperature difference between tube surface and heating media

Nu Nusselt number is a dimensionless parameter expressing the ratio of convective to conductive heat transfer between a solid boundary (tube bank) and a moving fluid (hot air), defined as hl/k where h is the heat-transfer coefficient, l is the characteristic length (tube diameter), and k is the thermal conductivity of the fluid

Eu Euler number is a dimensionless parameter that represents the ratio of pressure force (pressure drop) to inertial force (dynamic head), defined as $2\Delta P/(\rho v^2)$ where ρ is the fluid density, v is the flow velocity and ΔP is the pressure drop across the tube bank

Re Reynolds number is a dimensionless parameter representing the ratio of momentum force (velocity) to viscous force in fluid flow (fluid properties), defined as $\rho vD/\mu$ where ρ is the fluid density, v is the flow velocity, D is the tube diameter and μ is the fluid viscosity

Appendix 1

10 Cavendish Court, Centerra Resource Park
Lebanon, New Hampshire 03766-1442 · USA
Telephone: (603) 643-2600
Fax: (603) 643-3967

Final Report

Dimpled Tube Bundle Modeling

TM-471

CONFIDENTIAL

Prepared for:

Yaroslav Chudnovsky
Gas Technology Institute
1700 South Mount Prospect Road
Des Plains, IL 60018

Madhusuden Agrawal, M.Sc.
Samir Rida, Ph.D.
Karl H. Kuehlert, Dr.-Ing.

February 19, 2002

Table of Contents

1. Introduction

GTI is gearing up for the design of a dimpled tubes bundle and is seeking the simulation of the flow and heat transfer for staggered arrangement of dimpled tubes streamlining by turbulent cross flow. The goal is to validate the results against experimental measurements for a baseline model with bared tubes and to model the flow and heat transfer for a dimpled tubes bundle case. GTI is interested in the flow distribution, the temperature field, the total pressure drop, and the heat transfer coefficient for each tube. GTI asked Fluent to perform heat transfer and steady flow analysis for the two models.

The objective of this project was to develop a computational model for fluid flow and heat transfer calculations for a staggered arrangement of dimpled tubes streamlining by turbulent cross flow. Two calculations were performed: bared tubes case with 8 rows (baseline model) and a case with eight rows of dimpled tubes (dimpled case). Fluent generated the computational mesh, set up and ran the CFD problems, and post-processed the results from the CFD analysis. This CFD analysis was performed to provide GTI

1) a better understanding of the flow patterns and the effect of the dimples on the flow structure,
2) Comparison of CFD results with experimental results for the bared tubes bundle model,
3) The total pressure loss and
4) The temperature field and heat transfer coefficient (local and average).

2. Model Set-Up and Technical Approach

The transport of mass, momentum, energy, chemical species etc. are governed by a generalized conservation principle and can be described in the form of general differential equation. The overall CFD procedure involves numerical solution of these differential equations. During this process, first the calculation domain (extent of space) is divided into number of non-overlapping control volumes such that there is one control volume surrounding each grid point. Then, each governing differential equation is iteratively balanced over each control volume to conserve the mass, momentum, energy and other physical entities. During the iterative process, the residual error for each governing equation is monitored and reduced. This process is continue until overall balance in the conservation of all the governing entities is achieved up to an acceptable desired level. Finally such converged numerical solutions reveal a detailed distribution of pressure, velocities, turbulence parameters, temperature, concentration of chemical species, etc in the calculation domain.

GTI is seeking the simulation of flow distribution and heat transfer in the heat exchanger. Two models were considered which are, the baseline bared tubes bundle and the dimpled tubes bundle. The simulations were performed with FLUENT V5. The geometry of the staggered tubes arrangement is shown in Figure 1.

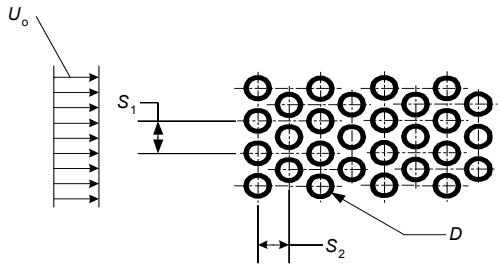

Figure 1: Staggered Tubes Geometry

a) Baseline Model

2D model for the baseline, bared tubes bundle, was generated and meshed in Gambit. The geometry of the computational domain is shown in Figure 2. Parameters for the baseline, bare tubes case, are given below:

Tubes: D = 1″; S_1=1.53″; S_2=1.32

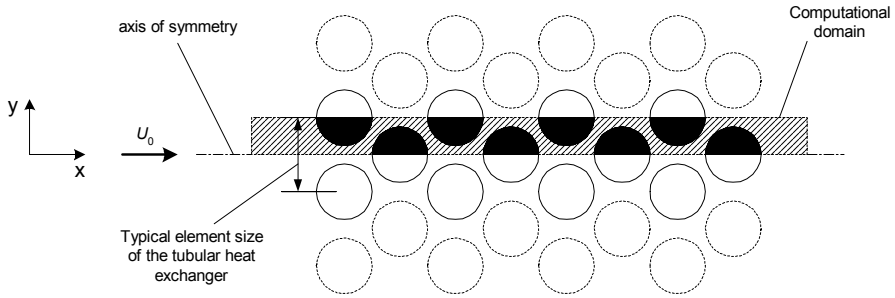

Figure 2: Computational Domain Geometry for the Bare Tubes Case (2D approach)

The computational mesh had about 36,500 quad cells. Proper attention was paid to resolve thermal boundary layers around the tubes. Figure 3 shows the picture of the computational mesh.

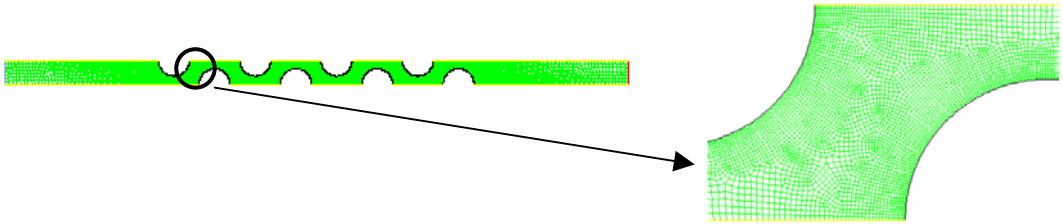

Figure 3: Computational Domain Geometry for the Bare Tubes Case (2D approach)

b) Dimpled Tubes Model

A 3D modeling is requested for the dimpled tubes case. The geometry of dimple arrangement on the tube surface is shown in Figure 4.

The details of the computational domain for the dimpled tubes case is shown in Figure 5. A 3d geometry and mesh was generated using gambit. Parameters used for the geometry generation of the dimpled tubes case are given below:

Tubes: $D = 1''$; S_1=1.53″; S_2=1.32
Dimpled surface geometry: r_{dimple}=7/128″; h=5/128″; a=0.1048″; b≈0.091″; t=5/32″

A hybrid mesh of about 900,000 cells was generated for the 3D dimpled case. Figure 6 shows a picture of the surface mesh.

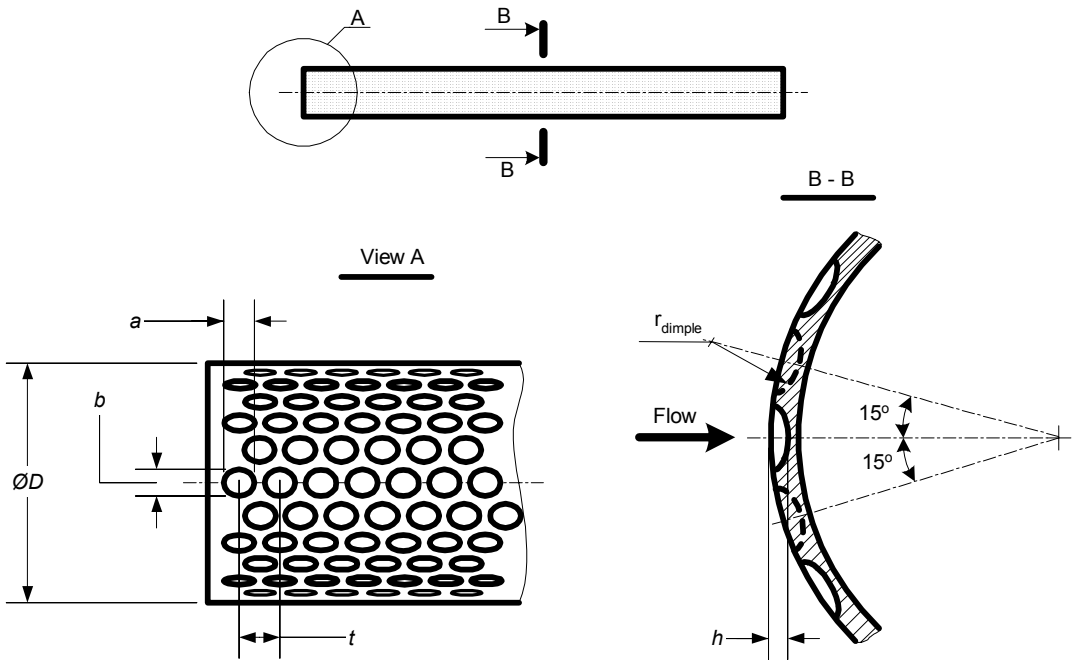

Figure 4: Surface Dimpled Tube Geometry

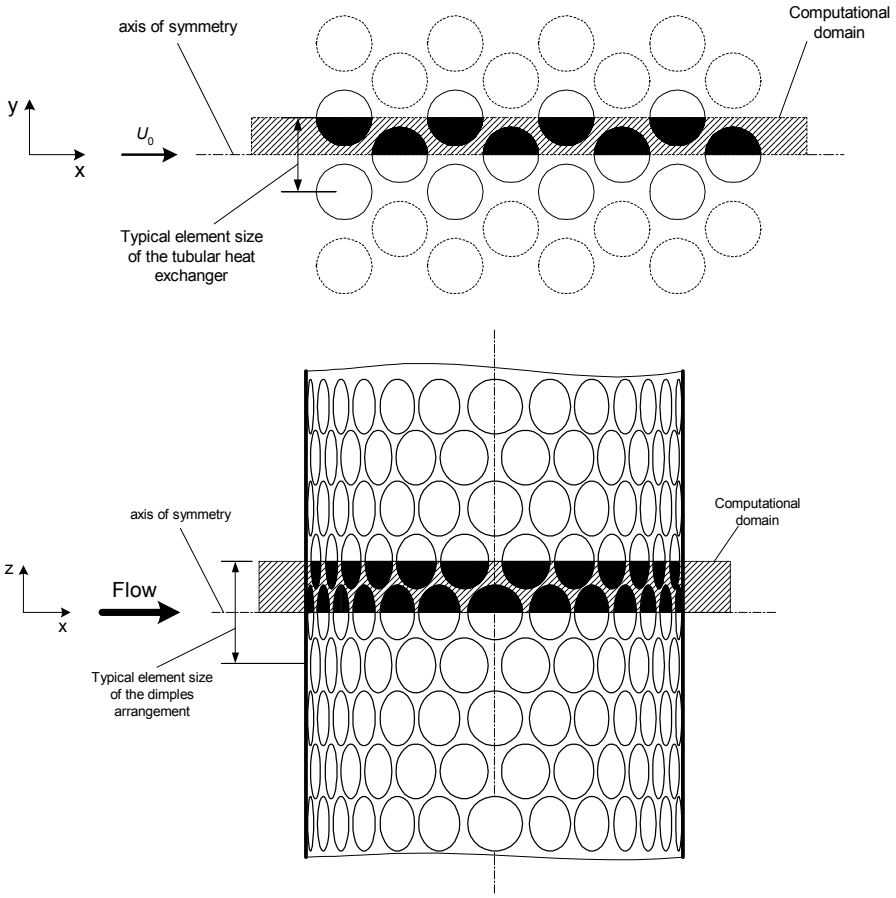

Figure 5: Computational Domain Geometry for the Dimpled Tubes

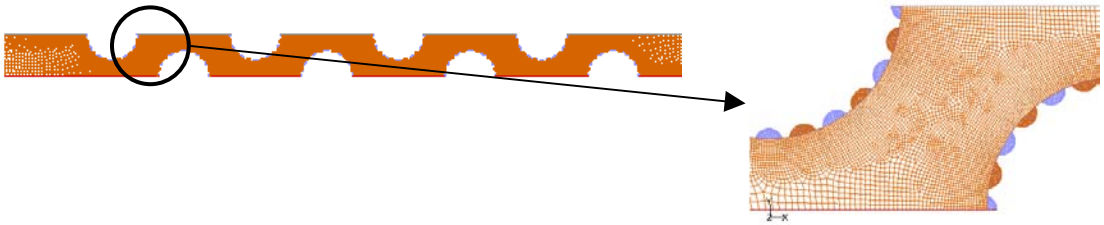

Figure 6: Surface mesh for the Dimpled case

In tube bundle problems, flow separates in the back of the tube, creating vortices that might become unstable and start shedding. The interaction of tubes with each other can often foster a certain flow periodicity and enhance heat transfer. The presence of dimples on the tube causes a disturbance that increases turbulence intensity as the flow goes in and out of the dimples, generating a small recirculation between them. Dimples act as turbulators, adding disturbances to move the separation away from the laminar region. This reduces the turbulent wake behind the tube and reduces drag at low Reynolds numbers.

In fact, an effective means to avoid the drag penalties and nonlinear behavior of lift and moment coefficients, caused by laminar separation bubbles, are turbulators. Turbulators force the transition from laminar to turbulent by artificial disturbances. This device will usually be attached just before the region of laminar separation and has to introduce enough of a disturbance to cause transition into the turbulent state, before the laminar separation can occur. This reduces the boundary layer thickness (and laminar separation bubble) at the surface. This is especially desirable for low Reynolds number applications. A small drag increase in the high-speed regime is the result, which is offset by the improvements at Reynolds numbers below 1 million. A turbulator increases the path length and heat transfer coefficients in heat exchangers. This is because the disturbances induce a large velocity gradient near the wall. The faster moving fluid in the vicinity of the wall will remain cooler than a slower more stagnant fluid resulting in a larger temperature gradient. A faster velocity gradient also results in a larger path length and increased heat transfer.

The flow over a tube bundle requires the use of RNG k-ε model because of the difficulty to predict separation with the standard k-ε model. The presence of dimples will make the flow more complex and generate even more vortices and flow separation as the dimples increase turbulence intensity. The RNG k-ε model is actually better than the standard of k-ε model for moderately complex behavior like separating flows, jet impingement, and swirling and secondary flows. With regards to wall treatment, both a non-equilibrium wall function and two-layer zonal model were used in the baseline case to validate which works better. Though the non-equilibrium wall function is better than the standard wall function because it accounts for the pressure gradient effects in the cases of separation and reattachment, yet it overpredicted the heat transfer coefficient value against the analytical observations. The two-layer zonal model, which does not rely on the law-of-the-wall, is good for complex flows and is especially applicable for low-Re flows. An addition simulation of the baseline case was performed in Fluent6 with k-w turbulence model, which is well known turbulence model for low-Re flows.

The air was modeled as incompressible ideal gas. A second order discretization of the governing equations was used to minimize numerical diffusion and enhance solution accuracy. These equations were solved in steady state using the segregated solver.

GTI has provided the following boundary conditions for the baseline bare tubes model and the dimpled tubes model. A uniform velocity profile in front of the tubes located at a distance of 5D from the first row was used at the inlet. The boundary conditions for both models were:

- Flow: air
- Inlet velocity: U_0=3 m/s
- Inlet temperature: T_0=140F;
- Tube temperature: T_{tube}=68F;
- Inlet turbulence intensity ε_0=1%;
- Inlet longitudinal and cross-flow turbulence integral scale: L_t=3″

3. Directions for Meshing and Convergence

Baseline case:

The mesh generation for the baseline geometry was fairly simple. A mesh with all quadrilateral elements was created on the one periodic model of the geometry. A fine mesh around the tube

walls was created using boundary layers feature of gambit. Eight layers with first row at 0.005 inches and growth rate of 1.1 was used in creating these boundary layers. Very fine interval size of about 0.01 inches was used near the tubes region and the coarse mesh of interval size about 0.1 inches in the far field region. Quad pave mesh was finally created, with a mesh size of about 36,500 cells.

Since mesh was of very good quality (maximum skewness of only 0.54), convergence was not very difficult. Default values of under-relaxation factors were used in all stages. First the solution was converged with first order descretization scheme for all variables and then the 2nd order scheme was switch on for pressure, momentum, turbulence and energy. To check the convergence, the average temperature at the outlet plane was monitored.

Dimpled Case:

The geometry and mesh generation on the dimpled model was reasonably complex. First the volume of one dimple was created which was rotated and translated around a tube to create a dimpled tube. And then this dimpled tube was copied and translated to create the whole dimpled tube arrangement. A hybrid mesh was created on this geometry. All the dimple volumes were meshed as tetrahedral elements with interval size of about 0.005 inches. A quad pave mesh on all tube surfaces was created. Five boundary layers with first row at 0.005 inches and growth rate of 1.15 was created around all tube surfaces. A cooper mesh was created for the big volume, which goes from inlet to outlet, leaving some space around tubes. In this cooper mesh appropriate grading was used so as to have a fine mesh around tubes and coarse mesh in far filed region. In the volumes near the tubes, tetrahedral mesh was created. The final mesh had about 1.07 millions hybrid cells.

In the dimpled case also, the mesh was reasonably good so convergence was not very difficult. Default values of under-relaxation factors were used in all stages. First the solution was converged with first order descretization scheme for all variables and then the 2nd order scheme was switch on for pressure, momentum, turbulence and energy. To check the convergence, the average temperature at the outlet plane was monitored.

4. Simulation Results

Baseline Case:

Three different simulations were performed for the baseline case –
1) using RNG turbulence model of Fluent5 with non-equilibrium wall function
2) using RNG turbulence model of Fluent5 with two layer zonal model
3) using k-w turbulence model of Fluent6 with two layer zonal model

The Figure 7, 8 and 9 show the distribution of the heat transfer coefficient on the tube wall surfaces. The computed heat transfer coefficient values are based on the reference temperature of air at 140F and defined as

Heat transfer coefficient = heat flux / (Twall – Tref)

The following table shows the average heat transfer coefficient on each tube for all three turbulence cases.

Tube No.	RNG turbulence model with 2layer zonal	RNG turbulence model with non-equilibrium wall	k-w turbulence model with 2layer zonal
1.	62.2 W/m2K	134.9 W/m2K	100.6 W/m2K
2.	73.3 W/m2K	161.7 W/m2K	94.0 W/m2K
3.	68.8 W/m2K	149.1 W/m2K	81.3 W/m2K
4.	68.2 W/m2K	141.1 W/m2K	72.5 W/m2K
5.	64.8 W/m2K	125.7 W/m2K	65.9 W/m2K
6.	61.7 W/m2K	110.8 W/m2K	60.9 W/m2K
7.	58.5 W/m2K	96.8 W/m2K	56.8 W/m2K
8.	54.6 W/m2K	82.2 W/m2K	52.9 W/m2K
Overall	**64 W/m2K**	**125.3 W/m2K**	**73.1 W/m2K**

For the baseline case experimental/analytical results were available for the overall heat transfer coefficient, appendix-1 shows the calculations for the overall analytical heat transfer coefficient. Its value is 76.64 W/m2K for the present configuration of staggered tubes. Fluent6 simulation with k-w model predicts overall heat transfer coefficient very close to the experimental results.

Figure 10 shows the angular variation of the heat transfer coefficient on the first tube for the RNG turbulence model with two layer zonal case. Figure 11 shows the contours of static temperature.

Figure 12 shows the static pressure contours. The total pressure drop is about 84.2 Pa, which is the difference between the average total pressure at inlet and outlet. Figures 13 and 14 show the velocity vectors plots.

Dimpled Case:

A three dimensional dimpled case was setup and simulated using RNG turbulence and 2-layer zonal model of Fluent5. Figure 15 shows the heat transfer coefficient plot on all tube surfaces, and figure 16 shows the enlarged view of heat transfer coefficient plot on the first tube.

Table below shows the comparison of the heat transfer rate for the baseline and the dimpled case.

Tube No.	For the Baseline Case			For the Dimpled Case		
	Heat Transfer Coefficient (W/m2K)	Surface Area*** (m2)	Heat Transfer Rate (W)	Heat Transfer Coefficient (W/m2K)	Surface Area*** (m2)	Heat Transfer Rate (W)
1.	62.2	0.03989	99.26	59.79	0.04852	115.91
2.	73.3	0.03989	116.99	73.71	0.04852	143.12
3.	68.8	0.03989	109.84	68.34	0.04852	132.53
4.	68.2	0.03989	108.88	66.47	0.04852	129.01
5.	64.8	0.03989	103.49	62.49	0.04852	121.45
6.	61.7	0.03989	98.49	58.64	0.04852	113.89
7.	58.5	0.03989	93.46	55.03	0.04852	106.83
8.	54.6	0.03989	87.15	50.39	0.04852	97.76
Overall	**64.0**	**0.31912**	**817.56**	**61.86**	**0.38819**	**960.5**

*Note*** : Surface Area based on one meter length in Z-Dir.*

Above table clearly shows that total heat transfer rate has increased with dimples as expected, however the overall heat transfer coefficient has come down slightly because of relatively low velocities within dimples.

Figure 17 shows the temperature contours on the symmetry plane and Figure 18 shows the contours of static pressure. The total pressure drop between inlet and outlet is 103.4 Pa.

Figure 19 shows the velocity vectors plot on the symmetry plane and Figure 20 shows the enlarged view of the velocity vectors plot in the tube area.

Dimpled Case with k-omega model in Fluent6:

A further simulation was performed for the dimpled case with SST k-omega turbulence model in Fluent6. Figure 21 shows the heat transfer coefficient plot on all the tubes and figure 22 shows an enlarged view of heat transfer coefficient on the 1st tube. The following table shows the comparison of heat transfer coefficient for each tube with RNG turbulence and k-omega turbulence model.

Tube No.	With RNG turbulence model	With k-omega turbulence model
1.	59.79 W/m2K	54.03 W/m2K
2.	73.71 W/m2K	82.02 W/m2K
3.	68.34 W/m2K	73.35 W/m2K
4.	66.47 W/m2K	67.59 W/m2K
5.	62.49 W/m2K	62.71 W/m2K
6.	58.64 W/m2K	58.41 W/m2K
7.	55.03 W/m2K	54.61 W/m2K
8.	50.39 W/m2K	50.65 W/m2K
Overall	**61.86 W/m2K**	**62.92 W/m2K**

Figure 23 shows the temperature contours on the symmetry plane and Figure 24 shows the contours of static pressure. The total pressure drop between inlet and outlet is 137.58 Pa.

Figure 25 shows the velocity vectors plot on the symmetry plane and Figure 26 shows the enlarged view of the velocity vectors plot in the tube area.

5. Conclusions and Recommendations

Based on the baseline simulation results, it is clear that the k-w model in Fluent6 is the best for these sort of low-Re type flow conditions. And the two layer zonal model is the preferred choice for near wall treatment. Comparison of the dimpled case results with the baseline case, clearly shows that total heat transfer rate has increased with dimples as expected.

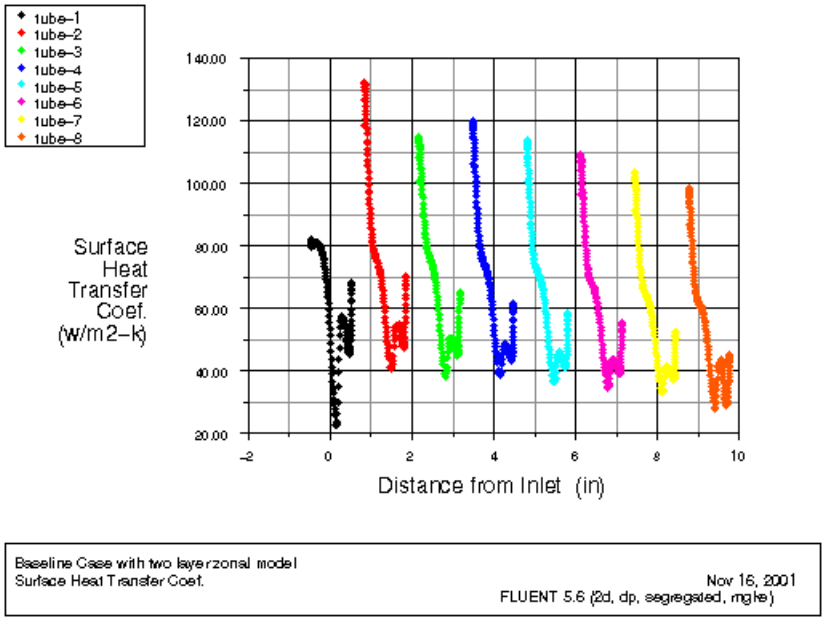

Figure 7: Distribution of Heat Transfer Coefficient for Baseline case with 2-layer zonal model and RNG turbulence

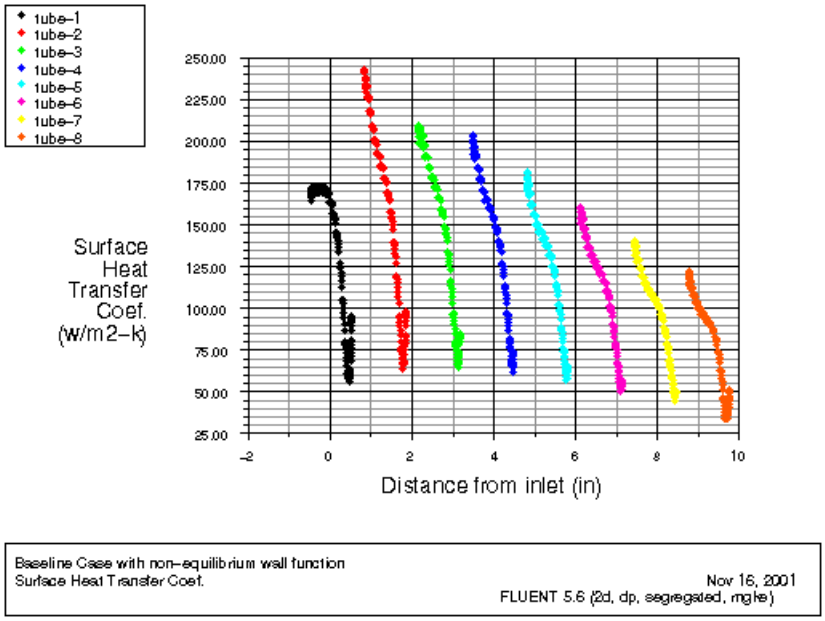

Figure 8: Distribution of heat transfer coefficient for baseline case with non-equilibrium function and RNG turbulence

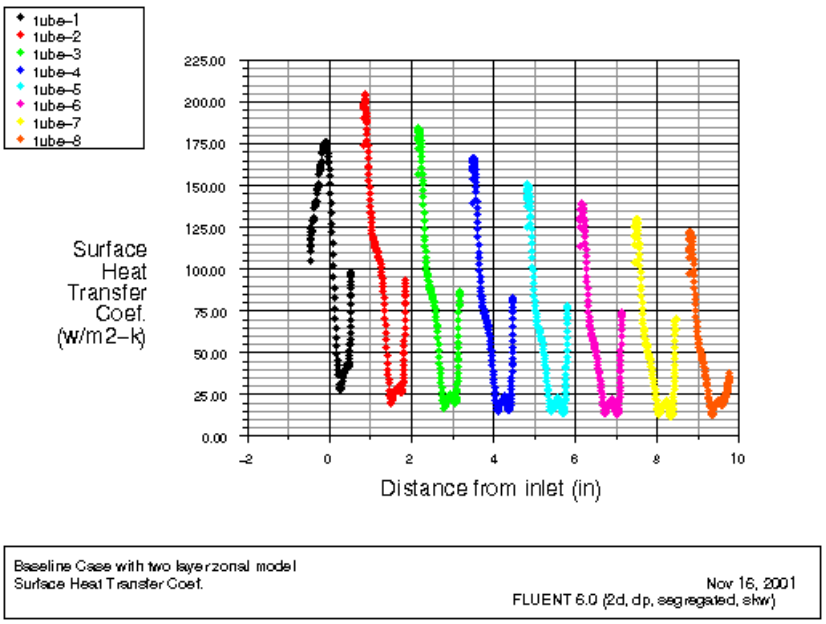

Figure 9: Distribution of heat transfer coefficient for baseline case with k-w model of Fluent6 and 2-layer zonal

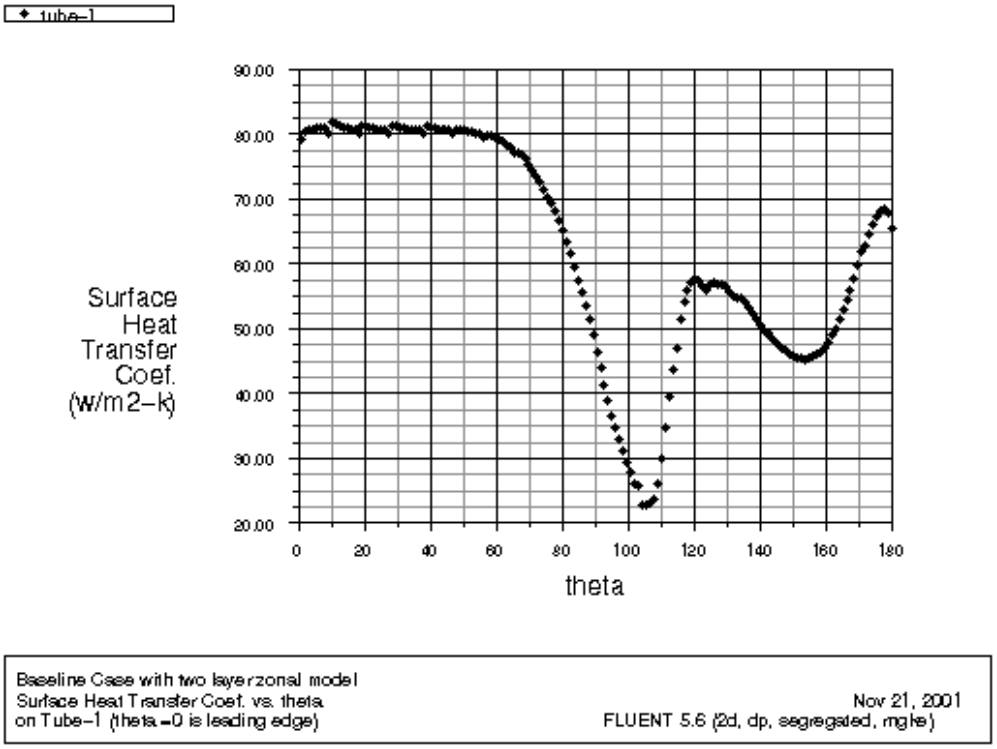

Figure 10: Angular distribution of heat transfer coefficient on the first tube

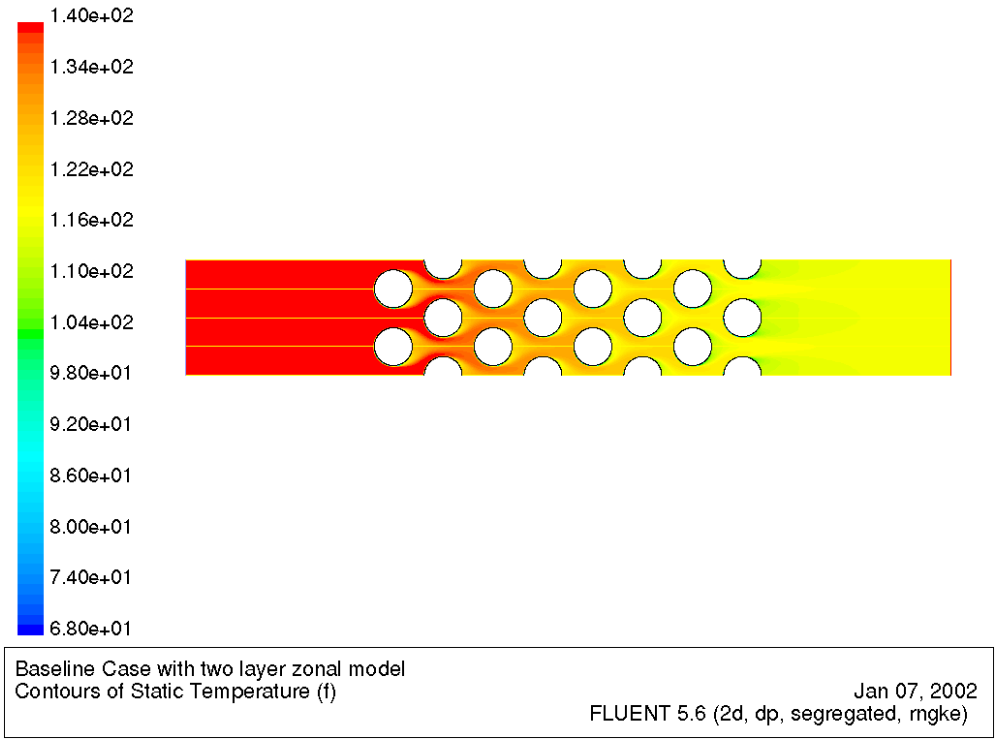

Figure 11: Contours of Static Temperature for the Baseline case

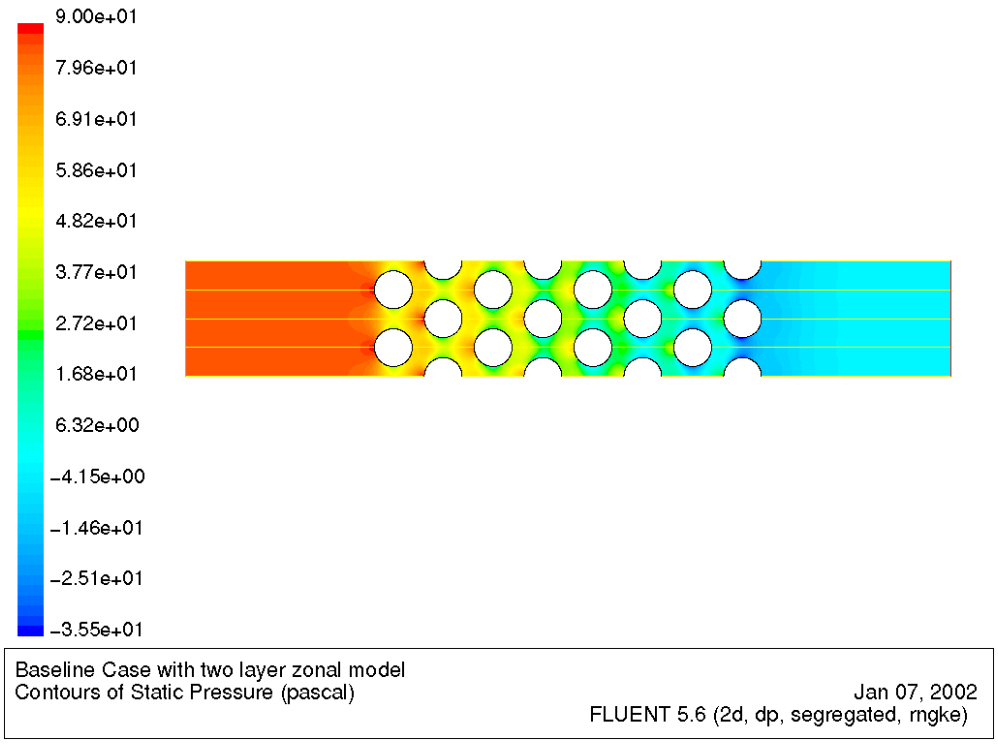

Figure 12: Contours of Static Pressure for the Baseline case

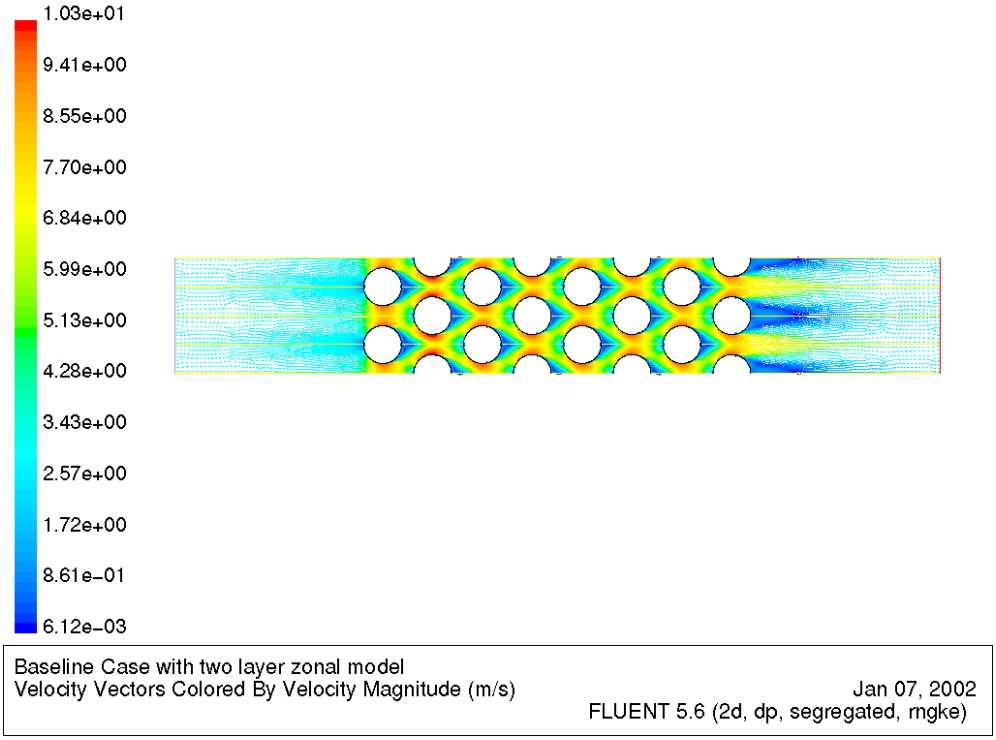

Figure 13: Velocity Vectors Plot for the Baseline case

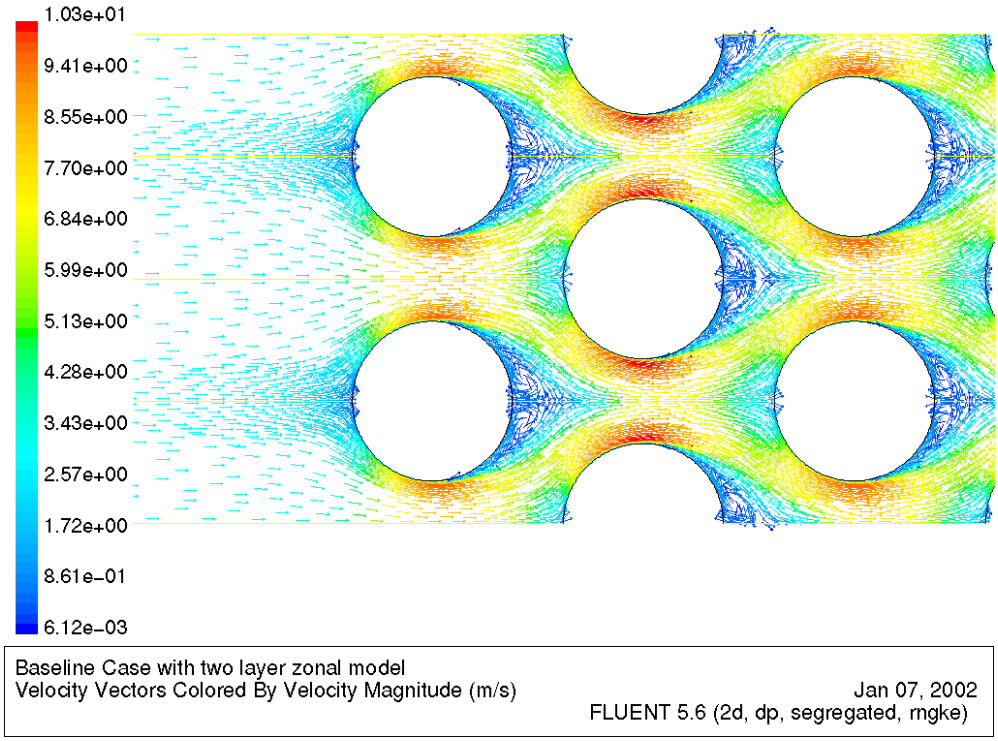

Figure 14: Enlarged View of Velocity Vectors plot

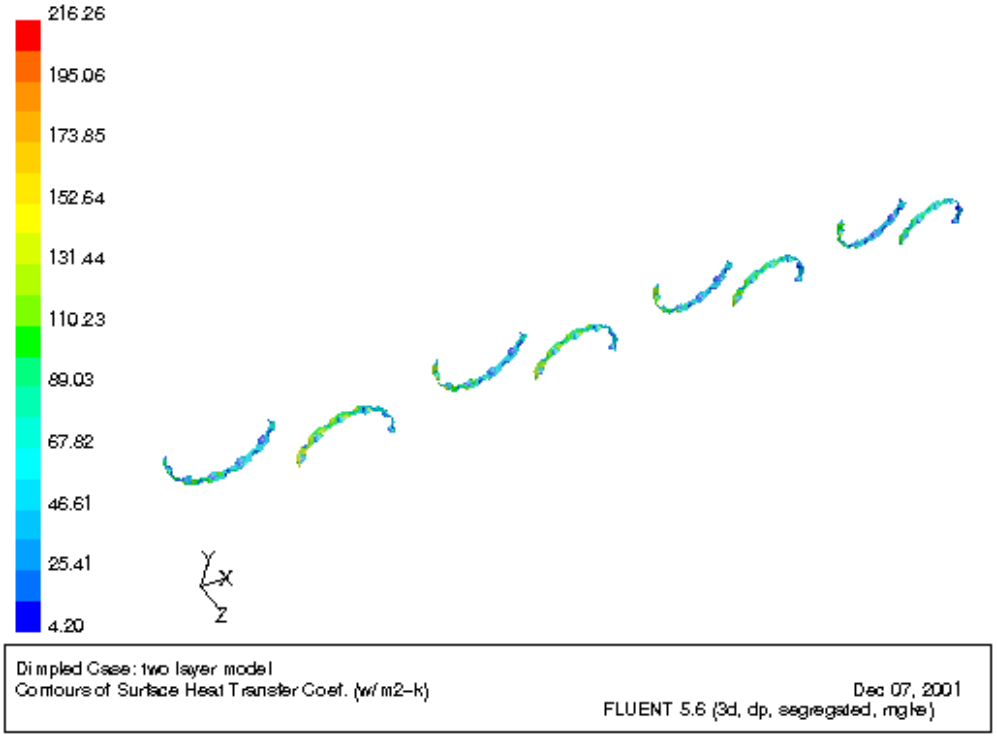

Figure 15: heat transfer coefficients on tube surfaces for the Dimpled Case

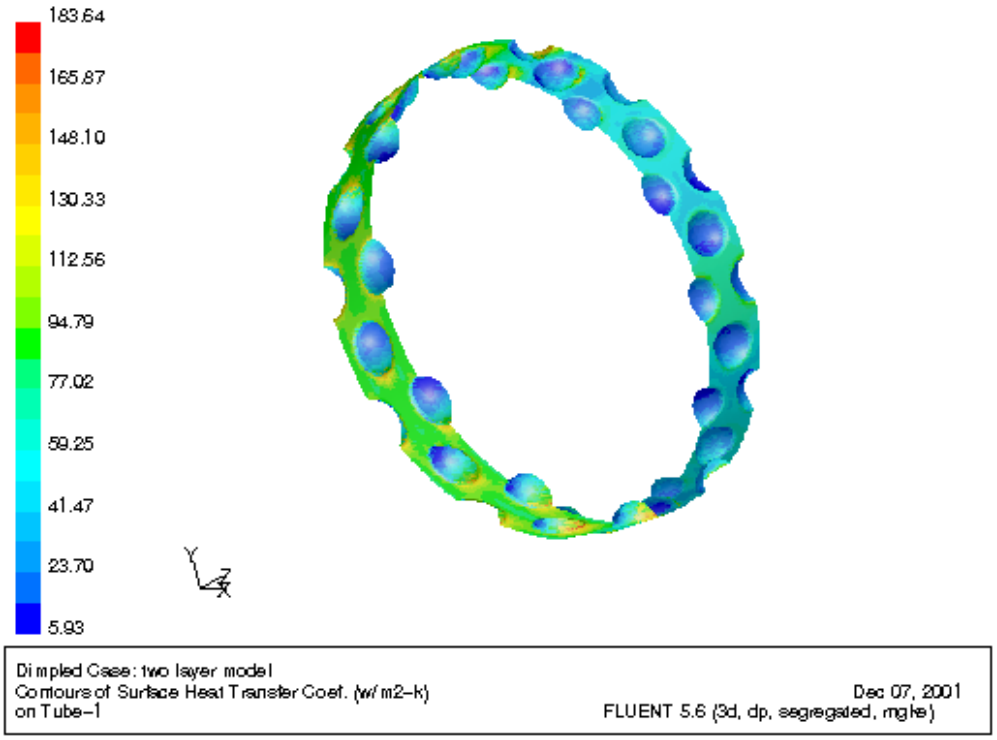

Figure 16: Enlarged View of heat transfer coefficient on first tube for Dimpled case

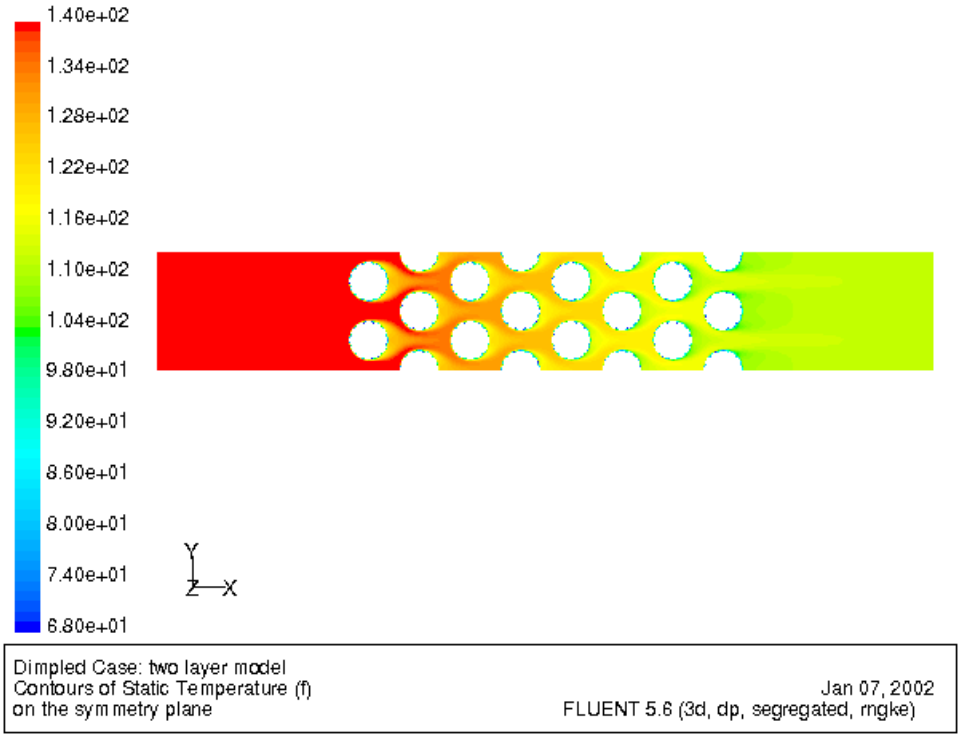

Figure 17: Temperature contours on symmetry plane for the Dimpled case

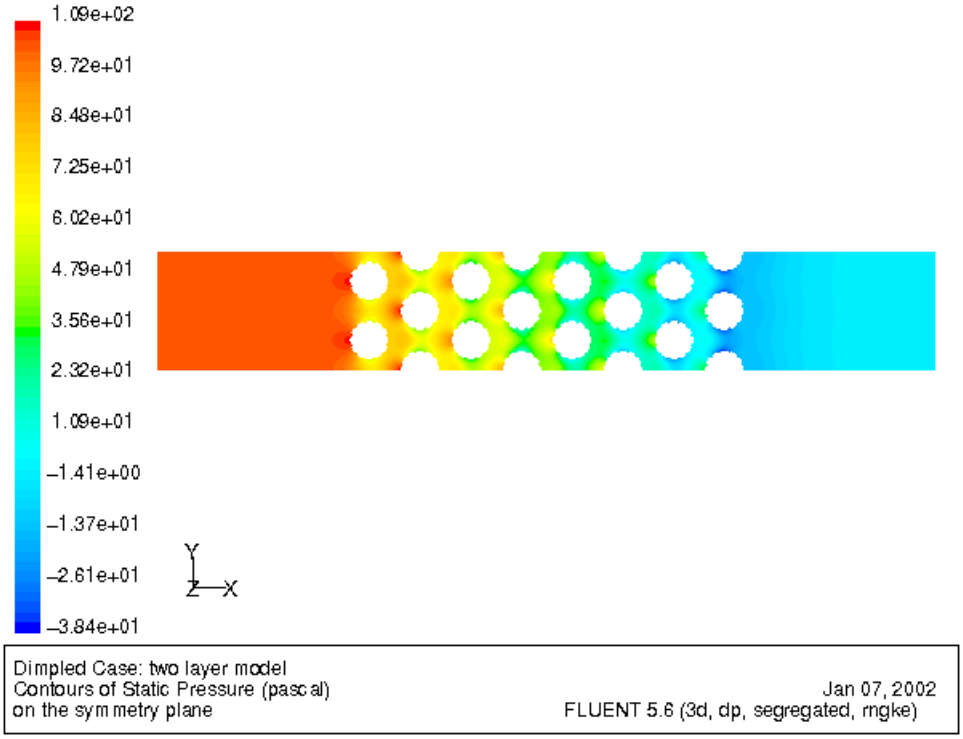

Figure 18: Contours of Static pressure on the symmetry for the Dimpled case

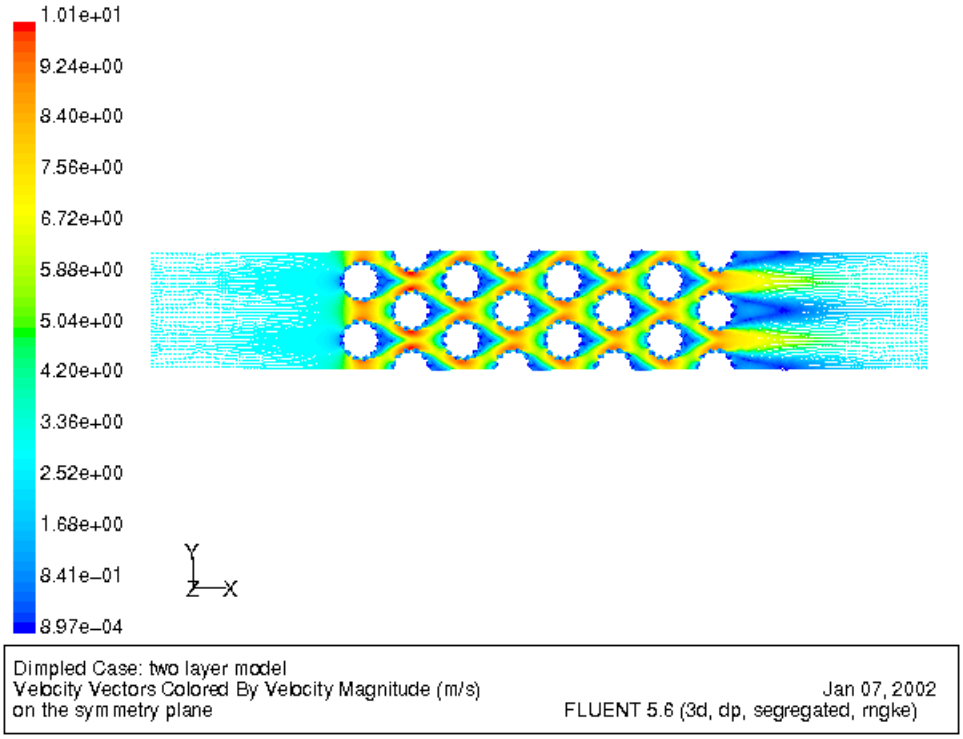

Figure 19: Velocity vectors plot on the symmetry plane for the Dimpled case

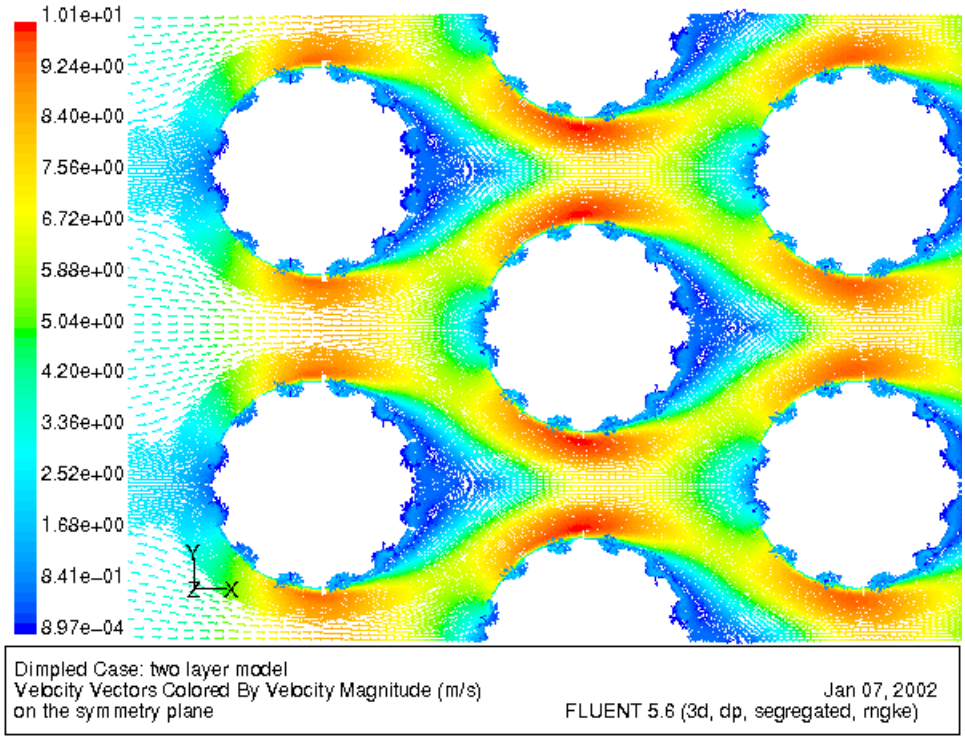

Figure 20: Enlarged View of view of velocity vectors plot for the Dimpled case

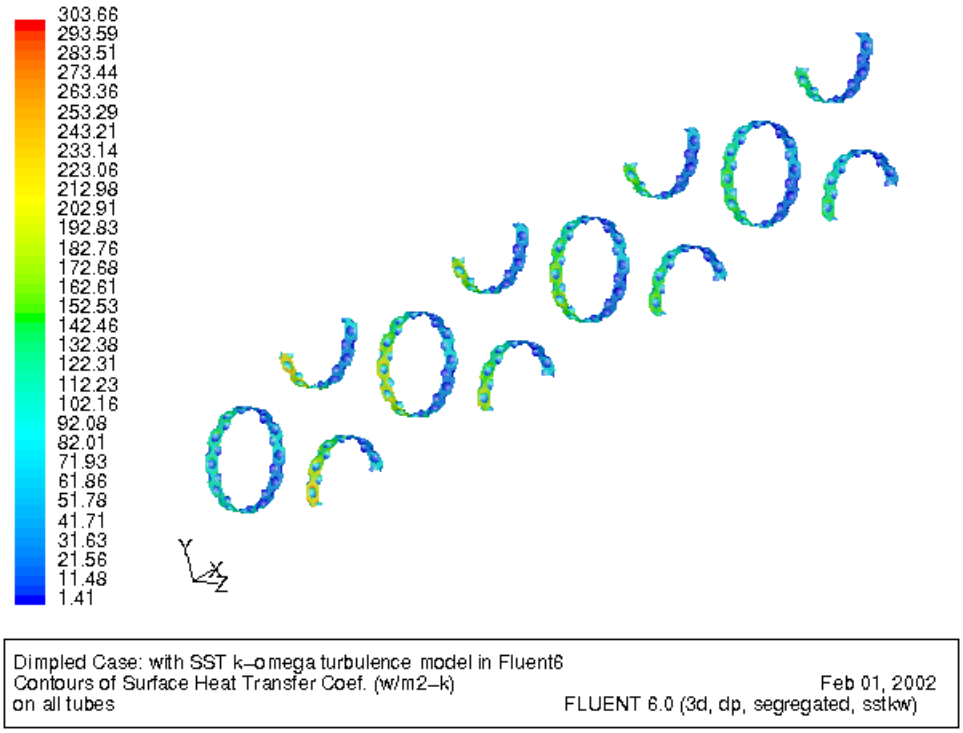

Figure 21: heat transfer coefficients on tube surfaces for the Dimpled Case with k-w turbulence model

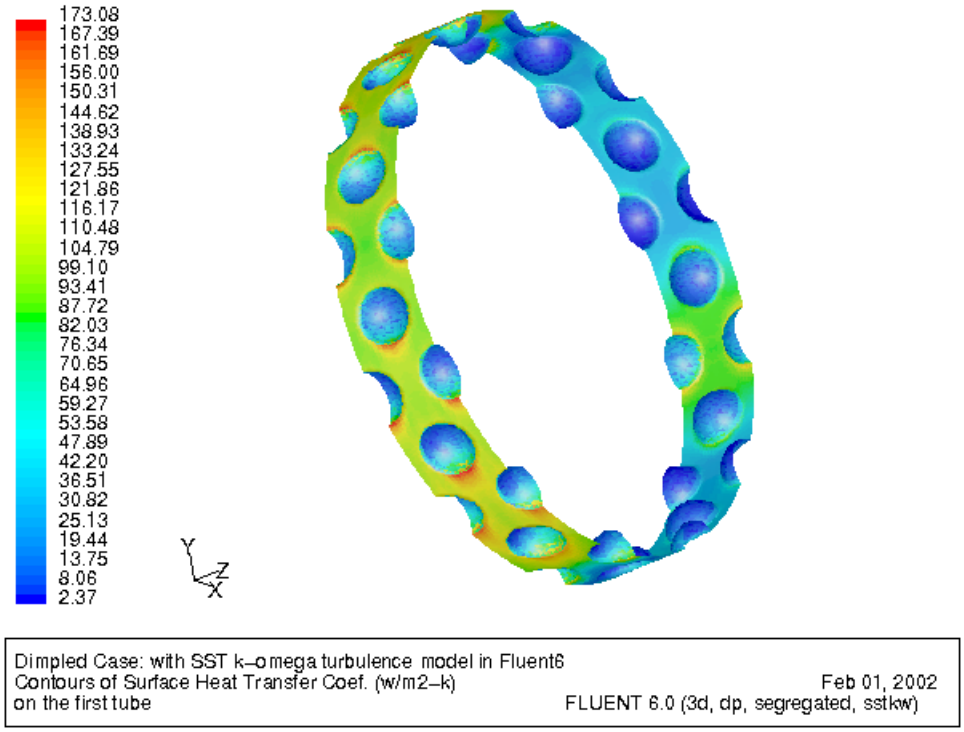

Figure 22: Enlarged View of heat transfer coefficient on first tube for Dimpled case with k-w turbulence model

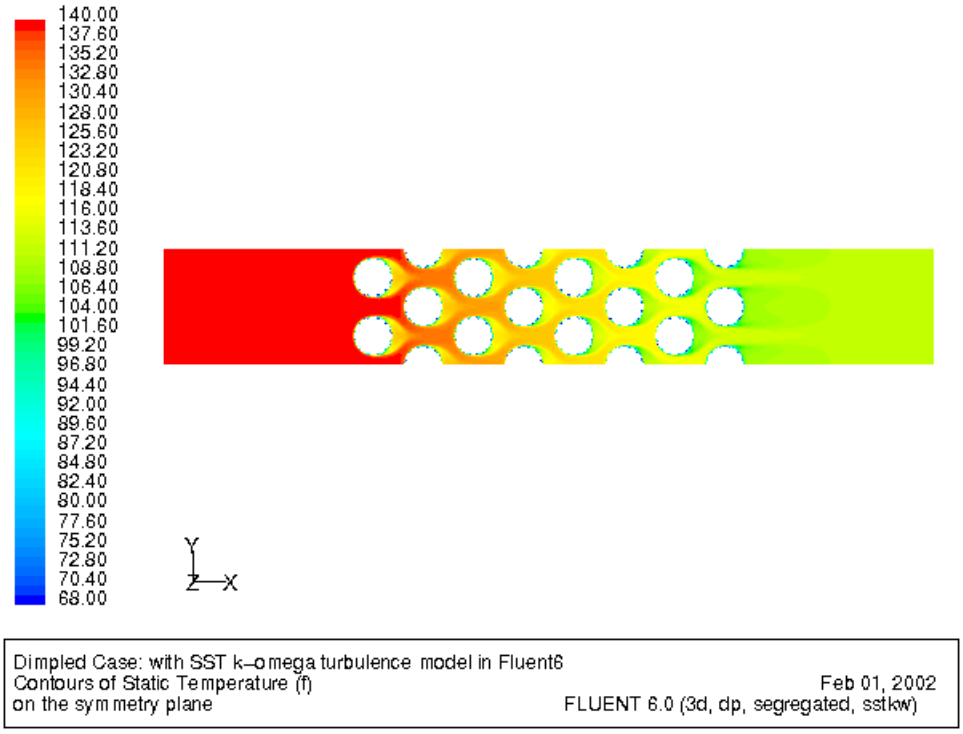

Figure 23: Contours of Static temperature on the symmetry for the Dimpled case with k-w turbulence model

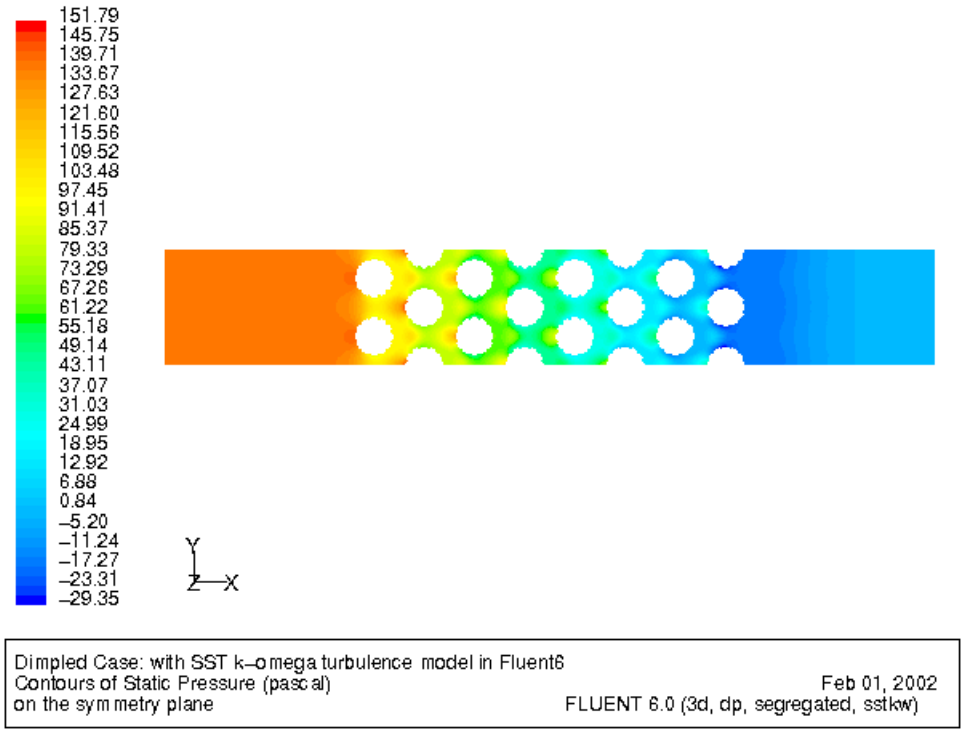

Figure 24: Contours of Static pressure on the symmetry for the Dimpled case with k-w turbulence model

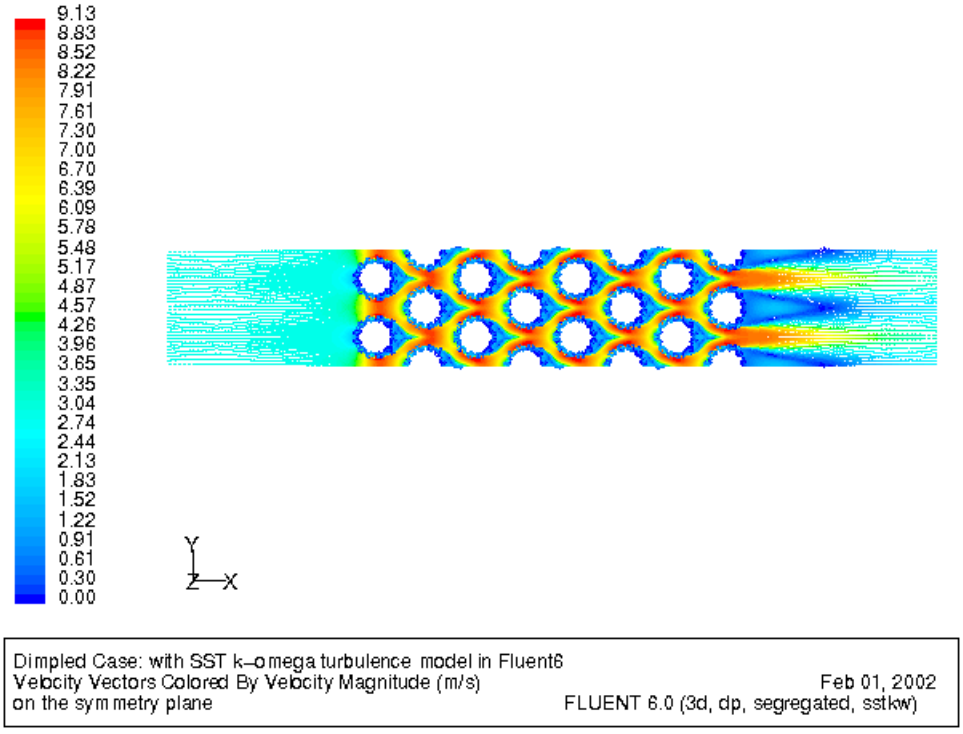

Figure 25: Velocity vectors plot on the symmetry plane for the Dimpled case with k-w turbulence model.

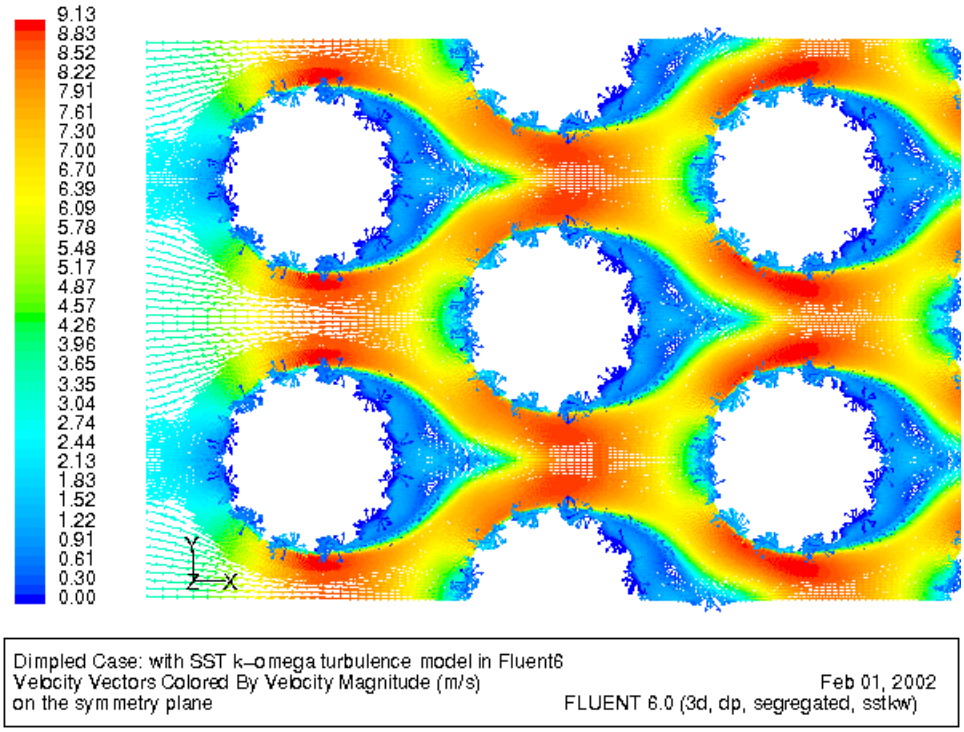

Figure 26: Enlarged View of view of velocity vectors plot for the Dimpled case with k-w turbulence model

Appendix-A

Empirical Calculation of Heat Transfer Coefficient for air flow normal to staggered circular tubes

S_2= 1.32", S_1 = 1.53" and D = 1"

$X_l = S_2/D = 1.32$ and $X_t = S_1/D = 1.53$
From fig 7-5: $C_h \approx 0.32$

$Pr = \mu C_p / k$
For air at 140^0F
μ = 1.7894e-5 Pa.s
C_p = 1006.43 J/kg K
k=0.0242 w/m K
Pr = 0.744176

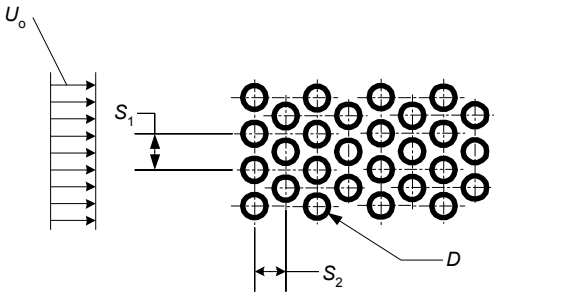

Fig. 7-5 Gas flow normal to an infinite bank of staggered circular tubes, heat transfer characteristics; a correlation of experimental data, average heat transfer coefficient around tube periphery. $StPr^{2/3} = C_h Re^{-0.4}$ $300 < Re < 15{,}000$.

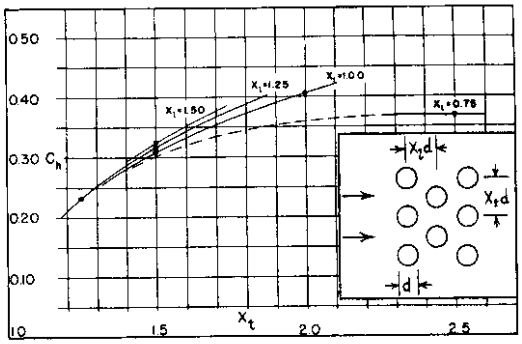

St = h / (ρ V_{max} C_p)
ρ = 1.0596 kg/m3
$V_{max} = V_{in} (S_1 - D) / S_1$
V_{in} = 3 m/s
V_{max} = 8.66 m/s
St = h / 9235.68

Re = 4 R_h ρ V_{max} / μ
$R_h = \sigma / \alpha$
σ = Free flow area / frontal area = $(S_1 - D) / S_1$ = 0.3464
α = Heat transfer area / total volume = π D / S_1 S_2 = 61.237 /m
R_h = 0.005656 m
Re = 11602

$St\ Pr^{2/3} = C_h\ Re^{-0.4}$
Substitute values for S_t, P_r, C_h and Re will leads to:
h = 85.16 W/m2 K

for 8 rows, (as shown in fig 7-7) the correction factor = 0.9

h = 85.16 * 0.9 = 76.64 W/m2 K

Fig. 7-7 Overall influence of row-to-row variations in the heat transfer coefficient in tube banks. Data are based on staggered tube banks but apply equally well to in-line tube banks and are a good approximation for crossed-rod and woven-screen matrices.

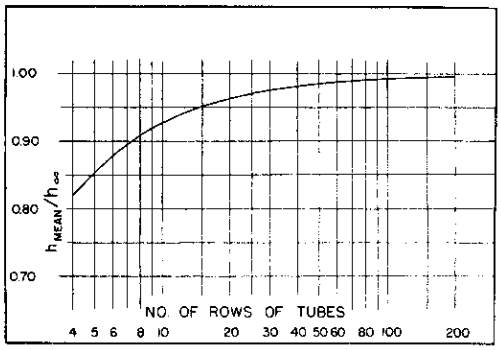

Reference: "Compact Heat Exchangers", 3rd Edition, W.M. Kays and A. L. London

Appendix 2

GTI-PF/11772

DIMPLED TUBE DEVELOPMENT

FINAL REPORT

Prepared by:

P. M. Ligrani
Department of Mechanical Engineering
University of Utah
50 S. Central Campus Drive, MEB 2202
Salt Lake City, Utah 84112-9208

Under subcontract to:

Gas Technology Institute
1700 South Mount Prospect Road
Des Plaines, IL 60018-1804

Prepared for:

Gas Technology Institute
Prime Contract No. DE-FC07-01ID14089
Subcontract No. PF11772
1700 South Mount Prospect Road
Des Plaines, IL 60018-1804

GTI Project Manager
Yaroslav Chudnovsky
Combustion Technology

March 2002

REPORT DOCUMENTATION PAGE

Form Approved
OMB No. 0704-0188

1. AGENCY USE ONLY (*Leave blank*)	2. REPORT DATE	3. REPORT TYPE AND DATES COVERED
	April 2002	Final Report (09/15/01 – 03/31/02)

4. TITLE AND SUBTITLE
Dimpled Tube Development

5. FUNDING NUMBERS
GTI contract no.
PF11772

6. AUTHOR(S)
Phillip M. Ligrani

7. PERFORMING ORGANIZATION NAME(S) AND ADDRESS(ES)
Gas Technology Institute
1700 South Mount Prospect Road
Des Plaines, IL 60018 - 1804

8. PERFORMING ORGANIZATION REPORT NUMBER

9. SPONSORING/MONITORING AGENCY NAME(S) AND ADDRESS(ES)

GTI
1700 S. Mt. Prospect Rd.
Des Plaines, IL 60018

10. SPONSORING/MONITORING AGENCY REPORT NUMBER

GTI-PF/11772

11. SUPPLEMENTARY NOTES

12a. DISTRIBUTION/AVAILABILITY STATEMENT

12b. DISTRIBUTION CODE

13. ABSTRACT (*Maximum 200 words)*

An experimental facility was designed, constructed, and tested to investigate the effects of adding either deep dimples, or shallow dimples to 6 tubes, contained in a total bank of 14 tubes. Significant heat transfer augmentations (compared to a bank of smooth tubes) are produced by using dimples on the surfaces of the tubes employed in the tube bank. The results show that these augmentations vary from one tube row to another, depending upon the type of dimples employed (either deep or shallow). The increases in form drag and pressure losses provided by the dimples are relatively small because of they do not protrude into the flow. From the measured results, it is estimated that overall friction factor ratios range from 0.97 to 1.03, and overall Nusselt number ratios are estimated to range from 1.35 to 1.57 if all 14 of the tubes in the tube bank contain shallow dimples. If all 14 of the tubes in the tube bank contain deep dimples, overall friction factor ratios are estimated to range from about 1.08 to 1.12, and overall Nusselt number ratios are estimated to range from about 1.25 to approximately 1.40.

14. SUBJECT TERMS
gas fired heat exchanger, dimpled tubes, heat transfer enhancment

15. NUMBER OF PAGES
35

16. PRICE CODE

17. SECURITY CLASSIFICATION OF REPORT	18. SECURITY CLASSIFICATION OF THIS PAGE	19. SECURITY CLASSIFICATION OF ABSTRACT	20. LIMITATION OF ABSTRACT
Unclassified	Unclassified	Unclassified	

RESEARCH SUMMARY

Title	Dimpled Tube Development
Contractor	Department of Mechanical Engineering, University of Utah, 50 S. Central Campus Drive, MEB 2202, Salt Lake City, Utah 84112- 9208
Principal Investigator	Phil Ligrani
Report Type Report Period	Final Report September 15, 2001 – March 31, 2002
Objective	To develop geometry/location recommendations for an effective tube surface profile for tube bundle that is representing convective section of the gas-fired process heater for the Chemical Industry.
Technical Perspective	The present project demonstrates cost-effective Dimpled Tube technologies for significantly improving the energy efficiency of chemical industry fired process heaters. Specifically, the results are intended to lead to a 3-5% increase in overall heater thermal efficiency with no significant increase in pressure drop or fouling. The technology was laboratory tested to define the tube/dimple design and acquire scale up data. The key overall targets for the entire project include: (a) design dimples into convective section tubes to increase fire-side heat transfer coefficients by over 30% without any increase in pressure drop, (b) maintain costs of Dimpled Tubes to be comparable to finned or studded tubes, and (c) demonstrate the Dimpled Tubes in a high temperature heater environment to: (i) increase overall fired process heater thermal efficiency by 3-5%, (ii) maintain/decrease fouling compared to smooth tubes/finned tubes, and (iii) effect a decrease in CO and NOx emissions and increase the burnout of any remaining combustibles in the combustion products.
Technical Approach	An experimental facility was designed, constructed, and tested especially for this study, including the manufacture of arrays of fully instrumented smooth tubes, shallow dimpled tubes, deep dimpled tubes. P&ID diagrams, and measurement system specifications were completed for the project. An experimental plan/matrix was developed for the experimental program. Experimental results were obtained which show the effects of adding deep dimples, and shallow dimples to 6 tubes, contained in a total bank of 14 tubes.
Results	Tube-averaged Nusselt number ratios for the deep dimpled tubes generally show only small variations with either $Re_{d\text{-}water}$ or $Re_{d\text{-}air}$. Comparisons of the results indicate that the highest heat transfer augmentations are measured on tube 2 (in the first upstream row of tubes), followed by tube 6 (in the second row of tubes). No augmentations are produced by tubes 10 and 13 (in the third and fourth rows). Tube-averaged Nusselt number ratios for the shallow dimpled tubes also generally show only small variations with either $Re_{d\text{-}water}$ or $Re_{d\text{-}air}$. The highest heat transfer augmentations are measured on tube 2 (in the first upstream row of tubes), followed by tube tube 10 (in the third row), and then by tube 13 (in the fourth row). No augmentations are produced by tube 6 (in the second row). A comparison of tube-averaged Nusselt numbers for the deep dimpled tubes for heating all 14 tubes and for heating 4 tubes only, shows that

significantly different values are measured for the two different heating arrangements, with higher tube-averaged Nusselt numbers when all 14 tubes are heated.

From comparisons of tube-averaged Nusselt numbers for the deep dimpled tubes, shallow dimpled tubes, and smooth, it is evident that the highest Nusselt numbers are obtained with deep dimpled tubes on the first row, smooth tubes on the second row, and shallow dimpled tubes on the third and fourth rows.

Comparisons of test section friction factors and Euler numbers shows that the highest Euler numbers and friction factors at each $Re_{d\text{-}air}$ are produced by the deep dimpled tubes. Values for the smooth and shallow dimpled tubes are then roughly the same magnitude at each value of $Re_{d\text{-}air}$. These data are obtained with a bank of 14 tubes total, with 6 tubes that have either shallow dimples or deep dimples.

If all 14 of the tubes in the tube bank contain shallow dimples, overall friction factor ratios range from 0.97 to 1.03, and overall Nusselt number ratios are estimated to range from 1.35 to 1.57. If all 14 of the tubes in the tube bank contain deep dimples, overall friction factor ratios range from about 1.08 to 1.12, and overall Nusselt number ratios are estimated to range from about 1.25 to approximately 1.40.

Project Implications

Significant heat transfer augmentations and reduced pressure penalties (compared to a bank of smooth tubes) can be produced by using dimples on the surfaces of the tubes employed in gas-fired process heaters for the Chemical Industry. Dimples augment surface heat transfer rates by producing arrays of vortex pairs which are shed from each dimple in a periodic manner. The increases in form drag and pressure losses provided by the dimples, as this occurs, is relatively minimal because of they do not protrude into the flow.

For a heat exchanger like the one investigated here, the most optimal heat transfer augmentation (with the minimum possible pressure drop penalty) will be obtained using deep dimpled tubes in row 1, smooth tubes in row 2, and shallow dimpled tubes in rows 3 and 4. For numerical code development, note that time-averaged predictions of flows over dimpled surfaces will be unable to capture some of the important physics in flows over dimpled surfaces, especially the unsteady vortex pair shedding which makes important contributions to surface heat transfer augmentation levels. To account for this in a time-averaged scheme, turbulence transport levels must be increased, however, the amount and distribution of eddy diffusivity values may not be easy to determine without additional detailed measurements of flows along dimpled surfaces.

GTI Project Manager

Yaroslav Chudnovsky
Combustion Technology
Gas Technology Institute
1700 South Mount Prospect Road
Des Plaines, IL 60018 - 1804

TABLE OF CONTENTS - Final Report
Dimpled Tube Development
Sponsored by the Gas Technology Institute

LIST OF SYMBOLS

A	test section flow cross-sectional area
A_s	total external surface area of all of the tubes in the tube bank.
$A_{surface}$	channel surface area for convective heat transfer, from the inlet of the test section, to the location where the local-mixed-mean temperature is determined
C	specific heat of water
C_p	air specific heat at constant pressure
D	outer tube diameter
Eu	Euler number based on pressure drop across the entire tube bank, $\Delta P / 0.5\rho V^2$
f	effective friction factor based on pressure drop across the entire tube bank, $\tau_o / 0.5\rho V^2$
f_o	baseline effective friction factor measured on smooth tubes, and based on pressure drop across the entire tube bank
h	local heat transfer coefficient, $\dot{q}_o'' / \Delta T$
k_{air-in}	thermal conductivity of air, based on the air temperature at the test section inlet
$\dot{m}_{air}$	air mass flow rate through the test section
$\dot{m}_w$	mass flow rate of water in one tube
Nu	Nusselt number measured on the dimpled tubes, hD / k_{air-in}
Nu_o	baseline Nusselt number measured on smooth tubes
$\dot{q}_o''$	surface convective heat flux from the tubes
$\mathrm{Re}_{\text{d-water}}$	Reynolds number based on average water velocity in one tube, and tube inner diameter
$\mathrm{Re}_{\text{d-air}}$	Reynolds number based on average air velocity at the inlet of the test section, and tube outer diameter
$T_{local-mixed-mean}$	local mixed-mean temperature
$T_{mm-inlet}$	local mixed-mean temperature at inlet of the test section
T_s	local surface temperature
T_{w-in}	temperature of the water at the tube inlet
T_{w-out}	temperature of the water at the tube outlet
V	spatially-averaged air velocity at the inlet of the test section
ΔT	temperature difference, $T_s - T_{local-mixed-mean}$
ΔP	streamwise pressure drop across the entire tube bank
ρ	air density based on inlet air temperature
τ_o	effective surface shear stress for the entire tube bank

I. INTRODUCTION

A. OVERALL OBJECTIVE

The overall objective of the project conducted at the University of Utah is to develop geometry/location recommendations for an effective tube surface profile for a tube bundle that is representative of a convective section in a gas-fired process heater for the Chemical Industry.

The overall goal of the portion of the project conducted at the University of Utah is to obtain more accurate information on heat transfer coefficients and friction factors as dependent upon relevant parameters for the tube bundle geometries. Activities in this task are thus arranged to give fundamental information and well as useful practical information on the effects of dimples on flow and heat transfer on the outsides of pipe surfaces.

B. BRIEF DESCRIPTION OF THE RESEARCH PROJECT

The work at the University of Utah is to perform physical modeling of dimpled profiles for CFD model validation, as well as developing the recommendations on effective dimple tube design for heat transfer enhancement with minimal pressure drop penalties. The key part of this effort is determination of optimal dimple pattern geometry of the tube bundle. The optimal arrangement is determined, by selecting the geometry arrangement tested, which gives the highest heat transfer augmentations with the lowest pressure penalties. This task involves tests on arrays of tubes with cross flow. Since liquid chemical product (ethylene, propylene, etc.) flows inside the tubes and combustion product cross flows the bundle of tubes, the dimple pattern is positioned on the outer surfaces of the tubes. Different dimple geometries are thus employed on the outsides of different tubes and tube arrays to determine optimal geometries for heat transfer enhancement with minimal pressure drops. The design of the dimple geometry, as well as the arrangement of the dimples on the tubes contained within each tube bank, were provided by GTI.

As mentioned above, the optimal dimple pattern and optimal design of the tube bundle was determined as part of this task, which was conducted at the University of Utah. Basic research was conducted to justify different geometry and design choices. The primary effects investigated were the influences of dimples geometry on bundle performance.

Measurements included local streamwise pressure drops as dependent upon streamwise distance, overall non-dimensional pressure drops, and peripherally averaged Nusselt numbers as dependent upon streamwise distance. This provided a global perspective of behavior of friction and heat transfer. Also measured were mass flow rates of air, mass flow rates of water, tube surface temperatures, test section inlet air temperatures, test section exit air temperatures, temperatures of water within the tubes as they enter into the test section, and temperatures of water within the tubes as they exit from the test section.

C. RATIONALE FOR UNDERTAKING THE RESEARCH PROJECT

The project is undertaken to determine the benefits, in the form of higher heat transfer augmentations and reduced pressure penalties, which can be produced by using dimples on the surfaces of the tubes employed in gas-fired process heaters for the Chemical Industry. Dimples augment surface heat transfer rates by producing arrays of vortex pairs which are shed from each dimple in a periodic manner. The increases in form drag and pressure losses provided by the dimples, as this occurs, are minimal because the dimples do not protrude into the flow. Form drag is defined as the pressure drop produced by an object which obstructs the flow in some manner.

II. TECHNICAL SECTION

A. WORK PLAN

The work plan involved 4 tasks overall.

Task 1. Design, develop, construct, fabricate, and assemble: (i) an experimental rig and (ii) thin-walled copper tubes with different test surfaces for testing. (iii) Also make measurement specifications. Due dates: (i) Dec. 31, 2001, (ii) smooth tubes-Nov. 30, 2001, (ii) dimpled tubes-Jan. 30, 2002, (iii) December 31, 2001. Deliverables: Drawings/sketches, P&ID (piping and instrumentation diagram), measurement system specifications.

Task 2. Develop an experimental plan/matrix. Due date was December 31, 2001. Deliverables: Experimental plan/matrix.

Task 3. Conduct experiments according to the plan/matrix, process data, and analyze results. Due date was March 15, 2002. Deliverables: Experimental data along with discussions of results.

Task 4. Preparation of final report and discussion of directions for future work. Due date was March 15, 2002. Deliverables: Final Report to GTI, which includes recommendations for the bench-scale unit design to be built and evaluated at GTI's Combustion Lab.

The experimental plan/matrix is as follows. The following surface arrangements were employed on the outsides of 6 of the tubes employed in the test section: (i) smooth, (ii) shallow dimples, (iii) deep dimples. A total of 14 cross-flow tubes were used. Of these, the 6 with different surface arrangements were removable. The following experimental parameters were measured for all 3 tube configurations at 3 different main flow Reynolds numbers, and at 3 different pipe flow Reynolds numbers.

(i) Dimensional and non-dimensional streamwise pressure drops in the mainflow passage.
(ii) Mass flow rates, temperatures, spatially-averaged velocities, and Reynolds numbers of the air and water.
(iii) Globally-averaged Nusselt numbers for heat transfer from the tube bank to the mainstream air.

B. WORK PERFORMED

For Task 1, all constructed items (smooth tubes, shallow dimpled tubes, deep dimpled tubes) were completed by January 30, 2002, including the P&ID diagrams, and measurement system specifications. Task 2, developing an experimental plan/matrix, was completed on December 31, 2001. Task 3, conducting experiments according to the plan/matrix, processing the data, and analyzing the results, was completed by March 15, 2002. Task 4, including the final report (first draft), was completed by March 31, 2002, including recommendations for the bench-scale unit design to be built and evaluated at GTI's Combustion Lab.

C. EXPERIMENTAL FACILITY DESCRIPTION, EXPERIMENTAL APPROACH DETAILS, EXPERIMENTAL RESULTS, EXPERIMENTAL UNCERTAINTY ESTIMATES

C.1. EXPERIMENTAL FACILITY DESCRIPTION, EXPERIMENTAL APPROACH DETAILS

Details of the experimental apparatus, developed especially for this study, are now described. Figure 1 shows a schematic and a photograph of the Dimpled Tube Heat Exchanger Test Facility. Figure 2 shows P&ID #1, with the test section layout, flow components, and some instrumentation and data acquisition equipment. This figure also shows the locations of the thermocouples used to measure the inlet air temperature. Figure 3 shows P&ID #2, with the test section layout, pressure tap locations, and tube arrangement, including the removable tubes. Figure 4, P&ID #3, shows the test section layout, flow components, and the instrumentation that is used on the removable tubes. Figure 5 subsequently gives P&ID #4 with the major components of the re-circulating water flow heating device. Figure 6 presents photographs of parts of the Dimpled Tube Heat Exchanger Test Facility, including: (a) the exit plenums, blower, computer, and data acquisition system, (b) the water heating device and test section, (c) the inlet nozzle and flow management devices, and (d) the test section and boundary layer bleed devices. Figure 7 then presents photographs of parts of the Dimpled Tube Heat Exchanger Test Facility, including: (a) the water heating device, (b) the total pressure probe and wall static pressure tap, and (c) the rotameter used to measure the water volumetric flow rate. Photographs and schematic diagrams showing the details of deep dimple tube geometry and shallow dimple tube geometry are given in Figures 8a and 8b, respectively.

Schematic diagrams and a photograph of the facility used for the heat transfer measurements are shown in Figs. 1, 2, and 3. The air used within the facility is circulated in an open-loop. As the air enters into the facility, it passes into a rectangular bell mouth inlet, followed by a honeycomb, two screens, and a two-dimensional nozzle with a contraction ratio of 4. This nozzles leads to a rectangular cross-section, inlet duct. This is located just upstream of the test section, which follows with the same cross-section dimensions. It exits to a large, rectangular plenum, which contains the blower. For all Reynolds numbers investigated, a Dayton 7C447 radial drive blower was employed to induce air flow through the test section. The air mass flow rate through the test section was determined (upstream of the tube bank) from measurements of the local air velocity and the local air density. The local air velocity was measured using a Kiel total pressure probe, a wall static pressure tap, and a Validyne M10 digital pressure manometer. The local air static density is based on the local air static temperature and the local air static pressure.

The mixed-mean stagnation temperature of the air entering the test section was measured using five calibrated copper-constantan thermocouples spread across the inlet cross-section. To determine this temperature, thermocouple-measured temperatures were corrected for thermocouple wire conduction losses, channel velocity variations, as well as for the differences between stagnation and recovery temperature. Magnitudes of the local mixed mean temperatures at different locations though the test section were then determined using energy balances, and the mixed mean temperature at the inlet of the test

section. The thermal conductivity used to determine local Nusselt numbers was based on the test section inlet temperature.

Five calibrated copper-constantan thermocouples are also spread over the exit of the test section duct. Mixed-mean temperatures, estimated from measured temperatures, match values determined from energy balances within 10-30 percent for all experimental conditions investigated. All measurements were obtained when the test facility is at steady-state, achieved when each of the temperatures from the thermocouples installed on the dimpled tubes, vary by less than $0.3\,^{\circ}\mathrm{C}$ over a 10 minute period.

To determine the surface heat flux (used to calculate heat transfer coefficients and local Nusselt numbers), the total convective power level, provided by each dimpled tube was measured based on an energy balance of the water passing through that tube. The overall water volumetric flow rate was measured using a single rotameter capable of operating with water at temperatures up to $100\,^{\circ}\mathrm{C}$. When 4 tubes were employed for heating, mass flow regulating valves were employed and adjusted so that the water mass flow rate in each of the 4 tubes was the same. All surface temperatures, and the temperatures of water and air were measured using calibrated, copper-constantan thermocouples. Voltages from the thermocouples were acquired using a Hewlett-Packard 44422T data acquisition card installed in a Hewlett-Packard 3497A data acquisition control unit, which was controlled by a Hewlett-Packard A4190A Series computer.

The heat flux from the tubes $\dot{q}_o''$ is determined using an energy balance around the water flowing into and out of the tubes, which is given by

$$\dot{q}_o'' = \dot{m}_w C(T_{w-in} - T_{w-out})$$

where $\dot{m}_w$ is the mass flow rate of water in one tube, C is the specific heat of water, T_{w-in} is the temperature of the water at the tube inlet, and T_{w-out} is the temperature of the water at the tube outlet. The heat transfer coefficient h and Nusselt number Nu are then determined using

$$Nu = hD/k_{air-in} \qquad\qquad h = \dot{q}_o''/\Delta T$$

respectively, where

$$\Delta T = T_s - T_{local-mixed-mean}$$

In these equations, k_{air-in} is the thermal conductivity of air, based on the air temperature at the test section inlet, and T_s is the local surface temperature. Nu_o utilizes the same Nusselt definition as above, but is used when values are measured on smooth tubes. The local mixed-mean temperature is determined through the tube bundle using energy balance equations, which are given by

$$T_{local-mixed-mean} = T_{mm-inlet} + \dot{q}_o'' A_{surface}/\dot{m}_{air} C_p$$

Here, $A_{surface}$ represents the channel surface area for convective heat transfer, from the inlet of the test section, to the location where the local-mixed-mean temperature is determined.

Wall static pressures are measured along the test section simultaneously as the heat transfer measurements are conducted, using static pressure taps, located along one of the test section side walls. The locations of these static pressure taps are shown in Figs. 2 and 3. These measurements are made with dimpled tubes placed in the test section, as well as with a baseline test section which employs smooth tubes. Friction factors and Euler numbers are then determined from streamwise pressure gradient magnitudes. With this approach, the Euler number is given by

$$Eu = \Delta P / 0.5 \rho V^2$$

Friction factors are determined using

$$f = \tau_o / 0.5 \rho V^2$$

The relation between the effective surface shear stress for the entire tube bank τ_o, and the overall pressure drop for the entire tube bank ΔP, is then given by

$$\tau_o = \Delta P \left(A / A_s \right)$$

where A is the flow cross-sectional area, and A_s is the total external surface area of all of the tubes in the tube bank.

Pressures from the wall pressure taps are measured using Celesco LCVR pressure transducers. Signals from these transducers are processed using Celesco CD10D Carrier-Demodulators. Voltages from the Carrier-Demodulators are acquired using a Hewlett-Packard 44422A data acquisition card installed in a Hewlett-Packard 3497A data acquisition control unit, which is controlled by a Hewlett-Packard A4190A Series computer. With this apparatus, 100 sequential measurements are acquired and measured from each pressure transducer, over a time period of about 20 seconds.

C.2. EXPERIMENTAL RESULTS

Figure 9 shows the variation of the local mixed mean temperature $T_{local-mixed-mean}$ with tube row for deep dimpled tubes, $Re_{d\text{-}air}$=12700 and $Re_{d\text{-}water}$=3460. Here, $Re_{d\text{-}air}$ is the air Reynolds number, which is based on average test section air inlet velocity and outside tube diameter. $Re_{d\text{-}water}$ is then the water-side Reynolds number, which is based on average water velocity inside of one tube, and the inside tube diameter D. These data are obtained with all 14 tubes heated and show the variation of mixed mean temperature with streamwise development, where the local mixed mean temperature throughout the tube bundle is determined using energy balances applied to successive tube rows. Note that the measured energy at the outlet of the test section is about equivalent in magnitude to the energy determined from an energy balance around the heated tubes. The measured

values are slightly lower due to conduction losses from the heated tubes. In spite of this small difference, the agreement between the measured outlet mixed mean temperature and the value from the energy balance validates the energy balances employed, which are applied to the test section.

A similar conclusion is also provided by the local mixed mean temperature data for other experimental conditions for the deep dimpled tubes, and for all experimental conditions investigated with the shallow dimpled tubes. In this case, these data are obtained with 4 tubes heated and show the variation of mixed mean temperature with streamwise development, where the local mixed mean temperature throughout the tube bundle is again determined using energy balances applied to successive tube rows.

Figure 10 gives tube-averaged Nusselt number ratios for the deep dimpled tubes for $Re_{d\text{-}air}$=10600. Figure 11 gives tube-averaged Nusselt number ratios for the deep dimpled tubes for $Re_{d\text{-}air}$=11300 and $Re_{d\text{-}air}$=12000. Each ratio represents a dimpled tube value divided by a smooth tube value. All of these data are obtained with only 4 tubes heated. This approach is employed because it results in data with lower experimental uncertainties than if heating is utilized in all 14 tubes. The results in Figures 10 and 11 show only small variations with either $Re_{d\text{-}water}$ or $Re_{d\text{-}air}$, apart from the data scatter which is present. Comparisons of the results indicate that the highest heat transfer augmentations are measured on tube 2 (in the first upstream row of tubes), followed by tube 6 (in the second row of tubes). No augmentations are produced by tubes 10 and 13 (in the third and fourth rows), as indicated by tube averaged Nusselt number ratios less than 1.

Several different physical effects are responsible for the variations shown in Figures 10 and 11. These include: (i) the increased mixing induced into the flow by the presence of the dimples on the surfaces of the tubes, (ii) the development and shedding of multiple vortex pairs by the flow as it is periodically ejected from each dimple, (iii) the unsteadiness of the flow as it is advected around the tubes, in the vicinity of the dimples, and then to the vicinity of tubes located farther downstream, (iv) the separated flow which develops within each dimple, (v) the advection of heat produced by the secondary flows shed from each dimple, and (vi) the increases in turbulent diffusion, which are caused by the flow which is periodically ejected from the dimples. These different effects are often in competition with each other. For example, the dominance of certain effects causes the heat transfer to be less than values measured on smooth tubes (at the same experimental conditions), whereas the dominance of other effects causes the heat transfer to be greater than values measured on smooth tubes (at the same experimental conditions). The higher values on tubes 2 and 6, shown in Figures 10 and 11, are likely due to stagnation point heat transfer effects on the first two rows of tubes and the high speeds of the fluid as is moves around these tubes. The lower Nusselt number ratios on tubes 10 and 13 (on the third and fourth streamwise rows of tubes) are speculated to be due to the absence of well defined stagnation regions, lower speeds in the fluid as is moves around these tubes, and more well developed re-circulating flows within the dimples that act like insulating pockets of air.

Figure 12 presents a comparison of tube-averaged Nusselt numbers for the deep dimpled tubes for heating all 14 tubes and for heating 4 tubes only. These data are given for $Re_{d\text{-}}$

$_{air}$=11400 and $Re_{d\text{-}water}$=3600. Significantly different values are measured for the two different heating arrangements, with higher tube-averaged Nusselt numbers when all 14 tubes are heated. Such differences are partially due to the effect of either heating or non-heating of the air around tubes located in the downstream part of the tube bank, by tubes which are located farther upstream in the tube bank. The differences, due to different thermal boundary conditions, are thus related to the coupling between the momentum and energy equations in variable property flows.

Figure 13 gives tube-averaged Nusselt number ratios for the shallow dimpled tubes for $Re_{d\text{-}air}$=10600. Figure 14 then presents tube-averaged Nusselt number ratios for the shallow dimpled tubes for $Re_{d\text{-}air}$=11300. Figure 15 presents tube-averaged Nusselt number ratios for the shallow dimpled tubes for $Re_{d\text{-}air}$=12000. All of these data are obtained with only 4 tubes heated. The results show only small variations with either $Re_{d\text{-}water}$ or $Re_{d\text{-}air}$, apart from the data scatter which is present. Comparisons of the results indicate that the highest heat transfer augmentations are measured on tube 2 (in the first upstream row of tubes), followed by tube tube 10 (in the third row), and then by tube 13 (in the fourth row). No augmentations are produced by tube 6 (in the second row), as indicated by tube averaged Nusselt number ratios less than 1.

The higher values on tube 2 in Figures 13, 14, and 15 are likely due to stagnation point heat transfer effects on the first row of tubes and the high speeds of the fluid as is moves around these tubes. Because of the high heat transfer in this first row of tubes, the air around the tubes in the second row (containing tube 6) is then heated appreciably. This then leads to Nusselt number ratios less than 1.0 at this location. The lower Nusselt number ratios on tube 6 are also speculated to be due to the absence of well defined stagnation regions, and perhaps lower speeds in the fluid as is moves around these tubes. Some recovery of the thermal flow then occurs as it advects father downstream, as evidenced by increased Nusselt number ratio magnitudes for tubes 10 and 13 (in the third and fourth streamwise rows). Here, increased secondary advection and increased magnitudes of turbulence diffusion are probably responsible for the Nusselt number ratios which are generally greater than 1.0. The different tube-averaged Nusselt number ratios in Figures 13, 14, and 15 are probably also related to different amplitudes and frequencies of the unsteady fluid structures which are shed from individual dimples, as well as each tube as it is subject to cross-flow.

Comparisons of tube-averaged Nusselt numbers for the deep dimpled tubes, shallow dimpled tubes, and smooth tubes are given in Figure 16 for $Re_{d\text{-}air}$=11400 and $Re_{d\text{-}water}$=5100. From these data, at this particular experimental condition, it is evident that the highest Nusselt numbers are obtained with deep dimpled tubes on the first row, smooth tubes on the second row, and shallow dimpled tubes on the third and fourth rows. These differences are due to different physical effects, which affect the transport of heat more strongly at some locations, than at others. For example, higher Nusselt number ratios are measured when the periodic development and shedding of multiple vortex pairs leads to increased mixing, increased secondary flow advection of heat, and increased turbulent diffusion. Lower Nusselt number ratios are measured when the separated flow which develops within each dimple leads to a region of stagnate air, which acts like an insulator.

Figures 17 and 18 present tube-averaged Nusselt numbers, measured on the tubes with smooth surfaces, and no dimples. These baseline data can be used to deduce Nusselt number values, from the Nusselt number ratio data presented in Figures 10, 11, 13, 14, and 15.

Figure 19 shows comparisons of test section friction factors for the deep dimpled tubes, shallow dimpled tubes, and smooth tubes for different $Re_{d\text{-}air}$. Figure 20 shows comparison of test section Euler numbers for the deep dimpled tubes, shallow dimpled tubes, and smooth tubes for different $Re_{d\text{-}air}$. Friction factors are determined using shear stress values, which are based upon the surface area of all of the tubes employed in the tube bank. The highest Euler numbers and friction factors in Figs. 19 and 20, at each Reynolds number, are produced by the deep dimpled tubes. Values for the smooth and shallow dimpled tubes are then roughly the same magnitude at each value of $Re_{d\text{-}air}$. The data in both of these figures are obtained with 14 tubes total in the bank, with 6 tubes that have either shallow dimples or deep dimples.

Friction factor ratios (dimpled surface friction factors divided by smooth tube friction factors) for the deep dimpled tubes, and shallow dimpled tubes for different $Re_{d\text{-}air}$ are given in Figure 21. Note that the f/f_o ratio is the same as the ratio of dimpled surface Euler number Eu to smooth surface Euler number. The data in this figure are also obtained with 14 tubes total in the bank, with 6 tubes that have either shallow dimples or deep dimples. The data in Figure 21 show augmentations of about 10 percent for the deep dimples, and from -2 percent to +2 percent for the shallow dimples.

In Figure 22, estimates of overall Nusselt number ratios and overall friction factor ratios for the entire test section for the deep dimpled tubes, and shallow dimpled tubes are presented for different $Re_{d\text{-}air}$. The estimated values are determined for a test section with a total either 14 tubes with shallow dimples or 14 tubes with deep dimples. Overall, the results suggest better overall performance is given by the shallow dimpled tubes, compared to the tubes with deep dimples.

To determine the overall friction factor ratios given in Fig. 22, the first step it to take f/f_o, the friction factor ratios in Figure 21 (which are obtained with 14 tubes total, of which 6 contain either shallow dimples or deep dimples), and then subtract the smooth contribution by subtracting 1.0 from each value. After this, these values are multiplied by 14/6 to obtain value representative of a tube bank arranged such that all 14 of tubes have either shallow dimples or deep dimples. This value is then added to 1.0 to give the $(f/f_o)_{overall}$ values which are plotted in Figure 22. A similar approach is used to obtain the overall Nusselt number ratios $(Nu/Nu_o)_{overall}$ which are also presented in Figure 22. In equation form, these approaches are given by

$$(f/f_o)_{overall} = (f/f_o - 1)(14/6) + 1.0$$

and

$$(Nu/Nu_o)_{overall} = (Nu/Nu_o - 1)(14/6) + 1.0$$

respectively.

C.3. EXPERIMENTAL UNCERTAINTY ESTIMATES

Uncertainty estimates are based on 95 percent confidence levels. Uncertainty of temperatures measured with thermocouples is ±0.4°C. Local Nusselt number uncertainty is then about ±8.9 percent. Corresponding Nusselt number ratio uncertainty is about ±0.25 (for a ratio of 2.00), or ±12.6 percent. Note that Nusselt number uncertainty values consider variations of the water mass flow rate from one tube to another. The uncertainty of friction factors (for both smooth tubes and dimpled tubes) is about ±12.0 percent. Reynolds number uncertainty is about ±2.0 percent for $Re_{d\text{-}air}$ of 12,000.

D. FINDINGS

Tube-averaged Nusselt number ratios for the deep dimpled tubes generally show only small variations with either $Re_{d\text{-}water}$ or $Re_{d\text{-}air}$. Comparisons of the results indicate that the highest heat transfer augmentations are measured on tube 2 (in the first upstream row of tubes), followed by tube 6 (in the second row of tubes). No augmentations are produced by tubes 10 and 13 (in the third and fourth rows).

A comparison of tube-averaged Nusselt numbers for the deep dimpled tubes for heating all 14 tubes and for heating 4 tubes only, shows that significantly different values are measured for the two different heating arrangements, with higher tube-averaged Nusselt numbers when all 14 tubes are heated.

Tube-averaged Nusselt number ratios for the shallow dimpled tubes also generally show only small variations with either $Re_{d\text{-}water}$ or $Re_{d\text{-}air}$. The highest heat transfer augmentations are measured on tube 2 (in the first upstream row of tubes), followed by tube tube 10 (in the third row), and then by tube 13 (in the fourth row). No augmentations are produced by tube 6 (in the second row).

From comparisons of tube-averaged Nusselt numbers for the deep dimpled tubes, shallow dimpled tubes, and smooth, it is evident that the highest Nusselt numbers are obtained with deep dimpled tubes on the first row, smooth tubes on the second row, and shallow dimpled tubes on the third and fourth rows.

Comparisons of test section friction factors and Euler numbers shows that the highest Euler numbers and friction factors at each $Re_{d\text{-}air}$ are produced by the deep dimpled tubes. Values for the smooth and shallow dimpled tubes are then roughly the same magnitude at each value of $Re_{d\text{-}air}$. These data are obtained with a bank of 14 tubes total, with 6 tubes that have either shallow dimples or deep dimples.

If all 14 of the tubes in the tube bank contain shallow dimples, overall friction factor ratios range from 0.97 to 1.03, and overall Nusselt number ratios are estimated to range from 1.35 to 1.57. If all 14 of the tubes in the tube bank contain deep dimples, overall friction factor ratios range from about 1.08 to 1.12, and overall Nusselt number ratios are estimated to range from about 1.25 to approximately 1.40.

III. MAJOR ACHIEVEMENTS OF THE RESEARCH PROJECT

An experimental facility was designed, constructed, and tested especially for this study, including the manufacture of arrays of fully instrumented smooth tubes, shallow dimpled

tubes, deep dimpled tubes. P&ID diagrams, and measurement system specifications were completed for the project. An experimental plan/matrix was developed for the experimental program. Experimental results were obtained which show the effects of adding deep dimples, and shallow dimples to 6 tubes, contained in a total bank of 14 tubes.

IV. MAJOR TECHNICAL PROBLEM AREAS ENCOUNTERED

During the course of the subcontract performance, three major technical hurdles were faced and overcome.

Tube heating. Originally, the tests were conducted with heating in all 14 tubes for the smooth and deep dimple configurations. Because of the difficulty in maintaining the same mass flow rate in each tube, the data associated with this arrangement had very high experimental uncertainties. Consequently, these data were repeated, and all subsequent data were obtained with heating in only 4 tubes, which were fully instrumented. This approach then resulted in higher quality data with less scatter and random variability.

Smoke visualizations. Smoke visualizations of the flow behavior around the tubes were planned in the original proposal scope of work. However, the detailed analysis of measurement approach in the beginning of the work led us to conclusion that information gained from visual observation will not be so useful for reaching the subcontract goals as reliability of the heat transfer and pressure drop results, so originally budgeted funds and time were reallocated to repeat data collection with heating in 4 tubes instead of heating in all 14 tubes. Anyway, flow visualizations and flow structural measurement studies can be conducted at a future data under follow on project. This would provide with additional information, which would further enhance our ability to interpret the heat transfer data, and to develop tube bundles with even better heat transfer enhancement rates.

Cooling agent (nitrogen). Another option considered in the original project plan was the use of liquid nitrogen to cool the mainstream air. As the facility was designed, the "nitrogen approach" was reconsidered and less expensive approach was selected and utilized. This approach involved heating the water used in the tubes of the experimental facility (with no mainstream air heating or cooling). This approach was more viable from a technical point of view (than using liquid nitrogen for mainstream air cooling) because there would be much difficulty in forcing the mainstream air at sufficient flow rates through a heat exchanger located in the main air passage. Such a heat exchanger would also add significant disturbances to the flow as it approached the tube bank. The use of water heating, instead of mainstream air cooling, thus provided a means to improve the experimental approach which was utilized without sacrificing measurement accuracy.

V. CONCLUSIONS

Significant heat transfer augmentations and reduced pressure penalties (compared to a bank of smooth tubes) can be produced by using dimples on the surfaces of the tubes employed in gas-fired process heaters for the Chemical Industry. Dimples augment surface heat transfer rates by producing arrays of vortex pairs which are shed from each dimple in a periodic manner. The increases in form drag and pressure losses provided by the dimples, as this occurs, is relatively minimal because of they do not protrude into the

flow. For example, if all 14 of the tubes in the tube bank contain shallow dimples, overall friction factor ratios are estimated to range from 0.97 to 1.03, and overall Nusselt number ratios are estimated to range from 1.35 to 1.57. If all 14 of the tubes in the tube bank contain deep dimples, overall friction factor ratios range from about 1.08 to 1.12, and overall Nusselt number ratios are estimated to range from about 1.25 to approximately 1.40.

VI. RECOMMENDATIONS

For a heat exchanger like the one investigated here, the most optimal heat transfer augmentation (with the minimum possible pressure drop penalty) will be obtained using deep dimpled tubes in row 1, smooth tubes in row 2, and shallow dimpled tubes in rows 3 and 4. The flow in the tube bundle is believed to be highly unsteady. Because of this, time-averaged predictions of flows over dimpled surfaces will be unable to capture some of the important physics in flows over dimpled surfaces, especially the unsteady vortex pair shedding which makes important contributions to surface heat transfer augmentation levels. To account for this in a time-averaged scheme, turbulence transport levels must be increased, however, the amount and distribution of eddy diffusivity values require additional detailed measurements of flows along dimpled surfaces.

DIMPLED TUBE HEAT EXCHANGER TEST FACILITY

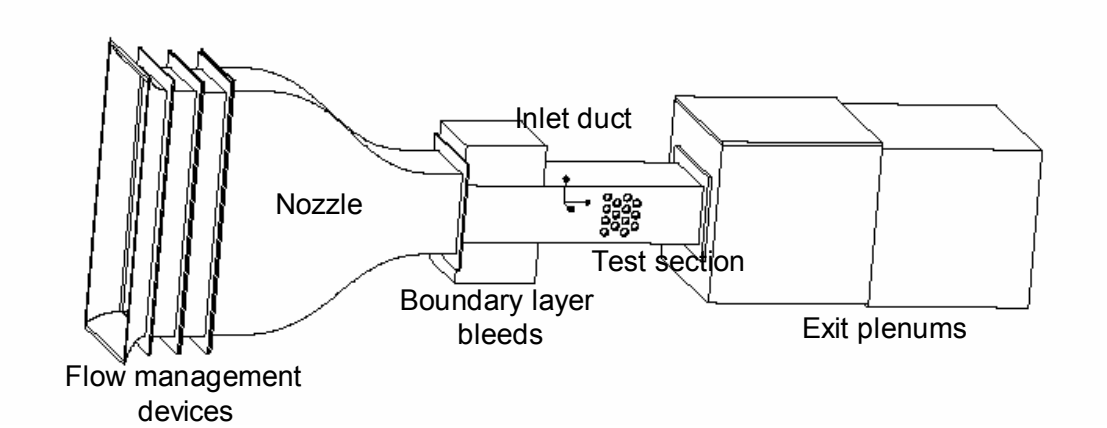

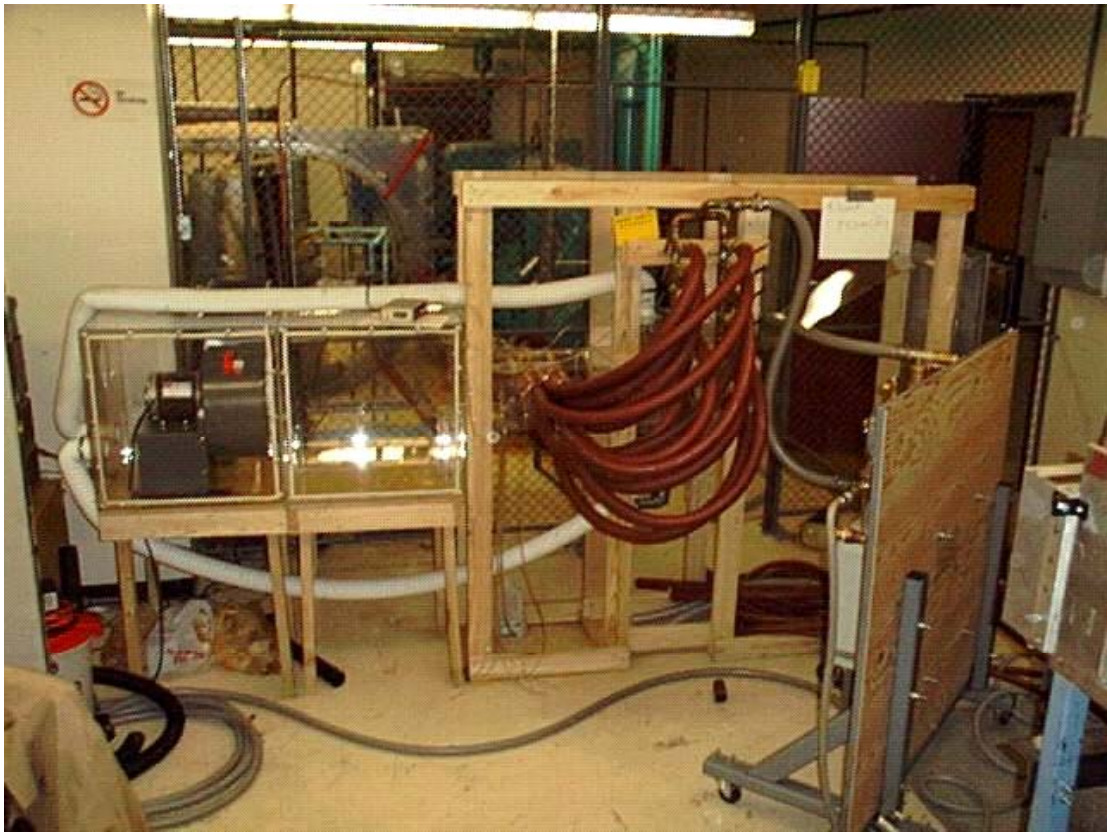

Figure 1. Schematic and photograph of Dimpled Tube Heat Exchanger Test Facility.

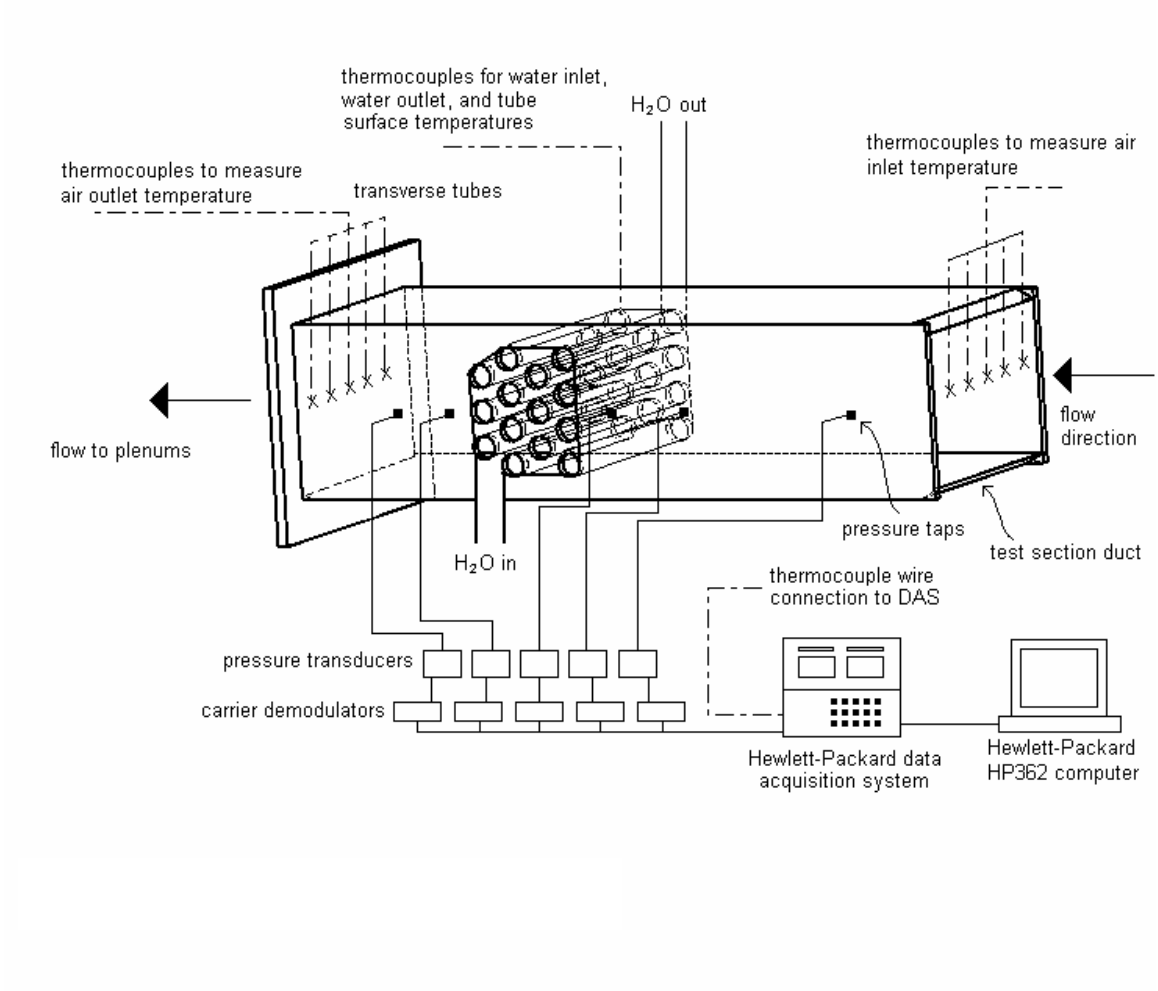

Figure 2. P&ID #1 showing test section layout, flow components, and some instrumentation and data acquisition equipment.

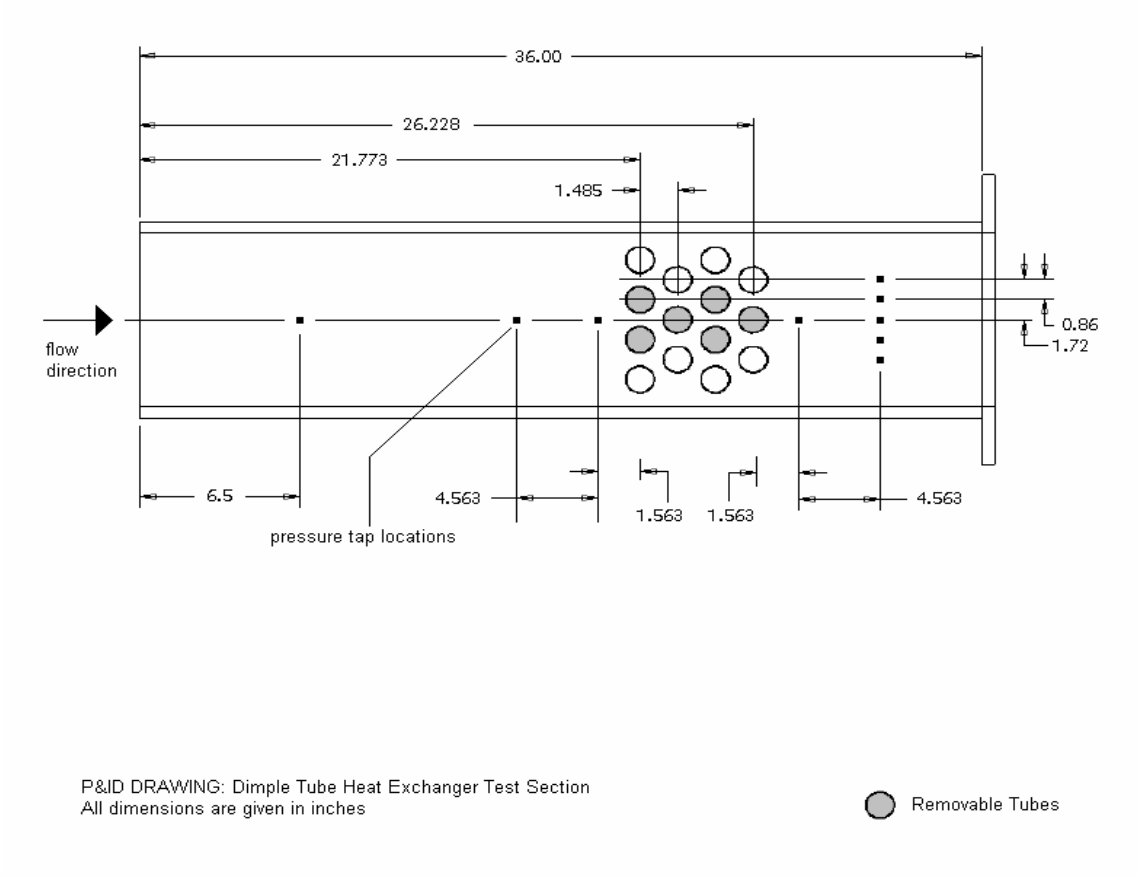

Figure 3. P&ID #2 showing test section layout, pressure tap locations, and tube arrangement, including the removable tubes. All dimensions are given in inches.

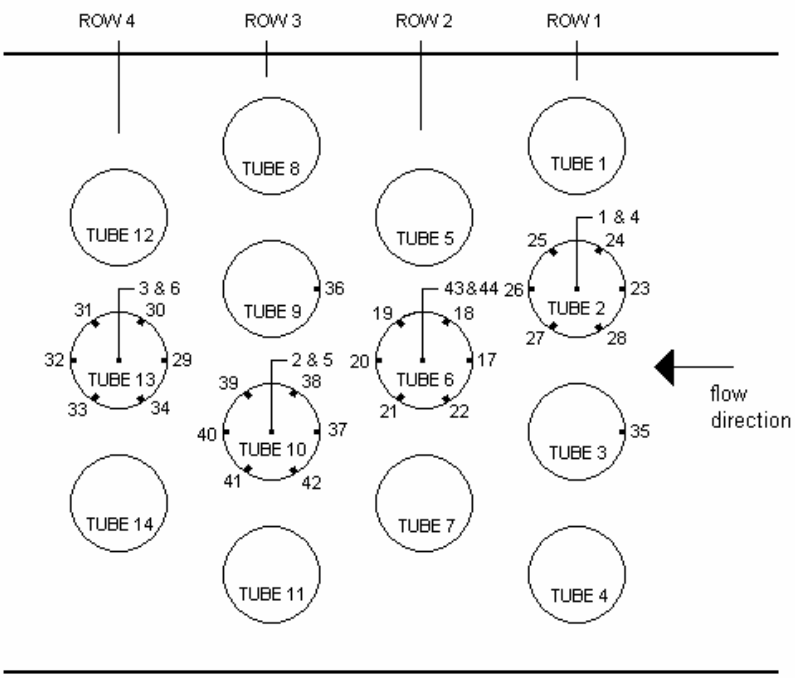

TC	POSITION/DESCRIPTION
1	Temp in of H2O, tube 2
2	Temp in of H2O, tube 10
3	Temp in of H2O, tube 13
4	Temp out of H2O, tube 2
5	Temp out of H2O, tube 10
6	Temp out of H2O, tube 13
7-11	Temp in of air
12-16	Temp out of air
17-22	Surface temp of tube 6
23-28	Surface temp of tube 2
29-34	Surface temp of tube 13
35	Surface temp of tube 3
36	Surface temp of tube 9
37-42	Surface temp of tube 10
43	Temp in of H2O, tube 6
44	Temp out of H2O, tube 6

Figure 4. P&ID #3 showing test section layout, flow components, and the instrumentation that is used on the removable tubes.

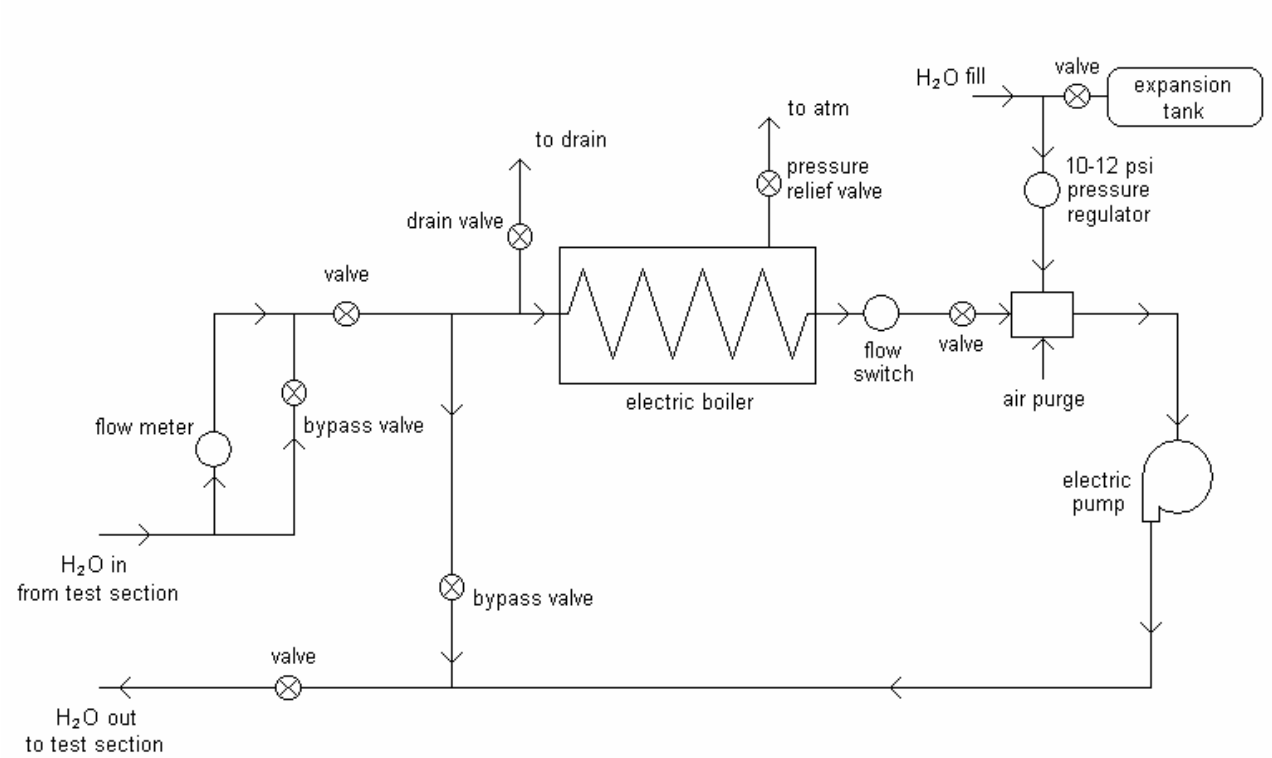

Figure 5. P&ID #4 showing the major components of the re-circulating water flow heating device.

(a)

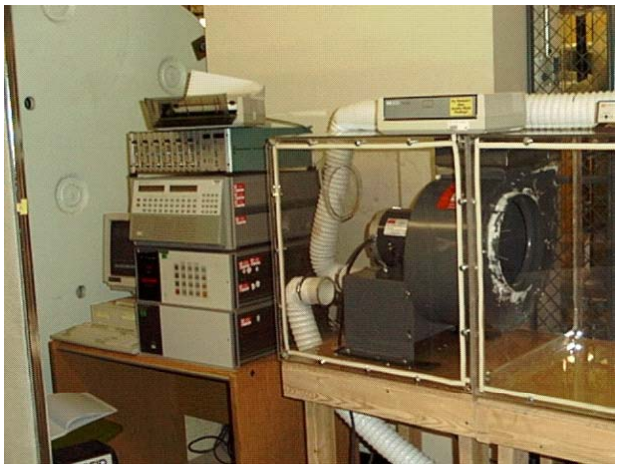

(b)

(c)

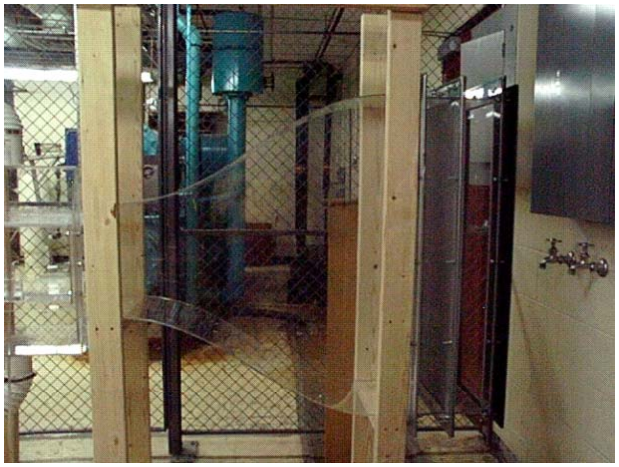

(d)

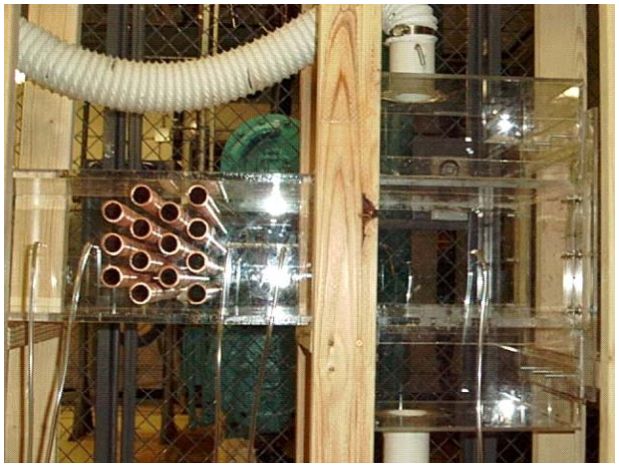

Figure 6. Photographs of parts of the Dimpled Tube Heat Exchanger Test Facility, including: (a) the exit plenums, blower, computer, and data acquisition system, (b) the water heating device and test section, (c) the inlet nozzle and flow management devices, and (d) the test section and boundary layer bleed devices.

(a)

(b)

(c)

Figure 7. Photographs of parts of the Dimpled Tube Heat Exchanger Test Facility, including: (a) the water heating device, (b) the total pressure probe and wall static pressure tap, and (c) the rotameter used to measure the water volumetric flow rate.

Instrumented tubes, deep dimples

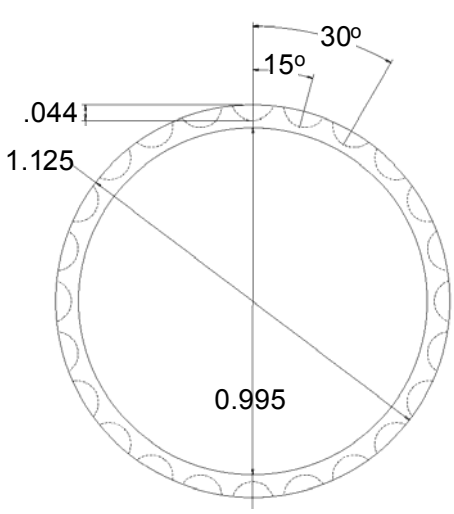

All dimensions in inches

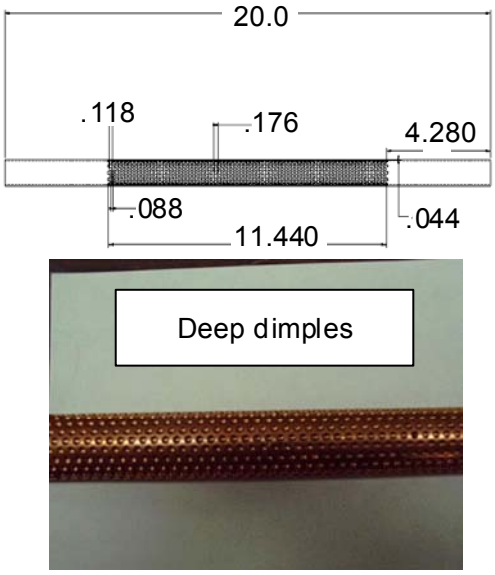

Deep dimple geometry

- Dimples have a spherical diameter of 0.123”
- The spherical tool (ball endmill) creates a dimple 0.044” deep, with a print diameter of 0.118”
- The dimples have a radial spacing of 30° with 12 dimples per row
- Additional rows are offset by 0.088” axially and 15° radially
- Center of the first row is placed 4.280” from end of the tube
- 131 rows of dimples
- 131 x 12 = 1572 dimples per tube
- 6 tubes with this dimple geometry and spacing
- All dimensions have a manufacturing tolerance of ±0.001”

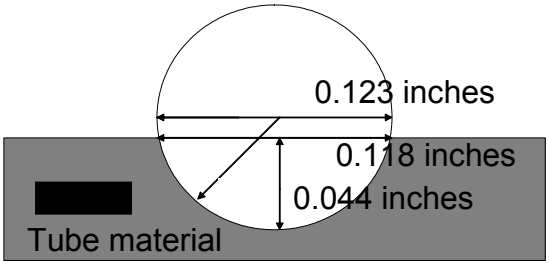

Figure 8a. Photographs and schematic diagrams showing the details of deep dimple tube geometry.

Instrumented tubes, shallow dimples

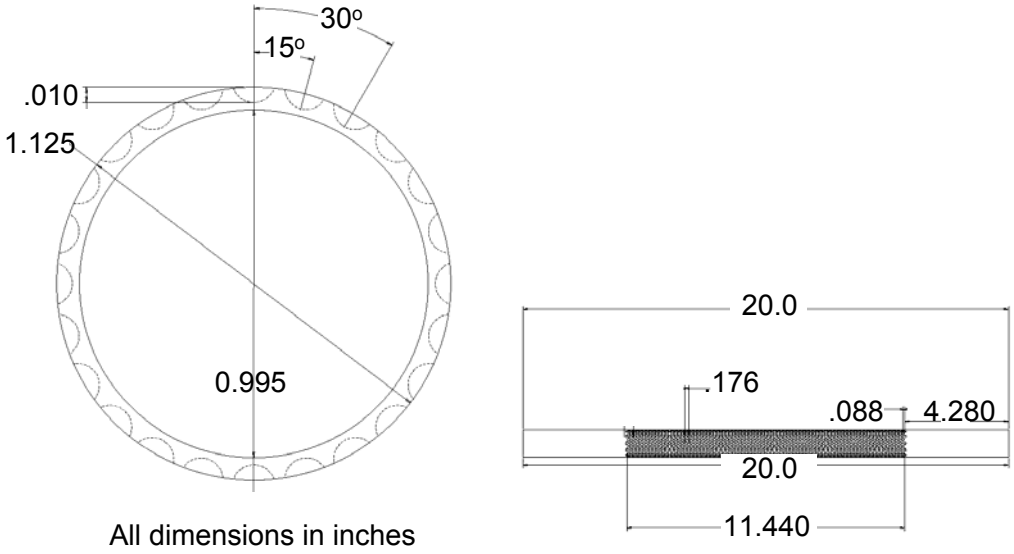

All dimensions in inches

Shallow dimple geometry

- Dimples have a spherical diameter of 0.369”
- The spherical tool (ball endmill) creates a dimple 0.010” deep with a print diameter of 0.118”
- The dimples have a radial spacing of 30° with 12 dimples per row
- Additional rows are offset by 0.088” axially and 15° radially
- Center of the first row is placed 4.280” from end of the tube
- 131 rows of dimples
- 131 x 12 = 1572 dimples per tube
- 6 tubes with this dimple geometry and spacing
- All dimensions have a manufacturing tolerance of ±0.001”

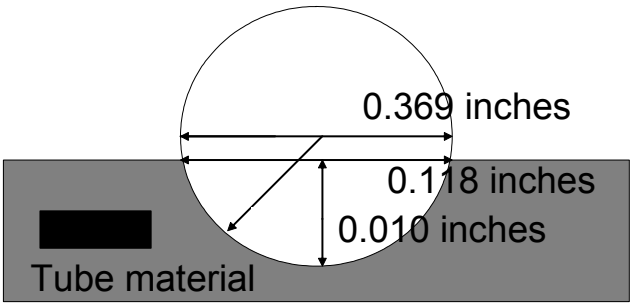

Figure 8b. Schematic diagrams showing the details of shallow dimple tube geometry.

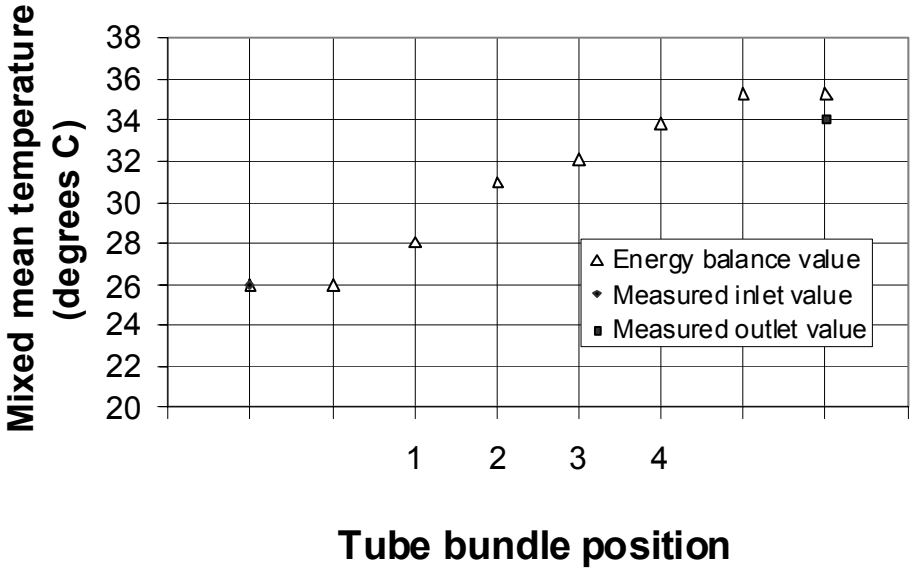

Figure 9. Variation of mixed mean temperature with tube row for deep dimpled tubes, $Re_{d\text{-}air}$=12700 and $Re_{d\text{-}water}$=3460, showing that the measured energy at the outlet of the test section is equivalent in magnitude to the energy determined from an energy balance around the heated tubes.

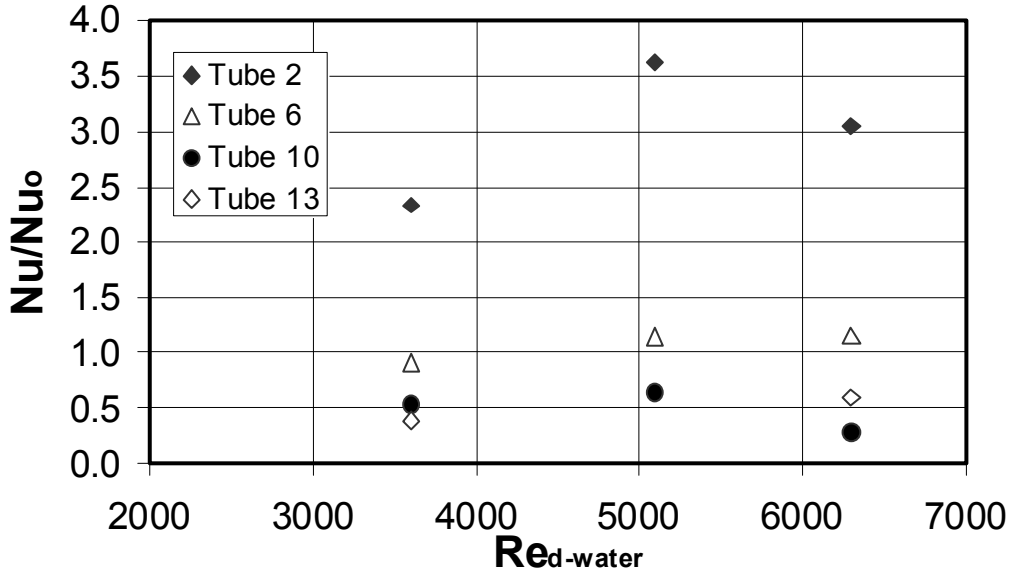

Figure 10. Tube-averaged Nusselt number ratios for the deep dimpled tubes for $Re_{d\text{-}air}$=10600.

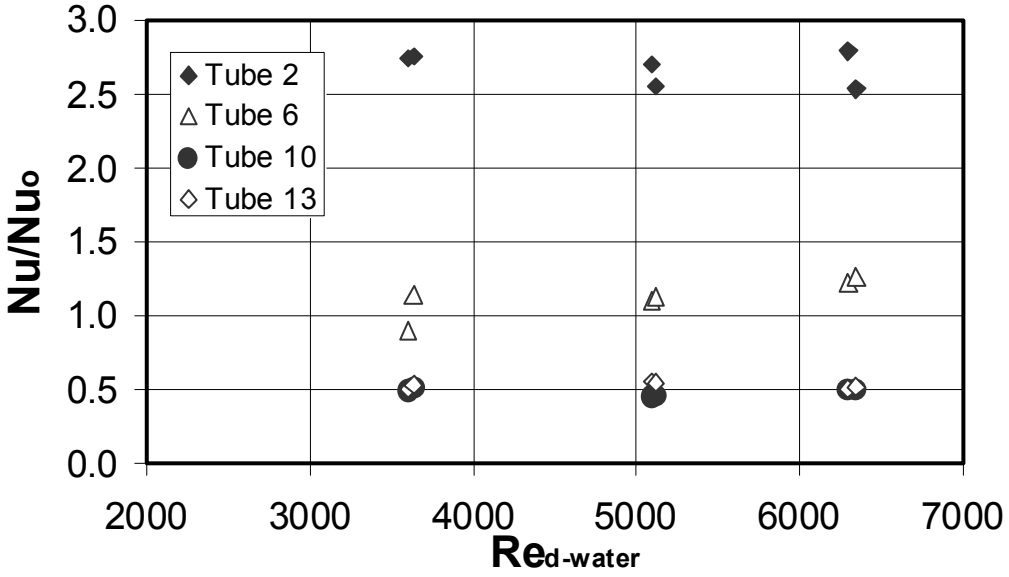

Figure 11. Tube-averaged Nusselt number ratios for the deep dimpled tubes for $Re_{d\text{-}air}$=11300 and $Re_{d\text{-}air}$=12000.

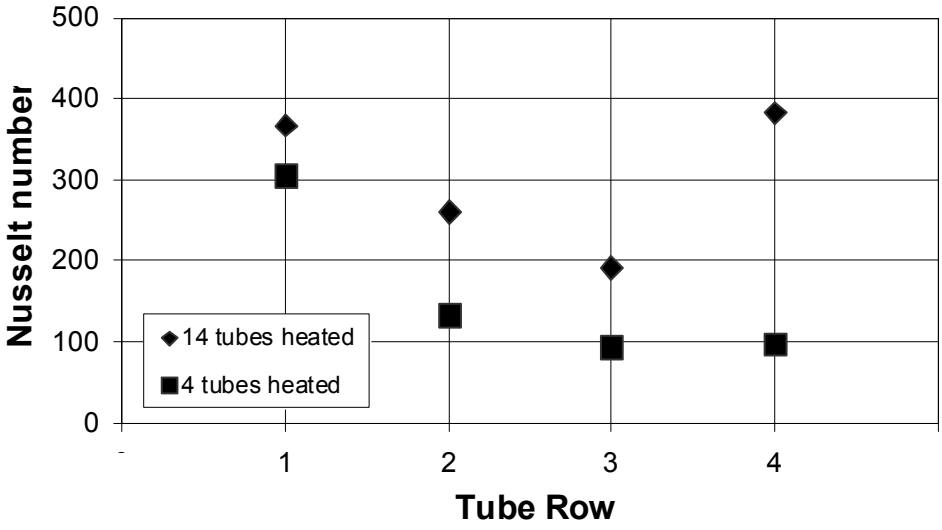

Figure 12. Comparison of tube-averaged Nusselt numbers for the deep dimpled tubes for heating all 14 tubes and for heating 4 tubes only, for $Re_{d\text{-}air}$=11400 and $Re_{d\text{-}water}$=3600.

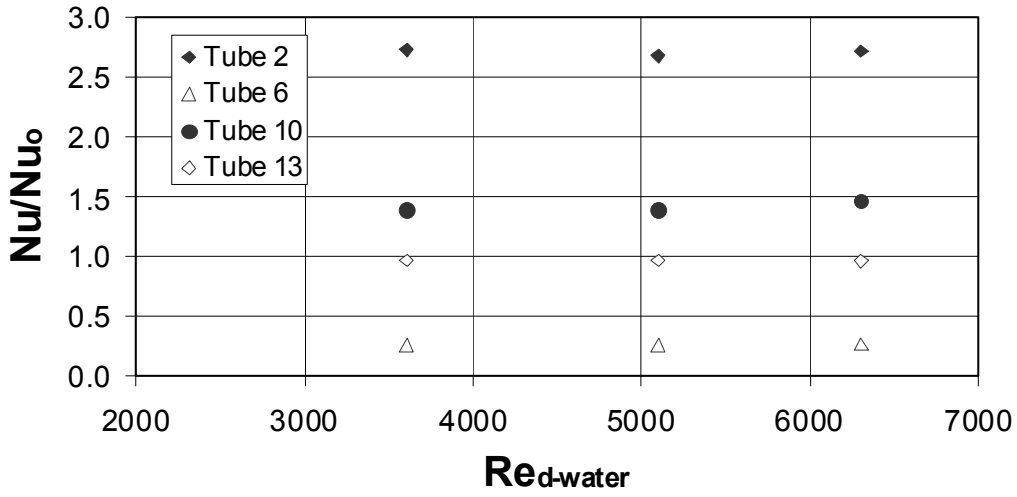

Figure 13. Tube-averaged Nusselt number ratios for the shallow dimpled tubes for $Re_{d\text{-}air}$=10600.

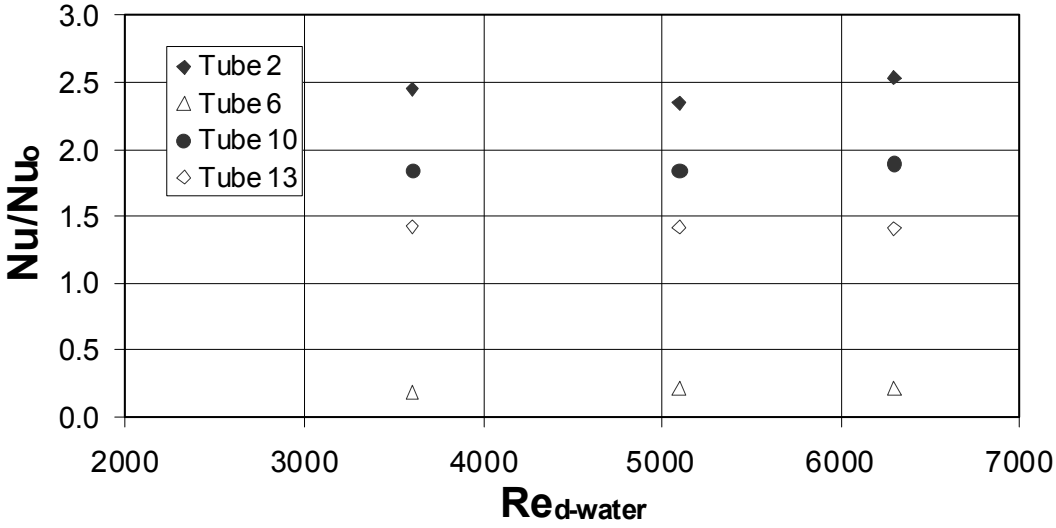

Figure 14. Tube-averaged Nusselt number ratios for the shallow dimpled tubes for $Re_{d\text{-}air}$=11300.

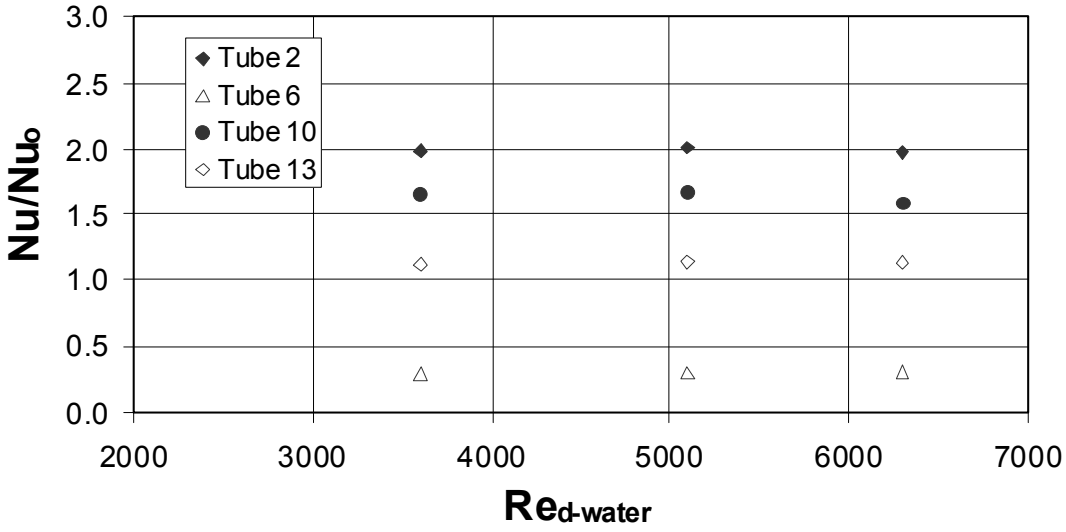

Figure 15. Tube-averaged Nusselt number ratios for the shallow dimpled tubes for $Re_{d\text{-}air}$=12000.

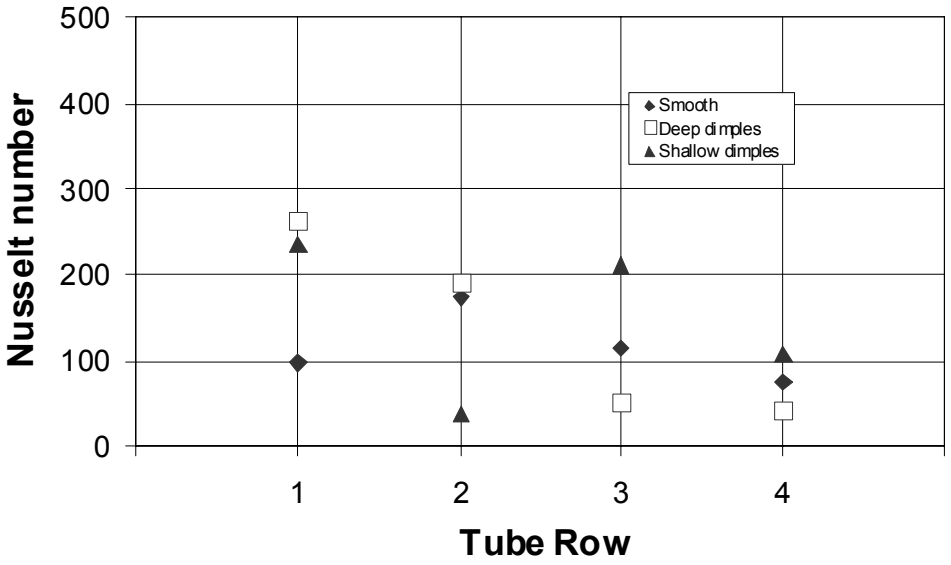

Figure 16. Comparison of tube-averaged Nusselt numbers for the deep dimpled tubes, shallow dimpled tubes, and smooth tubes for $Re_{d\text{-}air}$=11400 and $Re_{d\text{-}water}$=5100.

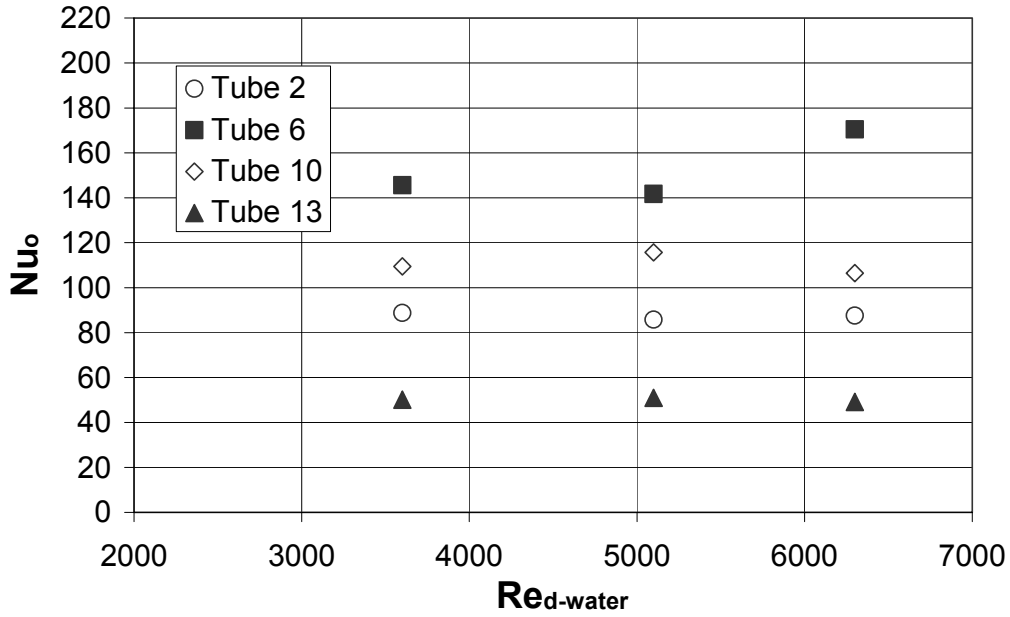

Figure 17. Tube-averaged Nusselt numbers for the smooth tubes for $Re_{d\text{-}air}$=10600.

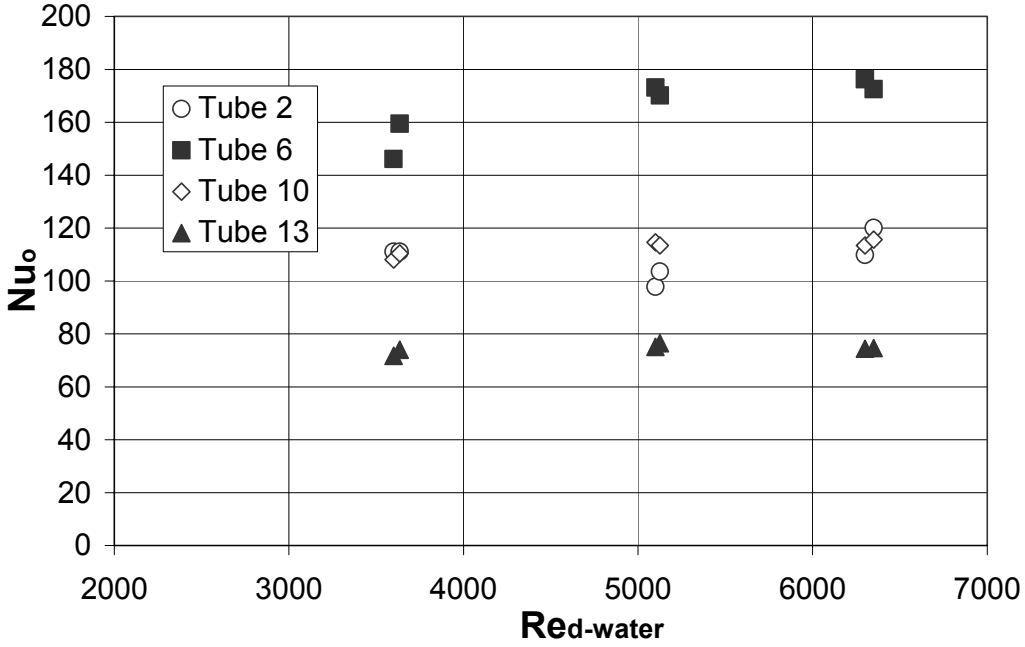

Figure 18. Tube-averaged Nusselt numbers for the smooth tubes for $Re_{d\text{-}air}$=11300 and $Re_{d\text{-}air}$=12000.

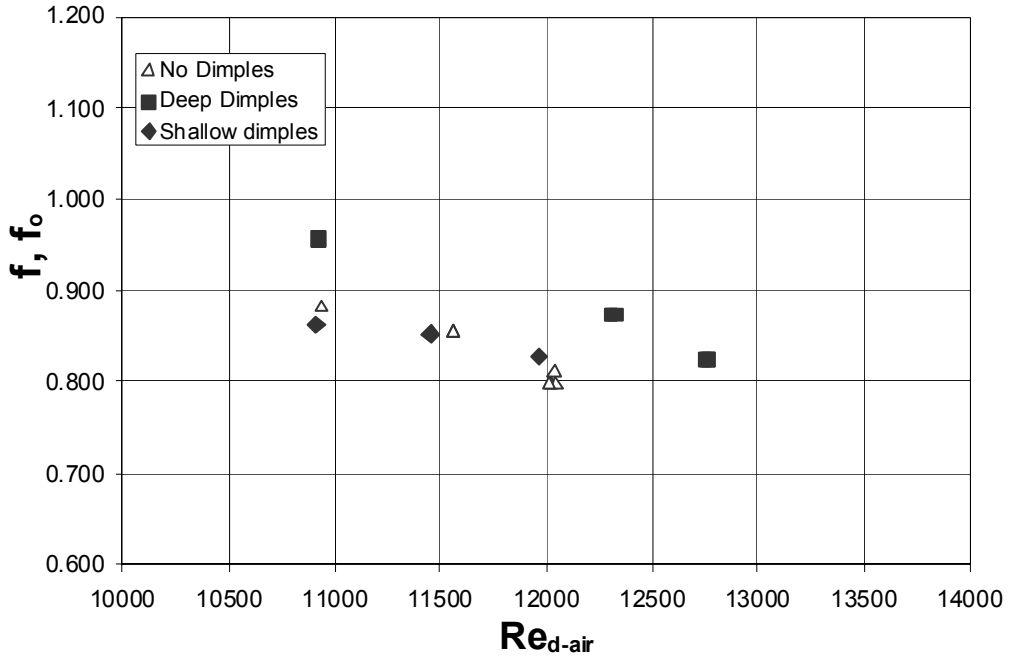

Figure 19. Comparison of test section friction factors for the deep dimpled tubes, shallow dimpled tubes, and smooth tubes for different $Re_{d\text{-}air}$.

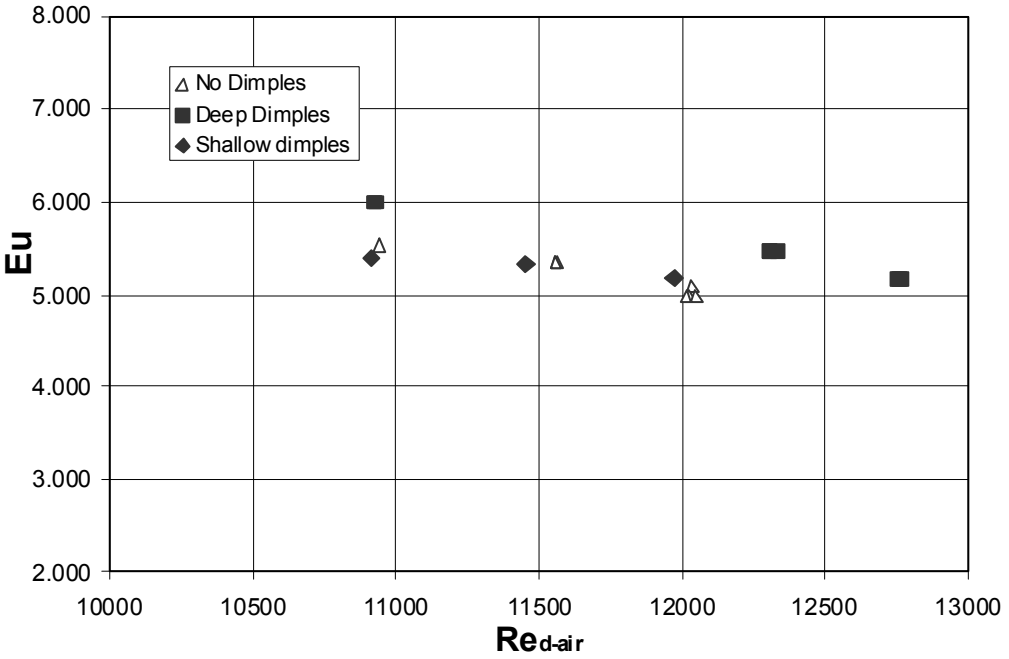

Figure 20. Comparison of test section Euler numbers for the deep dimpled tubes, shallow dimpled tubes, and smooth tubes for different $Re_{d\text{-}air}$.

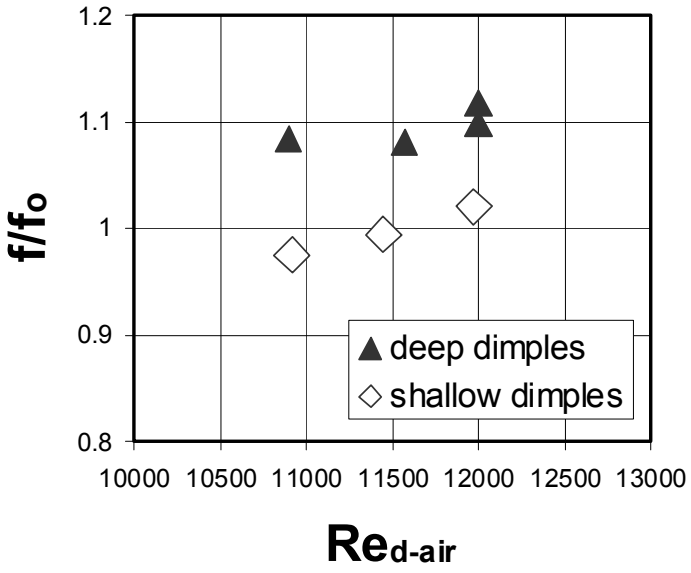

Figure 21. Comparison of test section friction factor ratios for the deep dimpled tubes, and shallow dimpled tubes for different $Re_{d\text{-}air}$.

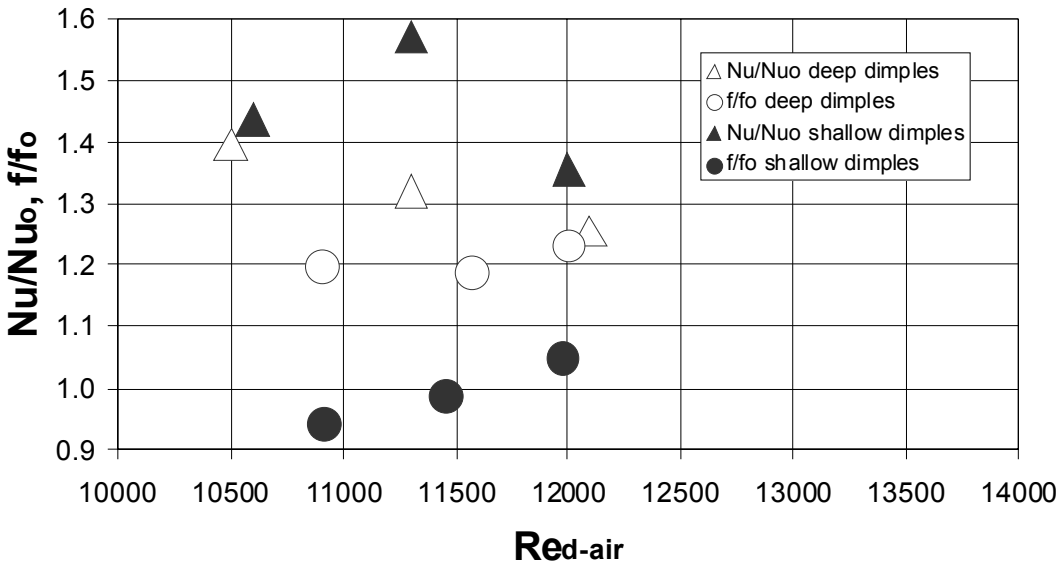

Figure 22. Estimates of overall Nusselt number ratios and overall friction factor ratios for the entire test section for the deep dimpled tubes, and shallow dimpled tubes for different $Re_{d\text{-}air}$. The estimated values are determined for a test section with a total either 14 tubes with shallow dimples or 14 tubes with deep dimples.

Appendix 3

Uncertainty Analysis for the Heat Transfer Coefficient Measurements

The average heat transfer coefficient for outside surface of the tubes is calculated using the following equation:

$$h = Q/(A*\Delta T_{LM}), \quad (1)$$

where:

Q = mean value of heat flow, Btu/hr

A = outside surface area of the tubes, ft^2

$\Delta T_{LM} = (T_{out} - T_{in})/\ln[(T_{wall} - T_{in})/(T_{wall} - T_{out})]$ = mean value of average logarithmic temperature drop, F

T_{out} = mean value of outlet air temperature, F

T_{in} = mean value of inlet air temperature, F

T_{wall} = mean value of average outside surface temperature of the tubes, F

Three error sources are identified for overall error estimate for the heat transfer coefficient measurement, namely, Q, A, ΔT_{LM}. Assume that A is exactly known, that is, there is no uncertainty in that value. The uncertainty in the mean value of heat transfer coefficient measurement would be (using the Kline and McClintock method):

$$\delta h = \{(\partial h/\partial Q*\delta Q)^2+(\partial h/\partial \Delta T_{LM}*\delta \Delta T_{LM})^2\}^{0.5}, \quad (2)$$

where δQ and $\delta \Delta T_{LM}$ represent uncertainties in Q and ΔT_{LM}.

Taking into account the partial derivatives in the equation (2), the uncertainty in h can be estimated using the following equation:

$$\delta h = \{(1/(A*\Delta T_{LM})*\delta Q)^2+(-Q/(A*\Delta T_{LM}^2)*\delta \Delta T_{LM})^2\}^{0.5}. \quad (3)$$

The heat flow Q is calculated using the following equation:

$$Q = M*c_p*\Delta T_f, \quad (4)$$

where:

M = water flow rate, lb/hr

c_p = 1 Btu/(lb*F) = water specific heat

$\Delta T_f = ((T_f)_{out} - (T_f)_{in})$ = water temperature difference, F

$(T_f)_{out}$ = outlet water temperature, F

$(T_f)_{in}$ = inlet water temperature, F

Assume that c_p is exactly known, that is, there is no uncertainty in that value. The uncertainty in the heat flow would be:

$$\delta Q = \{(\partial Q/\partial M*\delta M)^2+(\partial Q/\partial \Delta T_f*\delta \Delta T_f)^2\}^{0.5}, \quad (5)$$

or taking into account the partial derivatives:

$$\delta Q = \{(c_p*\Delta T_f*\delta M)^2+(M*c_p*\partial \Delta T_f)^2\}^{0.5}, \quad (6)$$

where δM and $\delta \Delta T_f$ represent uncertainties in M and ΔT_f.

The uncertainty in M would be:

$$\delta M = \{\delta M_1{}^2+(1.96*\delta M_2)^2\}^{0.5}, \quad (7)$$

where δM_1 and δM_2 represent uncertainties of the water flow meter and water flow rate estimated standard deviation. The value δM_1 is equal 0.01 of flow meter reading, the value δM_2 is calculated from measuring data as standard deviation. The multiplier 1.96 at the standard deviation means that we use 95% confidence level. In order to decrease uncertainty from random error, several measured values are averaged. In this case, uncertainty in mean value $\delta \bar{M}_2$ would be:

$$\delta \bar{M}_2 = \delta M_2/\sqrt{n}, \quad (8)$$

where n is number of measured values. Taking into account the mean value $\delta \bar{M}_2$, equation (7) becomes:

$$\delta M = \{\delta M_1{}^2+(1.96*\delta \bar{M}_2)^2\}^{0.5} \quad (9)$$

The uncertainty in ΔT_f would be:

$$\delta \Delta T_f = \{(\partial \Delta T_f/\partial (T_f)_{out}*\delta (T_f)_{out})^2+(\partial \Delta T_f/\partial (T_f)_{in}*\delta (T_f)_{in})^2\}^{0.5}, \quad (10)$$

or taking into account the partial derivatives:

$$\delta\Delta T_f = \{\delta(T_f)_{out}^2 + (-\delta(T_f)_{in})^2\}^{0.5}, \quad (11)$$

where $\delta(T_f)_{out}$ and $\delta(T_f)_{in}$ represent uncertaintis in $(T_f)_{out}$ and $(T_f)_{in}$.

The uncertainty of the water temperature measurement would be:

$$\delta(T_f) = \{\delta(T_f)_1^2 + (1.96*\delta(T_f)_2)^2\}^{0.5}, \quad (12)$$

where $\delta(T_f)_1$ and $\delta(T_f)_2$ represent uncertainties of the thermocouples calibration and water temperature standard deviation. Uncertainty in mean value $\delta(\bar{T}_f)_2$ would be:

$$\delta(\bar{T}_f)_2 = \delta(T_f)_2 / \sqrt{n}. \quad (13)$$

Taking into account the mean value $\delta(\bar{T}_f)_2$, equation (12) becomes:

$$\delta(T_f) = \{\delta(T_f)_1^2 + (1.96*\delta(\bar{T}_f)_2)^2\}^{0.5}, \quad (14)$$

The uncertainty of the average logarithmic temperature drop ΔT_{LM} would be:

$$\delta\Delta T_{LM} = \{(\partial\Delta T_{LM}/\partial T_{out}*\delta T_{out})^2 + (\partial\Delta T_{LM}/\partial T_{in}*\delta T_{in})^2 + (\partial\Delta T_{LM}/\partial T_{wall}*\delta T_{wall})^2\}^{0.5}, \quad (15)$$

where δT_{out}, δT_{in}, and δT_{wall} represent uncertainty in T_{out}, T_{in}, and T_{wall}.

The partial derivates are:

$$\partial\Delta T_{LM}/\partial T_{out} = \{\ln[(T_{wall} - T_{in})/(T_{wall} - T_{out})] - (T_{out} - T_{in})/(T_{wall} - T_{out})\}/$$
$$/\{\ln[(T_{wall} - T_{in})/(T_{wall} - T_{out})]\}^2$$

$$\partial\Delta T_{LM}/\partial T_{in} = \{-\ln[(T_{wall} - T_{in})/(T_{wall} - T_{out})] + (T_{out} - T_{in})/(T_{wall} - T_{in})\}/$$
$$/\{\ln[(T_{wall} - T_{in})/(T_{wall} - T_{out})]\}^2$$

$$\partial\Delta T_{LM}/\partial T_{wall} = (T_{in} - T_{out})^2 / \{(T_{wall} - T_{out})*(T_{wall} - T_{in})*\{\ln[(T_{wall} - T_{in})/(T_{wall} - T_{out})]\}^2\}$$

The uncertainty of the air inlet temperature would be:

$$\delta T_{in} = \{\delta(T_{in})_1^2 + (1.96*\delta(T_{in})_2)^2\}^{0.5}, \quad (16)$$

where $\delta(T_{in})_1$ and $\delta(T_{in})_2$ represent uncertainties of the thermocouples and air inlet temperature standard deviation. The k-type thermocouples were used to measure air temperature. Uncertainty of the thermocouples is ±2F. Uncertainty in mean value $\delta(\bar{T}_{in})_2$ would be:

$$\delta(\bar{T}_{in})_2 = \delta(T_{in})_2 / \sqrt{n}. \quad (17)$$

Taking into account the mean value $\delta(\bar{T}_{in})$ equation (12) becomes:

$$\delta T_{in} = \{\delta(T_{in})_1^2+(1.96*\delta(\bar{T}_{in})_2)^2\}^{0.5}, \quad (18)$$

The uncertainty of the air outlet temperature would be:

$$\delta T_{out} = \{\delta(T_{out})_1^2+(1.96*\delta(T_{out})_2)^2\}^{0.5}, \quad (19)$$

where $\delta(T_{out})_1$ and $\delta(T_{out})_2$ represent uncertainties of the thermocouples and air outlet temperature standard deviation. Uncertainty in mean value $\delta(\bar{T}_{out})_2$ would be:

$$\delta(\bar{T}_{out})_2 = \delta(T_{out})_2 /\sqrt{n}. \quad (20)$$

Taking into account the mean value $\delta(\bar{T}_{out})$ equation (12) becomes:

$$\delta T_{out} = \{\delta(T_{out})_1^2+(1.96*\delta(\bar{T}_{out})_2)^2\}^{0.5}, \quad (21)$$

The average outside surface temperature of the tubes is calculated using the following equation:

$$T_{wall} = T_f + f*d_o/d_i*1/h_f +f*d_o/(d_o - t_w)*t_w/k, \quad (22)$$

where:

$T_f = ((T_f)_{out} + (T_f)_{in})/2$ = mean water temperature, F

$f = Q/A$ = heat flux rate for outside surface of the tubes, Btu/(hr*ft^2)

d_o = outside tube diameter, ft

d_i = inside tube diameter, ft

t_w = tube wall thickness, ft

h_f = heat transfer coefficient for inside surface of the tubes, Btu/(hr*ft^2*F)

k = thermal conductivity of tube wall, Btu/(hr*ft*F)

Assume that d_o, d_i, t_w, and k are exactly known, that is, there is no uncertainty in those values. The uncertainty of the average outside surface temperature of the tubes would be:

$$\delta T_{wall} = \{(\partial T_{wall}/\partial T_f*\delta T_f)^2+(\partial T_{wall}/\partial f*\delta f)^2+(\partial T_{wall}/\partial h_f*\delta h_f)^2\}^{0.5}, \quad (23)$$

where δT_f and δf, and δh_f represent uncertainties in T_f and f, and h_f.

Taking into account the partial derivatives in the equation (15), the uncertainty in T_{wall} can be estimated using the following equation:

$$\delta T_{wall} = \{\delta T_f^2 + \{(d_o/d_i * 1/h_w + d_o/(d_o - t_w) * t_w/k) * \delta f\}^2 + \{(-f * d_o/d_i * 1/h_f^2) * \delta h_f\}^2\}^{0.5}, \quad (24)$$

The uncertainty of the mean water temperature would be:

$$\delta T_f = \{\delta(T_f)_{out}^2 + \delta(T_f)_{in}^2\}^{0.5}/2, \quad (25)$$

The uncertainty of the heat flux rate for outside surface of the tubes would be:

$$\delta f = (1/A)^{0.5} * \delta Q, \quad (26)$$

The value of the δQ is unknown. As the first approximation, we can take δQ equal $0.1*Q$, then calculated δf and other uncertainties, recalculate δQ using equation (7), and finally correct the δf value.

Heat transfer coefficient h_f for inside surface of the tubes is calculated based on reference data. Uncertainty of the data is not higher than ±5% of the h_f for 95% confidence level. Therefore, it is taken that $\delta h_f = 0.05 * h_f$.

Estimations showed that maximum heat transfer coefficient uncertainty takes place at low air inlet velocity and equals ±10% for bare tubes, ±6% for finned tubes, and ±16% for dimpled tubes of readings for 95% confidence level. The most important error source in this case is uncertainty in water temperature difference $\delta \Delta T_f$, as the temperature difference is reduced essentially (8F at 10 ft/s for bare tubes) at low air inlet velocity. The uncertainty is reduced when air inlet velocity is decreased. Thus, the heat transfer coefficient uncertainty equals ±3% for bare tubes, ±2% for finned tubes, and ±4% for dimpled tubes of readings for 95% confidence level at are inlet velocity 80 ft/s.

Uncertainty for heat transfer coefficient for finned tubes

Inlet velocity $\mathbf{V_{in}}$, ft/s	**10**			**20**			**40**		**60**		**80**	
Water flow rate **M**, lb/hr	710	1216	2562	703	1199	2515	1202	2559	1200	2506	1208	2539
Hea flux **f=Q/A**, Btu/(hr*ft2)	3635	3680	3798	6196	6389	6610	10269	10730	13123	13831	15630	16597
Heat flux uncertainty **df**, Btu/(hr*ft2)	301	481	1005	336	509	990	589	1060	627	1058	697	1111
Mean water temperature uncertainty $\mathbf{dT_f}$, F	0.6	0.6	0.6	0.6	0.6	0.6	0.6	0.6	0.6	0.6	0.6	0.6
Uncertainty of outside tube surface temperature $\mathbf{dT_w}$, F	2.1	2.2	2.7	2.3	2.3	2.7	2.6	2.8	2.7	2.8	2.9	2.9
Air intlet temperature uncertainty $\mathbf{dT_{in}}$, F	2.0	2.0	2.0	2.0	2.0	2.0	2.0	2.0	2.0	2.0	2.0	2.0
Air outlet temperature uncertainty $\mathbf{dT_{out}}$, F	2.0	2.0	2.0	2.0	2.0	2.0	2.0	2.0	2.0	2.0	2.0	2.0
Air inlet temperature $\mathbf{T_{in}}$, F	1083	1082	1081	1098	1098	1098	1098	1098	1098	1098	1099	1099
Air outlet temperature $\mathbf{T_{out}}$, F	202	186	175	325	308	286	451	424	535	508	599	573
Tube wall temperature $\mathbf{T_{wall}}$, F	176	134	100	247	193	141	266	196	316	237	355	269
Water temperature difference uncertainty $\mathbf{d(dT_f)}$, F	1.2	1.2	1.2	1.2	1.2	1.2	1.3	1.2	1.2	1.2	1.2	1.2
Water flow rate uncertainty **dM**, lb/hr	7.2	12.3	25.8	7.2	12.2	25.3	12.3	26.6	12.2	25.5	12.3	25.6
Water temperature difference $\mathbf{dT_f}$, F	52.0	30.7	15.1	89.5	54.1	26.7	86.8	42.6	111.1	56.1	131.3	66.4
Heat flow uncertainty **dQ**, Btu/hr	955	1550	3185	1089	1626	3177	1847	3371	2013	3416	2210	3571
Heat flow uncertainty **dQ/Q** for 95% confidence level, %	2.6	4.1	8.3	1.7	2.5	4.7	1.8	3.1	1.5	2.4	1.4	2.1
Heat transfer coefficient **h**, Btu/(hr*ft2*F)	14.7	11.9	10.8	19.2	16.7	15.4	23.9	21.9	29.6	27.1	34.9	31.7
Heat transfer coefficient uncertainty **dh/h**, %	4	5	8	2	3	5	2	3	2	3	2	2
Overall heat transfer coefficient uncertainty **dh**, Btu/(hr*ft2*F)	0.69			0.56			0.65		0.64		0.65	
Average heat transfer coefficient **h**, Btu/(hr*ft2*F)	12.5			17.1			22.9		28.4		33.3	
Overall heat transfer coefficient uncertainty **dh/h**	**6**			**3**			**3**		**2**		**2**	

Maximum heat transfer coefficient uncertainty is +-6% of reading for 95% confidence level

Uncertainty for heat transfer coefficient for bare tubes

Inlet velocity $\mathbf{V_{in}}$, ft/s	**10**			**20**			**40**			**60**			**80**		
Water flow rate **M**, lb/hr	697	1193	2516	708	1206	2542	695	1209	2521	705	1195	2496	699	1208	2524
Hea flux **f=Q/A**, Btu/(hr*ft2)	9089	9306	9801	14095	14374	14915	21245	21816	22606	26726	27408	28427	31354	32327	33690
Heat flux uncertainty **df**, Btu/(hr*ft2)	605	1023	2156	632	1040	2180	676	1073	2192	735	1110	2180	771	1123	2194
Mean water temperature uncertainty $\mathbf{dT_f}$, F	0.6	0.6	0.6	0.6	0.6	0.6	0.6	0.6	0.6	0.6	0.6	0.6	0.6	0.6	0.6
Uncertainty of wall temperature $\mathbf{dT_w}$, F	4.9	4.9	6.0	5.4	5.1	6.0	6.5	5.7	6.2	7.2	6.2	6.3	7.8	6.5	6.4
Air intlet temperature uncertainty $\mathbf{dT_{in}}$, F	2.0	2.0	2.0	2.0	2.0	2.0	2.0	2.0	2.0	2.0	2.0	2.0	2.0	2.0	2.0
Air outlet temperature uncertainty $\mathbf{dT_{out}}$, F	2.0	2.0	2.0	2.0	2.0	2.0	2.0	2.0	2.0	2.0	2.0	2.0	2.0	2.0	2.0
Air inlet temperature $\mathbf{T_{in}}$, F	1098	1097	1097	1098	1098	1098	1098	1099	1099	1098	1098	1098	1098	1098	1098
Air outlet temperature $\mathbf{T_{out}}$, F	615	611	609	713	707	702	799	793	788	844	838	831	875	869	863
Tube wall temperature $\mathbf{T_{wall}}$, F	120	93	74	154	119	90	200	153	113	229	178	131	255	198	145
Water temp. difference uncertainty $\mathbf{d(dT_f)}$, F	1.2	1.2	1.2	1.2	1.2	1.2	1.2	1.2	1.2	1.2	1.2	1.2	1.2	1.2	1.2
Water flow rate uncertainty **dM**, lb/hr	7.2	12.5	26.0	7.4	12.3	25.9	7.2	12.4	25.4	7.3	12.3	25.3	7.1	12.4	25.7
Water temperature difference $\mathbf{dT_f}$, F	27.3	16.3	8.2	41.7	25.0	12.3	64.0	37.8	18.8	79.3	48.0	23.8	94.0	56.0	28.0
Heat flow uncertainty **dQ**, Btu/hr	884	1490	3115	929	1521	3157	975	1566	3148	1050	1590	3139	1096	1646	3200
Heat flow uncertainty **dQ/Q**, %	4.6	7.6	15.2	3.1	5.1	10.1	2.2	3.4	6.7	1.9	2.8	5.3	1.7	2.4	4.5
Heat transfer coefficient **h**, Btu/(hr*ft2*F)	12.8	12.7	13.0	19.2	18.7	18.8	28.8	27.9	27.6	36.4	35.0	34.4	43.2	41.4	40.6
Heat transfer coefficient uncertainty **dh/h**, %	5	8	15	3	5	10	2	4	7	2	3	5	2	3	5
Overall uncertainty **dh**, Btu/(hr*ft2*F)		1.32			1.28			1.27			1.29			1.34	
Average **h**, Btu/(hr*ft2*F)		12.8			18.9			28.1			35.3			41.7	
Overall **dh/h, %**		**10**			**7**			**5**			**4**			**3**	

Maximum heat transfer coefficient uncertainty is +-10% of reading for 95% confidence level

Uncertainty for heat transfer coefficient for deep dimpled tubes in narrow channel

Inlet velocity $\mathbf{V_{in}}$, ft/s	**10**			**20**			**40**			**60**			**80**		
Water flow rate **M**, lb/hr	703	1200	2472	695	1202	2518	701	1205	2491	711	1204	2532	703	1200	2497
Hea flux **f=Q/A**, Btu/(hr*ft2)	8986	9598	10857	15112	16258	17877	25808	27025	29200	34726	36354	39138	42628	44370	47775
Heat flux uncertainty **df**, Btu/(hr*ft2)	975	1653	3393	984	1670	3466	1046	1681	3422	1105	1736	3511	1172	1798	3525
Mean water temperature uncertainty $\mathbf{dT_f}$, F	1.0	1.0	1.0	1.0	1.0	1.0	1.0	1.0	1.0	1.0	1.0	1.0	1.0	1.0	1.0
Uncertainty of wall temperature $\mathbf{dT_w}$, F	7.2	7.7	9.5	7.6	7.9	9.6	8.5	8.1	9.5	9.3	8.7	9.7	10.0	9.2	9.9
Air intlet temperature uncertainty $\mathbf{dT_{in}}$, F	2.0	2.1	2.1	2.0	2.0	2.0	2.0	2.0	2.0	2.0	2.0	2.0	2.0	2.0	2.0
Air outlet temperature uncertainty $\mathbf{dT_{out}}$, F	2.0	2.0	2.0	2.0	2.0	2.0	2.0	2.0	2.0	2.0	2.0	2.0	2.0	2.0	2.0
Air inlet temperature $\mathbf{T_{in}}$, F	1061	1062	1060	1098	1098	1099	1098	1098	1098	1098	1098	1098	1099	1098	1099
Air outlet temperature $\mathbf{T_{out}}$, F	416	411	403	527	519	509	614	601	587	662	647	631	695	680	663
Tube wall temperature $\mathbf{T_{wall}}$, F	118	94	76	162	126	96	225	175	132	270	214	159	310	246	185
Water temperature difference uncertainty $\mathbf{d(dT_f)}$, F	2.0	2.0	2.0	2.0	2.0	2.0	2.0	2.0	2.0	2.0	2.0	2.0	2.0	2.0	2.0
Water flow rate uncertainty **dM**, lb/hr	7.5	12.2	25.4	7.0	12.1	25.3	7.1	12.3	25.1	7.3	12.3	25.6	7.3	12.1	25.2
Water temperature difference $\mathbf{dT_f}$, F	26.8	16.8	9.2	45.5	28.3	14.9	77.0	47.0	24.5	102.2	63.2	32.4	127.0	77.4	40.1
Heat flow uncertainty **dQ**, Btu/hr	1409	2386	4906	1413	2407	5003	1494	2457	4974	1597	2513	5084	1676	2559	5053
Heat flow uncertainty **dQ/Q**, %	7.5	11.9	21.6	4.5	7.1	13.4	2.8	4.3	8.1	2.2	3.3	6.2	1.9	2.8	5.1
Heat transfer coefficient **h**, Btu/(hr*ft2*F)	16.0	16.5	18.2	24.9	25.4	26.9	43.1	42.1	43.0	59.6	57.5	57.6	75.7	71.6	71.0
Heat transfer coefficient uncertainty **dh/h**, %	8	12	22	5	7	13	3	5	8	3	4	6	3	3	5
Overall **dh**, Btu/(hr*ft2*F)	2.64			2.44			2.46			2.62			2.78		
Average **h**, Btu/(hr*ft2*F)	16.9			25.7			42.7			58.2			72.8		
Overall **dh/h, %**	**16**			**9**			**6**			**4**			**4**		

Maximum heat transfer coefficient uncertainty is +-16% of reading for 95% confidence level

Appendix 4

Uncertainty Analysis for the Pressure Drop Measurements

The total pressure drop is calculated using the following equation:

$$dP = dP_s + dP_d, \quad (1)$$

where:

dP_s = static pressure difference between inlet and outlet flow, in. WC

$dP_d = 0.004019 *(\rho_2*V_2^2/2 - \rho_1*V_1^2/2) = 0.004019*(1 - \rho_1/\rho_2)*\rho_1*V_1^2/2$ = additional pressure drop caused by flow deceleration due to density change, in. WC

ρ_1, ρ_2 = flow density before and after the tube bundle, kg/m^3

V_1, V_2 = flow velocity before and after the tube bundle, m/s

We use static pressure difference dP_s instead of total pressure difference in equation (1). This approach is valid because inlet and outlet velocity profiles are uniform, and static pressure across the flow is the same. In this case, total pressure difference equals static pressure difference.

The equation (1) becomes:

$$dP = dP_s + 0.004019*(\rho_1 - \rho_1^2/\rho_2)*V_1^2/2, \quad (2)$$

Four error sources are identified for overall error estimate for the pressure drop measurement, namely, dP_s, ρ_1, ρ_2, and V_1. The uncertainty in the mean value of pressure drop measurement would be (using the Kline and McClintock method):

$$\delta dP = \{(\partial dP/dP_s *\delta dP_s)^2+(\partial dP/\partial\rho_1*\delta\rho_1)^2+(\partial dP/\partial\rho_2*\delta\rho_2)^2+(\partial dP/\partial V_1*\delta V_1)^2\}^{0.5}, \quad (3)$$

where δdP_s, $\delta\rho_1$, $\delta\rho_2$, and δV_1 represent uncertainties in dP_s, ρ_1, ρ_2, and V_1.

Taking into account the partial derivatives in the equation (3), the uncertainty in dP can be estimated using the following equation:

$$\delta dP = \{\delta dP_s^2 + [0.004019*(V_1^2/2 - V_1^2*\rho_1/\rho_2)*\delta\rho_1]^2 + [0.004019*\rho_1^2*V_1^2/(2*\rho_2^2)*\delta\rho_2]^2 + + [0.004019*(\rho_1 - \rho_1^2/\rho_2)*V_1*\delta V_1]^2\}^{0.5}, \quad (4)$$

The uncertainty in dP_s would be:

$$\delta dP_s = \{\delta(dP_s)_1^2+(1.96*\delta(dP_s)_2^2\}^{0.5}, \quad (5)$$

where $\delta(dP_s)_1$ and $\delta(dP_s)_2$ represent uncertainties of the pressure transmitter and pressure estimated standard deviation. The value $\delta(dP_s)_1$ is equal 1% of pressure transmitter full scale, or 0.03 in. WC. The value $\delta(dP_s)_2$ is calculated from measuring data as standard deviation. The multiplier 1.96 at the standard deviation means that we use 95% confidence level. In order to decrease uncertainty from random error, several measured values are averaged. In this case, uncertainty in mean value $\delta(d\ \overline{P}_s)_2$ would be:

$$\delta(d\ \overline{P}_s)_2 = \delta(dP_s)_2 / \sqrt{n}, \tag{6}$$

where n is number of measured values. Taking into account the mean value $\delta(d\ \overline{P}_s)_2$, equation (5) becomes:

$$\delta dP_s = \{\delta(dP_s)_1^2 + [(1.96 * \delta(d\ \overline{P}_s)_2]^2\}^{0.5}, \tag{7}$$

Flow density is calculated using the following equation:

$$\rho = P/(R*T), \tag{8}$$

where:

P = total flow pressure, Pa

R = 287.05 = gas constant, J/(kg*K)

T = flow temperature, K

Assume that R is exactly known, that is, there is no uncertainty in that value. The uncertainty in density would be:

$$d\rho = \{(\partial\rho/\partial P * \delta P)^2 + (\partial\rho/\partial T * \delta T)^2\}^{0.5}, \tag{9}$$

or taking into account the partial derivatives:

$$d\rho = \{(\delta P/(R*T))^2 + (\delta T * P/(R*T^2))^2\}^{0.5}, \tag{10}$$

where δP and δT represent uncertainties in P and T.

Flow inlet velocity is measured as:

$$V_1 = (0.453515 * M/3600)/(A*\rho_1), \tag{11}$$

where:

M = air flow rate, lb/hr

A = channel cross section area, m^2
Assume that A is exactly known, that is, there is no uncertainty in that value. The uncertainty in the flow inlet velocity measurements would be:

$$\delta V_1 = \{(\partial V_1/\partial M*\delta M)^2 + (\partial V_1/\partial \rho_1*\delta \rho_1)^2\}^{0.5}, \quad (12)$$

Taking into account the partial derivatives in the equation (12), the uncertainty in V_1 can be estimated using the following equation:

$$\delta V_1 = \{[0.453515/(3600*A*\rho_1)*\delta M]^2 + [0.453515*M/(3600*A*\rho_1^2)*\delta \rho_1]^2\}^{0.5}, \quad (13)$$

The uncertainty in M would be:

$$\delta M = \{\delta M_1^2+(1.96*\delta M_2)^2\}^{0.5}, \quad (14)$$

where δM_1 and δM_2 represent uncertainties of the air flow meter and air flow rate estimated standard deviation. The value δM_1 is equal 0.01 of flow meter reading, the value δM_2 is calculated from measuring data as standard deviation. Uncertainty in mean value $\delta \bar{M}_2$ would be:

$$\delta \bar{M}_2 = \delta M_2/\sqrt{n}, \quad (15)$$

Taking into account the mean value $\delta \bar{M}_2$, equation (14) becomes:

$$\delta M = \{\delta M_1^2+(1.96*\delta \bar{M}_2)^2\}^{0.5} \quad (16)$$

Total pressure at outlet equals absolute pressure P_{out} = 101,300 Pa and is measured with an uncertainty of 1% of reading or δP_{out} = 1013 Pa. Inlet total pressure is calculated as:

$$P_{in} = P_{out} + dP, \quad (17)$$

The uncertainty of the inlet total pressure measurements would be:

$$\delta P_{in} = \{\delta P_{out}^2 + \delta dP^2\}^{0.5}. \quad (18)$$

The uncertainty of the air temperature measurement would be:

$$\delta T = \{\delta T_1^2 + (1.96*\delta T_2)^2\}^{0.5}, \quad (19)$$

where δT_1 and δT_2 represent uncertainties of the thermocouple calibration and air temperature standard deviation. The value δT_1 is equal ±2F, the value δT_2 is calculated from measuring data as standard deviation. Uncertainty in mean value $\delta \bar{T}_2$ would be:

$$\delta \bar{T}_2 = \delta T_2 /\sqrt{n}. \quad (20)$$

where n is number of measured values. Taking into account the mean value $\delta\ \bar{T}_2$, equation (19) becomes:

$$\delta T = \{\delta T_1^2 + (1.96 * \delta\ \bar{T}_2)^2\}^{0.5} \quad (21)$$

Estimations showed that maximum total pressure drop uncertainty takes place at low air inlet velocity and equals ±0.03 in. WC (±30%) at total pressure drop 0.1 in. WC for bare tubes; ±0.03 in. WC (±14%) at total pressure drop 0.22 in. WC for finned tubes; and ±0.03 in. WC (±11%) at total pressure drop 0.26 in. WC for dimpled tubes for 95% confidence level. The most important error source in this case is pressure transmitter uncertainty, which is ±0.03 in. WC. Total pressure drop uncertainty is reduced when air inlet velocity is decreased. Thus, total pressure drop uncertainty equals ±1% of readings for all cases for 95% confidence level at are inlet velocity 60ft/s–80 ft/s.

Uncertainty for pressure drop for bare tubes

Inlet velocity $\mathbf{V_{in}}$, ft/s	**10**			**20**			**40**			**60**			**80**		
Water flow rate **M**, lb/hr	697	1193	2516	708	1206	2542	695	1209	2521	705	1195	2496	699	1208	2524
Pressure drop **dP**, in. WC	0.10	0.10	0.10	0.32	0.32	0.32	1.27	1.26	1.24	2.62	2.59	2.56	4.38	4.33	4.27
Outlet total pressure uncertainty $\mathbf{dP_{out}}$, Pa	1013	1013	1013	1013	1013	1013	1013	1013	1013	1013	1013	1013	1013	1013	1013
Inlet total pressure uncertainty $\mathbf{dP_{in}}$, Pa	1013	1013	1013	1013	1013	1013	1013	1013	1013	1013	1013	1013	1013	1013	1013
Static pressure difference uncertainty $\mathbf{d(dP_s)}$, in. WC	0.03	0.03	0.03	0.03	0.03	0.03	0.03	0.03	0.03	0.03	0.03	0.03	0.03	0.03	0.03
Inlet flow velocity $\mathbf{V_1}$, m/s (eq. 11)	3.1	3.1	3.1	6.2	6.8	6.2	12.4	12.5	12.4	18.6	18.5	18.5	24.5	24.5	24.5
Inlet velocity uncertainty $\mathbf{dV_1}$, m/s (eq. 13)	0.04	0.04	0.044	0.09	0.10	0.089	0.18	0.18	0.176	0.26	0.26	0.262	0.35	0.35	0.346
Total pressure drop uncertainty **d(dP)**, in. WC	0.030	0.030	0.030	0.030	0.030	0.030	0.030	0.030	0.030	0.030	0.030	0.030	0.031	0.031	0.031
Overall total pressure drop uncertainty **d(dP)**, in. WC	0.030			0.030			0.030			0.030			0.031		
Average total pressure drop **dP**, in. WC	0.10			0.32			1.26			2.59			4.33		
d(dP)/h for 95% confidence level, %	**30**			**9**			**2**			**1**			**1**		

Maximum total pressure drop uncertainty is +- 30% (+- 0.03 in. WC) of reading (0.1 in.WC) for 95% confidence level

Uncertainty for pressure drop for finned tubes

Inlet velocity $\mathbf{V_{in}}$, ft/s	**10**			**20**			**40**			**60**			**80**		
Water flow rate **M**, lb/hr	710	1216	2562	703	1199	2515	#REF!	2559	1200	#REF!	1208	2539	#REF!	1208	2524
Pressure drop **dP**, in. WC	0.27	0.26	0.26	1.02	1.01	1.02	#REF!	4.10	4.10	#REF!	9.05	8.87	#REF!	16.61	16.38
Outlet total pressure uncertainty $\mathbf{dP_{out}}$, Pa	1013	1013	1013	1013	1013	1013	#REF!	1013	1013	#REF!	1013	1013	#REF!	1013	1013
Inlet total pressure uncertainty $\mathbf{dP_{in}}$, Pa	1013	1013	1013	1013	1013	1013	#REF!	1013	1013	#REF!	1013	1013	#REF!	1014	1014
Static pressure difference uncertainty $\mathbf{d(dP_s)}$, in. WC	0.03	0.03	0.03	0.03	0.03	0.03	#REF!	0.10	0.10	#REF!	0.10	0.10	#REF!	0.10	0.10
Inlet flow velocity $\mathbf{V_1}$, m/s (eq. 11)	3.1	3.0	3.1	6.1	6.2	6.2	#REF!	12.3	12.2	#REF!	18.1	18.1	#REF!	23.8	23.8
Inlet velocity uncertainty $\mathbf{dV_1}$, m/s (eq. 13)	0.04	0.04	0.044	0.09	0.09	0.088	#REF!	0.17	0.173	#REF!	0.25	0.254	#REF!	0.33	0.332
Total pressure drop uncertainty **d(dP)**, in. WC	0.030	0.030	0.030	0.030	0.030	0.030	#REF!	0.100	0.100	#REF!	0.100	0.100	#REF!	0.100	0.100
Overall total pressure drop uncertainty **d(dP)**, in. WC		0.030			0.030			0.082			0.082			0.082	
Average total pressure drop **dP**, in. WC		0.26			1.02			2.73			5.97			11.00	
d(dP)/h for 95% confidence level, %		**11**			**3**			**3**			**1**			**1**	

Maximum total pressure drop uncertainty is +- 11% (+- 0.03 in. WC) of reading (0.26 in.WC) for 95% confidence level

Uncertainty for pressure drop for deep dimpled tubes in narrow channel

Inlet velocity $\mathbf{V_{in}}$, ft/s	**10**			**20**			**40**			**60**			**80**		
Water flow rate **M**, lb/hr	703	1200	2472	695	1202	2518	701	1205	2491	711	1204	2532	703	1200	2497
Pressure drop **dP**, in. WC	0.22	0.22	0.22	0.78	0.80	0.80	3.18	3.16	3.15	7.48	7.48	7.39	13.83	13.67	13.57
Outlet total pressure uncertainty $\mathbf{dP_{out}}$, Pa	1013	1013	1013	1013	1013	1013	1013	1013	1013	1013	1013	1013	1013	1013	1013
Inlet total pressure uncertainty $\mathbf{dP_{in}}$, Pa	1013	1013	1013	1013	1013	1013	1013	1013	1013	1013	1013	1013	1014	1014	1014
Static pressure difference uncertainty $\mathbf{d(dP_s)}$, in. WC	0.03	0.03	0.03	0.03	0.03	0.03	0.03	0.03	0.03	0.10	0.10	0.10	0.10	0.10	0.10
Inlet flow velocity $\mathbf{V_1}$, m/s (eq. 11)	2.3	2.3	2.3	4.5	4.6	4.7	9.2	9.3	9.3	13.7	13.7	13.7	18.0	18.0	18.0
Inlet velocity uncertainty $\mathbf{dV_1}$, m/s (eq. 13)	0.03	0.03	0.033	0.06	0.07	0.066	0.13	0.13	0.131	0.19	0.19	0.193	0.25	0.25	0.252
Total pressure drop uncertainty **d(dP)**, in. WC	0.030	0.030	0.030	0.030	0.030	0.030	0.030	0.030	0.030	0.100	0.100	0.100	0.100	0.100	0.100
Overall total pressure drop uncertainty **d(dP)**, in. WC	0.030			0.030			0.030			0.100			0.100		
Average total pressure drop **dP**, in. WC	0.22			0.79			3.16			7.45			13.69		
d(dP)/h for 95% confidence level, %	**14**			**4**			**1**			**1**			**1**		

Maximum total pressure drop uncertainty is +- 14% (+- 0.03 in. WC) of reading (0.22 in.WC) for 95% confidence level

Appendix 5

BRIEF SUMMARY OF DIMPLED TUBE STRENGTH EVALUATION

Computation of stressed-deformed state was performed by Energetic System Consulting under subcontract KI24443 for the SA-178A tube. Dimpling geometry was copied directly from the fabricated samples given in Figure 1 below.

A

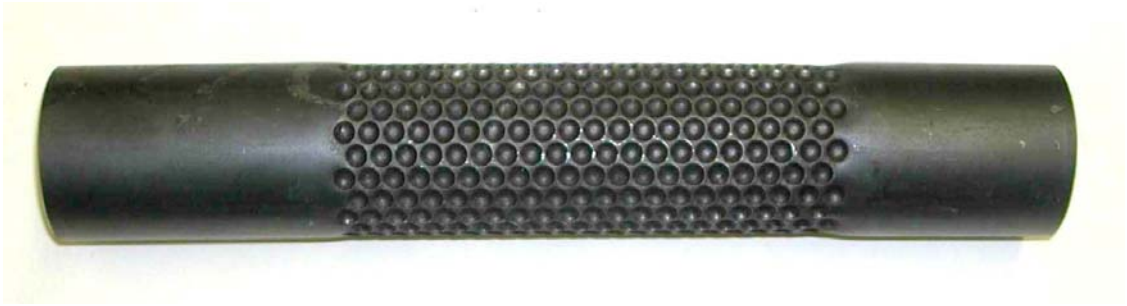

B

C

Figure 1. Dimpled tube samples for computation geometry and "burst" tesing:
A – test sample, B – cuts for profile measurement, C – profiles (wall thickness of 0.2", 0.15" and 0.1")

Two values of inner pressure (52 MPa/7,500 psi and 104 MPa/15,000 psi) were considered for all calculations. The first pressure value of 52 MPa was selected from the destruction tests. As shown down below the obtained maximum stresses appear more than yield point meaning that process should be considered within the plasticity theory frame. The second pressure value

doubles the inner pressure value and it was expected that all the stresses will be related to elasticity range, so all the result may be considered as real characteristics of tube stress-deformed state.

Computation of stress-deformed state was performed by finite element method using computation complex ANSYS (certificate № 145 2002). For determination of stressed and deformed state of the tube two finite-element models were used (see Figures 2 and 3). In finite–element model presented in Figure 1 four-node finite elements type of "thin shell" were used. Shell finite elements are assigned on middle surface of computed construction and thickness is assigned as element parameter.

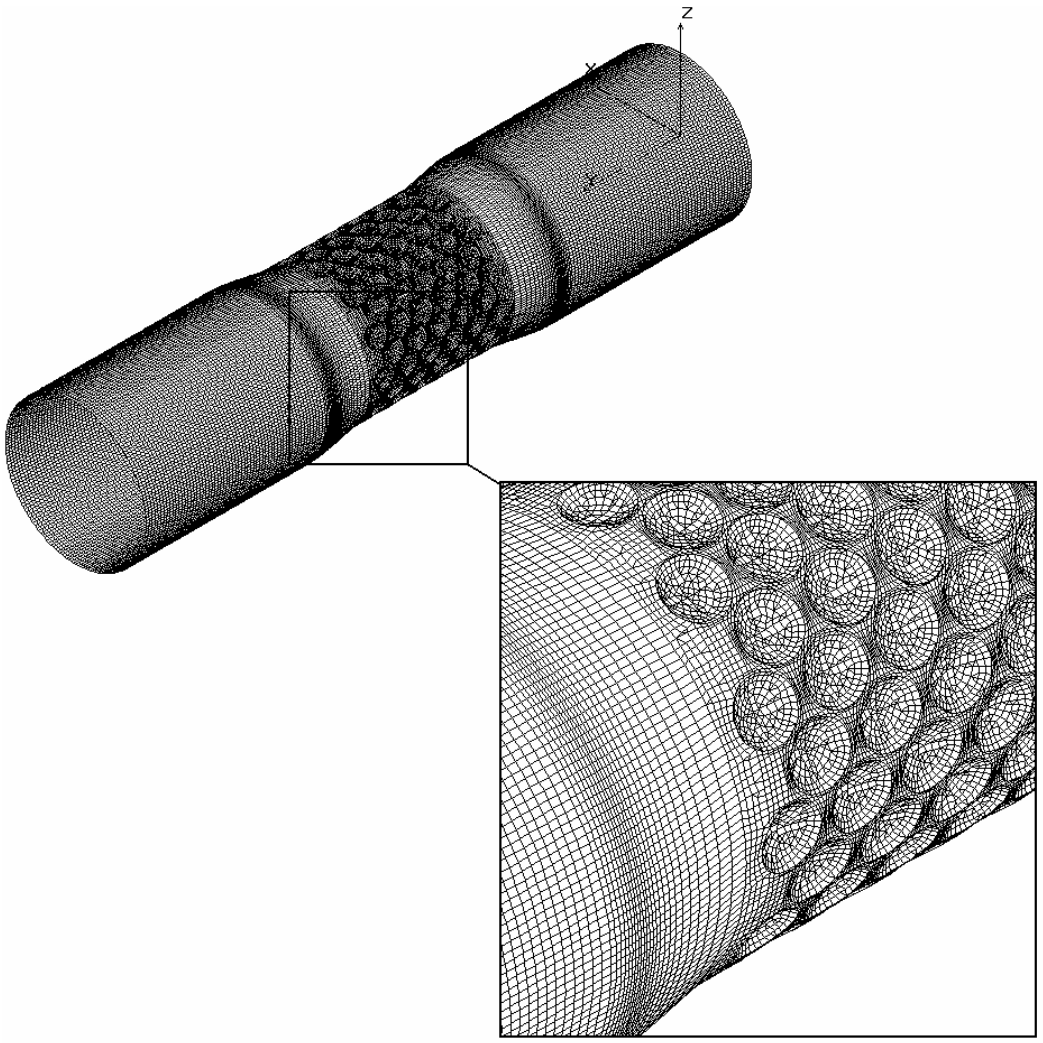

Figure 2. Finite-element model #1

In finite-element model presented in Figure 3 space ten-node elements type of "volumetric body" were used. Inner pressure was used as given load.

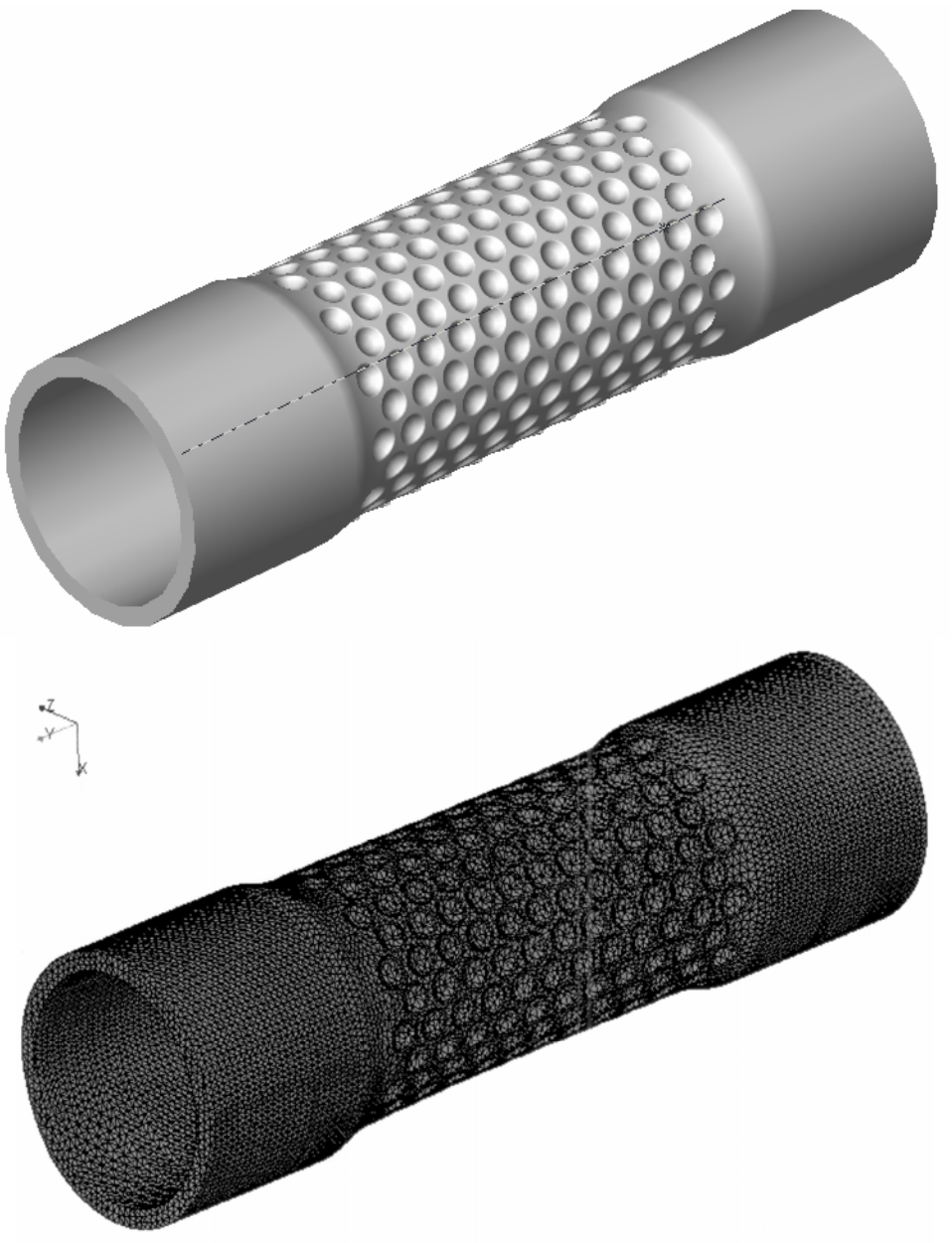

Figure 3. Finite-element model #2

In Figure 4 a reduced membrane stresses distribution due to inner pressure of 52 MPa/7,500 psi is presented. It is known that the reduced membrane stresses govern by system state for static conditions. Calculations demonstrated, that for such conditions a dimpled surface part is stronger part of the tube as opposed to the bare parts. It perfectly corresponds to the results of destruction tests (see Figure 5), when the test sample destruction occurred at the bare part of the tube.

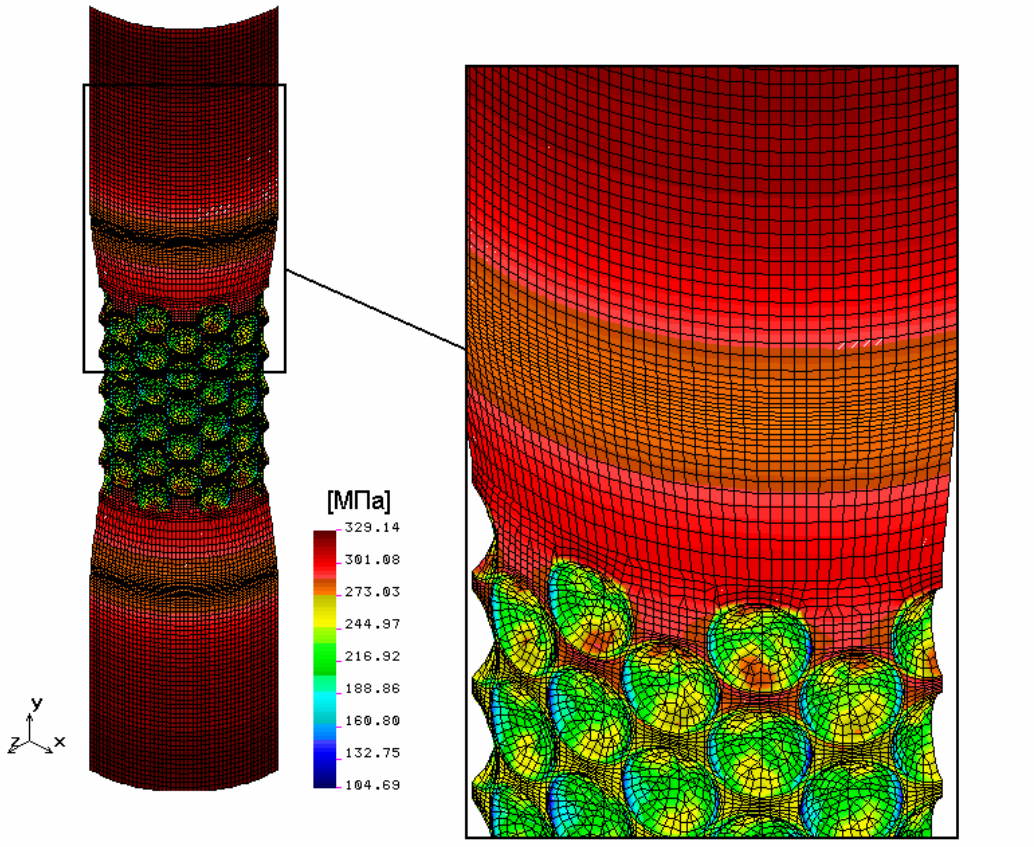

Figure 4. Reduced membrane stresses distribution (52 MPa/7,500 psi, definite-element model #1)

Figure 5. Dimpled tube sample after "burst" test

In Figure 6 the reduced stresses for local conditions are presented. These stresses are very important for fatigue destruction only, because for static conditions it relaxed with the plasticity mechanisms participation. So those stresses are of conditional sense, because were computed without plasticity effects account. Stresses on outer surface are shown in Figure 6A and the maximum local stresses zones on inner surface (very small area) are shown in Figure 6B.

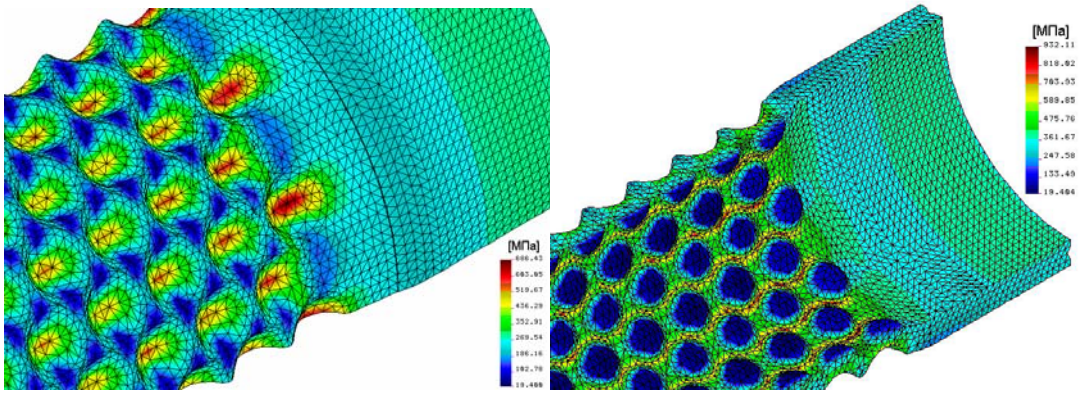

A B

Figure 6. Reduced stresses distribution (52 MPa/7,500 psi, definite-element model #2):
A - outer surface, B – inner surface

The following results were obtained for non-destructive level and without accounting plasticity. For that computation 10 MPa (~1,400 psi) inner pressure load was selected as double exceeding the operational pressure of 5 MPa (~700 psi) assuming to stay in the elasticity range. Results of those computations are presented in Figure 7 below.

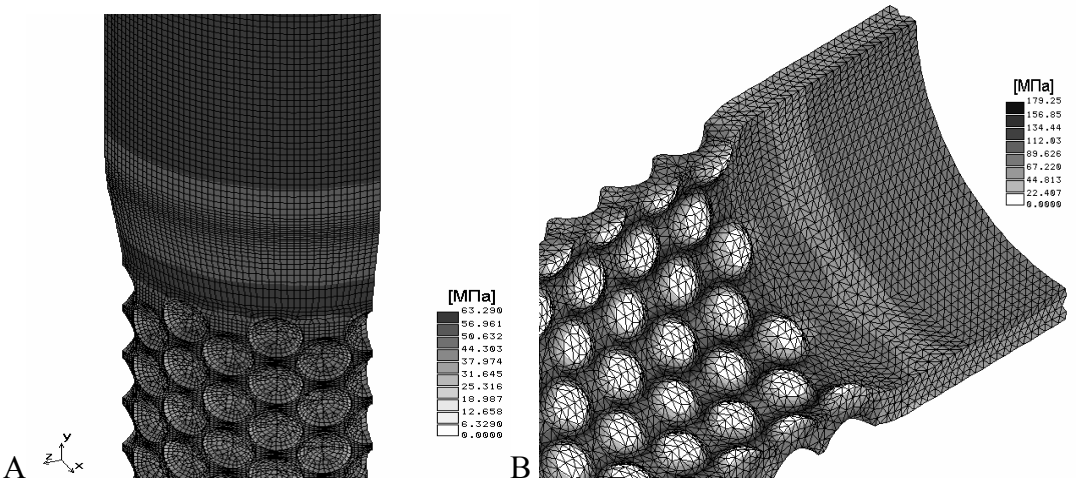

A B

Figure 7. Reduced membrane stresses distribution (10 MPa/1,400 psi, definite-element model #1) and reduced stresses distribution (10 MPa/1,400 psi, definite-element model #2)

Figure 7A represents a reduced membrane stresses distribution due to inner pressure of 10 MPa (~1,400 psi). As opposed to previous case those computations are quantitatively valid, because all the stresses are into elasticity range. Because of practical proportionality between inner pressure value and stresses, their values are approximately 5.2 times less, than in previous case. As well as above, calculations proved, that dimpled part of the tube is much stronger than bare one. Reduced membrane stresses are small enough in comparison with yield strength as well as deformations. Figure 7B demonstrates a reduced stresses distribution due to inner pressure of 10 MPa (~1,400 psi) according to definite-element model #2. Comparing the maximum stress value (~179 MPa/26,000 psi) with a yield strength value (~ 200 MPa/29,000 psi) and taking into account the double pressure assumption (10 Mpa/1,400 psi)) it can be concluded that there is a reliable safety assurance factor for the “real-life” operating conditions.

AUTHORIZED TESTING INC.
2522 Kansas Avenue • Riverside, CA 92507 USA

Appendix 6

Phone: (951)682-4110 • Fax: (951) 682-6090
Email: fjensen@authorizedtestinginc.com
URL: www.authorizedtesting .com

TEST REPORT

CUSTOMER: **Gas Technology Institute** **TEST DATE:** **August 2, 2004**

PART NUMBER: **Tube** **SUBMITTED BY:** **L. Sherrow**

SERIAL NUMBERS: **1- 4** **P.O. NUMBER:** **RF00030400**

TEST DESCRIPTION:

PROOF TEST

The above listed samples were submitted for hydraulic proof test in accordance with Gas Technology Institute purchase order RF00030400.

Each tube was filled with water and pressurized to 2,800 psi, then held for a period of 30 seconds. During this time each tube was visually inspected for leaks or deformation of which none was noted.

Upon completion of the proof test, pressurization resumed until failure occurred. Results of the test are as follows:

SERIAL NUMBER	*BURST PRESSURE*	*FAILURE MODE*
1	12,650 psi	Pinhole leak; lower sidewall
2	13,750 psi	Ductile; upper sidewall
3	13,700 psi	Ductile; upper sidewall
4	14,200 psi	Ductile; upper sidewall

Testing and the results of the tests were in accordance with the applicable specification.

I certify the above information to be true and correct.

Signed by: _____ Date: August 23, 2004

Frank Jensen, Special Programs Administrator
Authorized Testing, Inc.


GTI
Proof / Burst Test
S/N: 1
Burst Pressure: 12,650


GTI
Proof / Burst Test
S/N: 2
Burst Pressure: 13,750


GTI
Proof / Burst Test
S/N: 3
Burst Pressure: 13,700


GTI
Proof / Burst Test
S/N: 4
Burst Pressure: 14,200